**Free-energy-based lattice Boltzmann method for emulsions with soluble surfactant**

by

Yash Devangkumar Kothari

A thesis submitted in partial fulfillment of the requirements for the degree of

Master of Science

Department of Mechanical Engineering
University of Alberta

# Abstract

A diffuse interface model to simulate a system of two immiscible liquids with surfactants is proposed. This model is based on a modified Ginzburg-Landau free energy functional to account for non-ionic soluble surfactants and couples the Navier-Stokes equations with two Cahn-Hilliard equations representing the transport of immiscible liquids and surfactant concentration. The governing equations are solved using a free-energy-based lattice Boltzmann framework.

The proposed model is validated for Langmuir and Frumkin adsorption isotherms when applied to simulate a planar interface and a spherical drop equilibration. The model ensures numerical stability and accurate results for low and high surfactant concentrations, and the diffuse interface thickness remains constant even for high surfactant loads.

The methodology is suggested to correlate the strength of the nonlinear surfactant coupling with the packing of surfactant molecules in the interfacial region. The proposed model allows for a reduction in surface tension of 45-50% compared to the clean system at low surfactant concentrations for the Langmuir isotherm, which follows the experimental results observed for liquid-liquid systems. The appropriate surfactant mobility and solubility values are recommended for different values of the strength of nonlinear surfactant coupling.

# Preface

The work presented in this thesis has been published as Y. Kothari and A. E. Komrakova, "Free-energy-based lattice Boltzmann model for emulsions with soluble surfactant," Chemical Engineering Science, 285, 119609 (2024). A. E. Komrakova was the supervisory author and was involved in discussions of the results and manuscript composition. I modified the computer code developed in Fortran 90 by A. E. Komrakova to incorporate the physics of soluble surfactants and performed the simulations for the present work. With the help of Dr. Marco Ferrari, I devised an efficient procedure to perform the sensitivity analysis of the model parameters. This procedure consists of two parts: automation of multiple simulations using Python and shell scripting and post-processing of the simulation results using MATLAB and ParaView.

# Acknowledgements

I would like to express my heartfelt gratitude to my supervisor for providing me with the opportunity to engage in research and introducing me to the interesting field of multiphase flows. This research work was possible owing to her guidance, trust, and patience for which I am deeply thankful. Beyond academic research, her kindness and strong work ethic play a key role in shaping my professionalism and providing guidance for both academic and professional aspirations.

I extend my gratitude to my colleagues, Dr. Marco Ferrari and Ashley Chen, for engaging in valuable discussions regarding emulsion modeling through the lattice Boltzmann method and methodologies for integrating meso- and macro-scale results. These conversations have contributed partly to the development of the research work presented in this thesis.

My sincere thanks to the Vaja family for embracing me as one of their own from the moment I arrived in Edmonton. Additionally, my special thanks go out to my dear friends for their unwavering support throughout this journey and I am truly grateful for that.

I dedicate this thesis to my parents for their unwavering love and support. To my dear sister, Krupa, for being the constant support through both the highs and lows.

Lastly, to my late grandparents, whose enduring life lessons continue to inspire me.

# Table of Contents

# List of Figures

# List of Symbols

$\Delta G$     Free energy

$\Delta t$     Time step

$\Delta x$     Grid spacing

$\mathbf{M}, \mathbf{S}, \mathbf{M}^{-1}$ Matrices related to the multiple-relaxation-time collision operator

$\mathcal{F}$     Free energy density functional

$A, B$     Model parameters related to the Ginzburg-Landau free energy density functional

$C$     Self-interaction strength between neighbouring surfactant molecules

$c_{q\alpha}$     Discrete velocity vector

$c_s$     Speed of sound

$D$     Model parameter related to the free energy density functional accounting for the adsorption of surfactant at the interface

$E$     Difference in the solubility strength of surfactant in two bulk phases

$f, g, h$     Particle populations

$f_q, g_q, h_q$     Particle distribution functions for particle populations $f$, $g$, and $h$

$f_q^{eq}, g_q^{eq}, h_q^{eq}$ Equilibrium distribution functions for particle populations $f$, $g$, and $h$

$k_B$     Boltzmann constant

$M$     Mobility

$p$     Thermodynamic pressure

$P_{\alpha\beta}^{chem}$     Chemical pressure tensor

$P_{\alpha\beta}^{th}$     Thermodynamic pressure tensor

$p_b$     Bulk pressure

$Q$      Total number of discrete velocity directions

$T$      Temperature

$t$      Time

$u$      Velocity

$V$      Volume

$W$      Model parameter defining the solubility of surfactant in bulk phases

$w_q$      Weight coefficients

$x_q$      Position vector

F      Free energy functional

**Dimensionless numbers**

$Ex$      Dimensionless number controlling the solubility of surfactant in bulk phases

**Greek letters**

$(\psi_0)_{lim}$      Limiting value of the surfactant concentration at the interface

$(\psi_b)_{lim}$      Limiting value of the bulk surfactant concentration

$\alpha$      Proportionality coefficient

$\delta(x)$      Dirac delta function

$\delta_{\alpha\beta}$      Kronecker delta function

$\epsilon$      Expansion parameter for the Chapman-Enskog analysis

$\Gamma$      Mobility coefficient

$\hat{\delta}(x)$      Nascent delta function

$\kappa_{int}$      Model parameter related to the Ginzburg-Landau free energy density functional

$\lambda_1, \lambda_2$      Coefficients incorporating different combinations of nonlocal surfactant couplings

$\mu$      Chemical potential

$\nu$      Kinematic viscosity

$\nu_B$      Bulk viscosity

$\Omega_q^f, \Omega_q^g, \Omega_q^h$      Collision operators for particle populations $f$, $g$, and $h$

$\phi$      Order parameter representing two immiscible liquids

$\phi_0$     Value of order parameter representing two immiscible liquids in bulk phases

$\phi_b$     Value of order parameter representing two immiscible liquids in bulk phases in the presence of surfactant

$\psi$     Order parameter representing a soluble surfactant

$\psi_0$     Surfactant concentration at the interface

$\psi_b$     Bulk surfactant concentration

$\Psi_c$     Adsorption constant

$\psi_c$     Adsorption constant for the Langmuir isotherm

$\psi_{xs}$     Excess surfactant concentration accounting for the local variation of $\psi$ in the interfacial region

$\rho$     Density

$\sigma$     Surface tension in the presence of surfactant

$\sigma_0$     Surface tension of the pure system

$\tau_f, \tau_g, \tau_h$ Relaxation times for particle populations $f$, $g$, and $h$

$\xi$     Interface thickness in the presence of surfactant

$\xi_0$     Interface thickness of the pure system

**Subscript**

$b$     Bulk phase location

$q$     Discrete velocity number

# Abbreviations

**BC** Boundary condition.

**BGK** Bhatnagar-Gross-Crook.

**CFD** Computational Fluid Dynamics.

**CMC** Critical micelle conentration.

**DPD** Dissipative particle dynamics.

**DSMC** Direct simulation Monte Carlo.

**EOS** Equation of State.

**LB** Lattice Boltzmann.

**LBE** Lattice Boltzmann equation.

**LBM** Lattice Boltzmann method.

**lu** lattice units.

**MD** Molecular dynamics.

**MPI** Message-passing interface.

**MRT** Multiple-relaxation-time.

**SRT** Single-relxation-time.

# Chapter 1

# Introduction

## 1.1    Background and motivation

An emulsion is a system of two or more immiscible liquids, for example, oil and water. Emulsions can be categorized into three types: coarse emulsions, mini- or nanoemulsions, and microemulsions [1]. These emulsion types differ from each other in various aspects, such as their formation process, the drop size of a dispersed phase in a continuous phase, physio-chemical properties, and their appearance [1]. Coarse and nanoemulsions are thermodynamically unstable, meaning the free energy of emulsion formation, $\Delta G_{formation}$ is positive [2]. This energy level indicates the requirement for external energy in the form of mechanical stirring or shearing to maintain the stability of the emulsion [1]. Due to the spontaneous trend toward a minimal interfacial area between the dispersed phase and the continuous phase [3], the emulsion will naturally break into separate phases, i.e., a state of lowest free energy. To slow down conversion from the state of a colloidal dispersion to the state of separated phases or increase its kinetic stability, a surfactant is used as an emulsifier to ensure the stability of the emulsions from seconds to years, depending on the application [1]. Microemulsions, consisting of two immiscible liquids and a surfactant, form spontaneously ($\Delta G_{formation} \leq 0$) [2]. Microemulsions are thermodynamically stable because their interfacial tension is lower compared to that of coarse and nanoemulsions, making the interfacial energy comparable to or lower than the entropy of dispersion and

favors the spontaneous formation of microemulsions [1].

Surfactant molecules are amphiphilic in nature, which means that the chemical structure of a surfactant molecule consists of a hydrophilic head and a hydrophobic tail [4], increasing its affinity for adsorbing at the water-fluid interfaces. As a result, the surfactant facilitates the emulsification of two immiscible liquids by decreasing the free energy formation of emulsion ($\Delta G_{formation}$) or reducing the interfacial tension between two immiscible liquids and promotes thermodynamic stability of the system [1]. Due to these properties, surfactants are used in various applications, ranging from improving detergent foaming capacity [5], preventing drops from coalescence in drop-based microfluidic systems [6], emulsifying cosmetic products such as sunscreens [7], and separating minerals in the froth flotation process [8] to altering rock wettability to more water-wet states for enhanced oil recovery [9].

The design or prediction of the surfactant-induced phenomena, such as the adsorption of surfactant molecules at the fluid interface, reduction of surface tension, micelle formation above the critical micelle concentration (CMC), and the appearance of Marangoni stresses is a challenging task. For example, estimating surface tension reduction based on surfactant adsorption on a water-hydrocarbon interface is of great importance for surfactant flooding applications [10]. There are several experimental/laboratory methods to measure the surface tension between water and hydrocarbons in the presence of surfactants, such as the weight of drop method [11], [12], pendant drop [13]–[15], and spinning drop [16]–[18]. These laboratory techniques are costly when factoring in the time spent, the expense of chemicals used to perform a test, and the cost of conducting tests [10]. In addition, experimental measurements of surface tension become difficult at very low surfactant concentrations (below 10 ppm in water) due to a significant increase in equilibration time for a typical measurement [19]. For this case, numerical modelling becomes critically important for the prediction of surface tension reduction. Considering the advances in numerical modelling of surfactant-laden systems, from studying the spontaneous emulsification of

2

the oil-water mixture by surfactant [20] to analyzing the role of surfactant in promoting drop breakup and preventing drop coalescence in turbulent flow [21], numerical simulations have shown great potential to study the system of two immiscible liquids with surfactant.

In the present study, we focus on developing a numerical model for a microemulsion to study the adsorption dynamics of non-ionic soluble surfactants on the interface of two immiscible liquids and to investigate surface tension reduction at low and high surfactant concentrations. Here, a non-ionic soluble surfactant is a type of surfactant that does not have an electric charge [10] and can dissolve in the liquid below the interface [4].

In the following sections, we explore various interface modelling approaches and justify the choice of a suitable interface model and a numerical method for simulating microemulsions. Based on the choice of the interface model, we discuss the existing numerical models of microemulsions in detail and outline the objectives of the present study.

## 1.2   Interface modeling approaches

When we consider modelling of a ternary system comprising two immiscible liquids and a non-ionic soluble surfactant, the initial step involves the selection of a suitable model for investigating the nature of the interface between two immiscible liquids. Subsequently, the second step entails the incorporation of the relevant physics pertaining to the behaviour of the non-ionic soluble surfactant into the chosen model.

Modelling of the interfacial flows is often classified into two categories based on a representation of the interface: sharp interface and diffuse interface approaches. The sharp interface approach assumes the interface between two immiscible fluids as a surface of zero thickness [22]. This means that the fluid properties, such as density, velocity, and viscosity at the interface, are discontinuous. The interface is treated as a free boundary that deforms and moves in time, resulting in a free boundary

problem [23]–[27], where the interfacial boundary condition upon applying the stress balance at the interface relates the jump in stress across the interface to the interfacial curvature [22]. The phase transition from one phase to another is sharp. For example, in a stair-step method [28], the interface between two immiscible fluids is represented as a vertical surface in a computational domain by modelling the interface as a Dirac delta function ($\delta$).

Several numerical methods have been developed using the sharp interface approach to model incompressible immiscible two-phase flows. One group among these methods, such as the front-tracking method [29] and the Marker in Cell method [30] tracks the interface explicitly using Lagrangian markers, while in another group, the interface is represented implicitly by a phase indicator function discretized on an Eulerian mesh, and this function is updated to capture the position of the interface. Examples of these methods include the volume of fluid method [31], the level set method [32], the coupled level set and volume of fluid methods [33], and the ghost fluid method [34].

On the other hand, the formulation of a diffuse interface assumes that the interface has a non-zero thickness, where the fluid properties change continuously. This idea was developed based on gradient theories proposed by Lord Rayleigh [35] and van der Waals [36]. Based on these gradient theories, Kortweg [37] proposed a capillary stress tensor in terms of density and spatial gradients for the diffuse interface model. Later, Cahn and Hilliard [38] showed the use of local mass fraction as an order parameter (i.e., phase indicator function) to represent a smooth change of material properties and physical quantities from one phase to another. The non-zero thickness of the interface is represented by regularizing the Dirac delta function [28] or the nascent delta function. The diffuse interface approach was implemented in the continuum surface force model [39] and the phase field model [40] to study surface tension and internal waves in a near-critical fluid, respectively.

In diffuse interface models, the models based on surface tension forces, such as

4

Brackbill et al.'s model [39] are difficult to implement for topological changes, for example, the breakup of a liquid drop, and these models have instability as well as convergence issues [41]; whereas, the phase field model is based on the fluid free energy and provides numerical stability for the flows with large topological changes [42].

In the phase field model, the physical quantities, such as the chemical potentials and surface tension force, are derived from the free energy functional, representing the thermodynamics of the system. In addition, the continuous transition from one phase to another phase is represented by introducing a phase field variable or an order parameter with distinct constant values in each bulk phase [22]. The local difference in the densities of binary liquids is taken as the order parameter [43]. The dynamics of immiscible two-phase flows are represented by either the Cahn-Hilliard or Allen-Cahn equations based on the Gingburg-Landau-Wilson free energy functional [44]. Due to the lack of conservation of mass in the Allen-Chan equation, the Cahn-Hilliard equation is typically used to study the two-phase flows [44]. Normally, the scale of the interface thickness is observed to be in the range of a few nanometers for multiphase flow problems [45], which makes the implementation of the diffuse interface computationally difficult. For this reason, the interface width is diffused by the length scale of the numerical spatial step size [22].

The difference between the sharp and diffuse interface formulations is shown in Figure 1.1. In the sharp interface, the change in the field variable representing two immiscible fluids from Fluid 1 to Fluid 2 is discontinuous, resembling a step-like change. In contrast, in the diffuse interface, the transition occurs smoothly over a finite thickness, creating an interfacial region.

Sharp interface models have shown the potential to simulate immiscible two-phase flows. The study conducted by Shaikh et al. [46] shows that the sharp interface-based level set method significantly reduces spurious velocity near the interface compared to the diffuse interface-based level set method, thus, leading to accurate results for capillary-induced flow. However, there are some limitations of the sharp interface
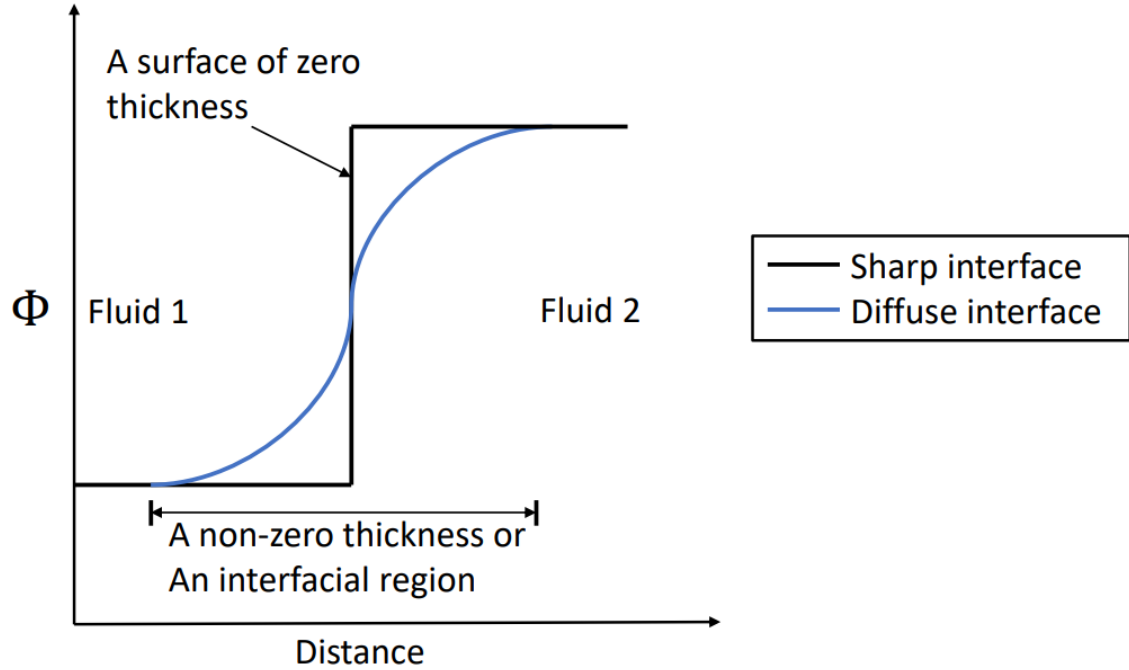
Figure 1.1: Change of the field variable representing two immiscible fluids for sharp and diffuse interface methods.

models:

- The assumption of a surface of zero thickness is not applicable for a near-critical fluid [22] because the interface thickness diverges at a critical point [47].

- The influence of the interface thickness on the bulk fluid needs to be accounted for when the length scale of any bulk fluid at two sides of the interface is comparable to the realistic interface thickness [22], [48].

- The numerical methods based on the free boundary problem are difficult to implement for interfacial flows where the free boundary shape or the sharp interface becomes self-intersecting or complicated [22].

- Sharp interface models are prone to numerical instability for the flows with large topological changes such as the drop breakup and coalescence [42], where the length scale of these physical mechanisms is comparable to the interface thickness [22].

- The interface reconstruction processes in the sharp interface-based models are complex [49] and computationally expensive.

Unlike sharp interface models, the description of a narrow interface thickness allows the phase field model to study the near-critical fluid [40] and the topological changes of the interface, such as drop coalescence [50]. Furthermore, the free energy governed diffuse interface model/phase field model provides a physical basis [42]. The interface dynamics captured by the evolution of the phase field variable makes the computations of the phase field model easier compared to the sharp interface models [49]. Therefore, we will adopt the phase field model for the investigation of surfactant-laden systems.

In the next section, we will explain the choice of a numerical method to simulate the binary fluid-soluble surfactant system.

## 1.3 Choice of a numerical method to solve governing equations for multiphase flows

For multiphase flows, the governing equations include the continuity equation, the momentum equation, and any additional convention or convection-diffusion equations, such as the Cahn-Hilliard equations for the present study.

The set of governing equations can be solved by two methods: the macroscopic and particle-based discrete methods. The macroscopic methods involve the conventional computational fluid dynamics (CFD) methods such as finite difference, finite volume, and finite element methods. In these methods, the governing equations are directly discretized and solved on a finite number of nodes, volumes, or elements, respectively, that make up a physical space or domain of interest for numerical simulations [51]. There are several examples of the use of these methods for binary fluid-surfactant systems, for instance, the finite difference-based front tracking method [52] to study axisymmetric flow with soluble surfactants, finite volume [53], [54] and finite element methods [55] to solve surfactant transport equations. However, these methods fall

short when applied to model complex fluid phenomena involving multiphase flows such as drop formation, breakup, and coalescence [56], where the characteristic length scale of the problem is of the same order of magnitude as the interface thickness. In addition, the continuum assumption of these methods becomes inadequate for studying the physical phenomena occurring at micro- and meso-scales [57].

On the other hand, particle-based discrete methods such as molecular dynamics (MD), lattice gas models, dissipative particle dynamics (DPD), direct simulation Monte Carlo (DSMC), and lattice Boltzmann method (LBM) do not solve the governing equations directly, but they represent the fluid as particles, which themselves can represent atoms, molecules, collections or distributions of molecules, or portions of the macroscopic fluid [51]. Contrary to the macroscopic view of the conventional CFD methods, the microscopic or mesoscopic view of the particle-based discrete methods benefits them in handling physical mechanisms involving large interfacial topological changes. However, the higher computational cost involved in MD, DPD, and DSMC simulations and the problem of statistical noise in lattice gas models [51] make these methods an impractical choice for solving the governing equations.

Unlike other particle-based discrete methods, the LBM is a mesoscopic method that represents the entire fluid using the collection of particles and tracks the particle distribution function [51] instead of the particles themselves. The particle distribution function is governed by the discretized Boltzmann equation or lattice Boltzmann equation. Considering the fact that the LBM is developed from lattice gas models, the LBM can recover hydrodynamic behaviour at the macroscopic scale by preserving microscopic kinetic principles [58]. For example, macroscopic properties such as density and velocity can be obtained from the moments of the particle distribution function. In addition, the governing equations can be recovered from the lattice Boltzmann equations formulated for the problem of interest by the Chapman-Enskog analysis [51]. The LBM method is described in detail in Section 2.7.

The LBM is comparatively better than macroscopic methods in dealing with com-

plex geometries for multiphase flows involving interfacial topological changes [59]. In addition, the linear convective term in the lattice Boltzmann equation makes its implementation easier, in contrast to the non-linear convective terms of Navier-Stokes equations, which are difficult to discretize [57]. The mesoscopic characteristics of the LBM allow it to eliminate the problem of statistical noise that existed in the lattice gas models [51]. Furthermore, it makes the lattice Boltzmann algorithm simple and amenable for parallelization compared to other particle-based discrete methods [51], [60]. The capability of the LBM to incorporate the microscopic physics (i.e., intermolecular interactions) without surrendering the computational efficiency of the macroscopic methods [56] makes it a promising candidate for simulating multiphase flows. At the same time, the LBM is not well suited for certain applications, such as simulating strong compressible flows. It is memory-intensive as significant memory is required to store and update the particle populations. Moreover, it suffers from spurious currents near fluid-fluid interfaces because of its lattice-based formulation [51].

In conclusion, it can be said that LBM is not suitable for all possible applications, but it has matured into a powerful and efficient alternative to other methods in recent years, particularly for multiphase flow simulations, for instance, the study of phase separation in non-ideal two-component fluids [61], the investigation of incompressible two-phase flows with large density differences [62], [63], the emulsion drop deformation and breakup study [64], and the simulation of binary fluid-soluble surfactant systems [20], [42], [60], [65], [66]. Therefore, we select the LBM for the present study of the ternary system consisting of two immiscible liquids with soluble surfactants.

In the next section, we will discuss a detailed literature review of the existing phase field models for microemulsions.

## 1.4 Literature review on the modeling of microemulsions

Before we delve into the discussion of existing phase field models for the system involving two immiscible liquids with soluble surfactants, it is important to highlight the advancements made in sharp interface models for simulating the same system.

For the sharp interface model, Stone and Leal [67] formulated the equation of state (EOS) to describe the effect of surfactant on the reduction of surface tension. Later, Milliken and Leal [68] coupled fluid mechanics and surfactant mass transfer to study the effect of surfactant solubility on drop breakup and deformation using the boundary integral method based on a sharp interface model. Following the work of Stone and Leal [67] and Milliken and Leal [68], different numerical methods such as front tracking methods [52], [69], [70], ghost-cell immersed boundary method [71], [72], volume of fluid method [73], and the hybrid numerical method combining boundary integral method with a fixed grid solution of the bulk surfactant equation [74] have been developed in the sharp interface framework to study the topological changes of the interface in the presence of surfactants for two-dimensional and three-dimensional multiphase flows. The recent progress of sharp interface methods shows that it has overcome some of the limitations mentioned in Section 1.2 such as the modelling of interface topological changes. Still, the phase field models are more physical than the sharp interface models, for example, the interface is artificially reconstructed in the sharp interface model; whereas, the interface evolves according to the chemical potential gradients derived from the fluid's free energy functional in the phase field model [65]. Second, to account for the mass transfer of a soluble surfactant between the interface and the bulk fluids, the sharp interface models require an external boundary condition that cannot arise uniquely from the model itself [42], [75].

In the phase field model, Laradji et al. [43] modified the Gingburg-Landau free energy functional describing the Cahn-Hilliard theory of an immiscible binary fluid

mixture [38] by incorporating the additional free energy terms associated with the physics of soluble surfactant. These additional terms in the free energy functional represent the adsorption of the surfactant at the binary fluid interface, the solubility of the surfactant in bulk phases, the diffusion of the surfactant, and the self-interaction strength between surfactant molecules. In addition to the Cahn-Hilliard equation for the order parameter representing two immiscible liquids, another Cahn-Hilliard equation for the soluble surfactant was introduced to account for the surfactant mass transfer. A local surfactant concentration is used to represent the soluble surfactant [43].

Later, Theissen and Gompper [20], Teramoto and Yonezawa [76], van der Sman and van der Graaf [65], and Teng et al. [77] proposed notable modifications to the free energy functional terms proposed by Laradji et al. [43] to study the surfactant effects on the spontaneous emulsification, drop growth dynamics, and adsorption dynamics. Li and Kim [78] compared these four models and modified the surfactant term that describes the diffusion of the surfactant, which allows a larger time step compared to these four models with severe time step constraints due to nonlinear coupling of the order parameters. During the comparison of these four models along with the Li and Kim [78]'s model for the case of a planar interface between two immiscible fluids in the presence of surfactant, it was found that the models suggested by Theissen and Gompper [20], Teramoto and Yonezawa [76], and Li and Kim [78] suffer from negative values of the surfactant volume fraction during the calculation of the equilibrium profile of surfactant for a certain set of numerical parameters that is unphysical and clearly outside of the range of surfactant volume fraction (i.e., $[0, 1]$). Similarly, the model of van der Sman and van der Graaf [65] and Teng et al. [77] also suffer from unphysical oscillations in the equilibrium profile of the surfactant volume fraction. However, the logarithmic free energy term inducing a Fickian-type diffusion for the surfactant in the van der Sman and van der Graaf [65]'s model restricts the value of surfactant volume fraction to be in the range $[0, 1]$ and ensures the physical results

for the surfactant profile.

The phase field model proposed by van der Sman and van der Graaf [65] is the most widely adopted model for binary fluid-surfactant systems. The free energy functional of this model is partly formulated based on the free-energy-based, sharp interface models of Diamant and Andelman [75] and Diamant et al. [79]. Specifically, in these models, the Dirac delta function used in the free energy term to account for surfactant adsorption at the interface was modified by regularizing it as a squared gradient of the order parameter representing two immiscible liquids for the phase field model. This allows the model of van der Sman and van der Graaf [65] to possess a realistic Langmuir adsorption isotherm. In addition, this model captures the expected relation between surface tension reduction and surfactant concentration. It also couples the surfactant adsorption with hydrodynamics to study the correct drop dynamics in the presence of surfactant.

Several modifications have been made to the van der Sman and van der Graaf [65]'s model, improving its stability and extending its capability to capture the adsorption dynamics for high surfactant concentrations. Liu and Zhang [42] extended this model to account for the Frumkin isotherm and different surfactant solubility in the bulk phases. In addition, they demonstrated the capability of their phase field model by investigating the drop dynamics with large topological changes in a shear flow. The model of Liu and Zhang [42] exhibits both Langmuir and Frumkin isotherms, which are the well-developed adsorption isotherms for non-ionic surfactants under the thermodynamic equilibrium state with a bulk surfactant concentration below CMC. However, their model works only for low concentrations of surfactants.

Yun et al. [80] investigated the van der Sman and van der Graaf [65]'s model for high surfactant concentrations. They observed that the equilibrium profile of the binary fluid becomes sharp, indicating the decrease of the interface thickness with an increase in the surfactant load. This phenomenon occurs due to the presence of surfactant in the chemical potential of the binary fluid system and the effect imposed

by the regularized Dirac delta function/nascent delta function. For instance, as the surfactant load increases, the squared gradient representation suggested in the van der Sman and van der Graaf [65]'s model mathematically leads to the decrease of the interface thickness. To overcome this problem, they suggested removing the surfactant terms from the chemical potential of the binary fluid system to keep the thickness constant regardless of the surfactant concentration. This modification makes the equilibrium profile of the binary fluid independent of the surfactant concentration. We categorize this description of the interface thickness as non-variational, where the interface thickness remains unaffected by the surfactant load.

Engblom et al. [81] performed the stability analysis of the van der Sman and van der Graaf [65]'s model considering the "frozen" coefficient formulation. It was reported that the use of the squared-gradient nascent delta function or squared-gradient nonlocal coupling between the surfactant and binary fluid makes the model mathematically ill-posed under a large set of physically relevant parameters. In addition, they suggested that the natural requirement that the interface sharpness be independent of the surfactant loading is sacrificed to improve the stability of the phase field model for binary fluid-surfactant systems. To improve the well-posedness of the squared-gradient based phase field models, they proposed three different models namely Model 1 - where a complete logarithmic free energy term is considered instead of the partial one used in the model of van der Sman and van der Graaf [65], Model 2 - where a square hyperbolic secant function in terms of the order parameter representing the binary fluid is suggested as the nascent delta function, and Model 3 - where a quartic hyperbolic secant function in terms of the order parameter representing the binary fluid is suggested as the nascent delta function. Note that the nascent delta functions used in Model 2 and Model 3 are the gradient-free representations of the nascent delta function. In addition, the authors did not neglect the presence of surfactant terms from the chemical potential of binary fluid. Hence, we define this description of the thickness of the interface as variational, where the

13

interface thickness depends on the concentration of the surfactant. They compared these models and determined that Model 1 does not theoretically possess a natural adsorption isotherm. Model 2 and Model 3 are stable and possess realistic adsorption isotherms. The results of Model 2 match the analytical predictions, but it produces slightly more diffuse results compared to Model 3. The model 3 has been shown to be the most reliable among these three models. From hereafter, whenever we mention the gradient-free nascent delta function, it means that we refer to the quartic hyperbolic secant function of Model 3 proposed by Engblom et al. [81].

Toth and Kvamme [82] observed that the gradient-free nascent delta function appears to increase the thickness of the interface with increasing surfactant concentration. They combined the squared-gradient and gradient-free representations of the nascent delta function to avoid interface-related problems, such as sharpening and broadening of the interface thickness at high concentrations of surfactant. Consequently, this formulation prompted the phenomenon of no phase separation, i.e., perfect miscibility at the critical surfactant concentration, the concentration at which the bulk phase order parameter representing the binary fluid becomes zero. The concept of a critical surfactant concentration can be thought of as similar to that of the theory of liquid-vapor critical point. Van der Sman and Meinders [83] also analyzed the squared-gradient and gradient-free surfactant couplings and concluded that the squared-gradient coupling leads to numerical instability for high surfactant concentrations. Furthermore, they questioned the physical meaning of the interface broadening when gradient-free surfactant coupling is used.

Shi et al. [66] adopted the strategy of Yun et al. [80] to resolve the interface sharpening phenomenon that occurred when using the squared-gradient representation of the surfactant coupling. Similarly, Soligo et al. [21] and Zong et al. [60] have successfully kept the thickness of the interface stable and addressed the Marangoni effect on the dynamics of the drop following the suggestions of Engblom et al. [81] and Yun et al. [80].

From the literature review, it is clear that the definition of interface thickness changes in the phase field model when investigating the binary fluid-surfactant systems at high surfactant concentrations. For example, one group of researchers including Shi et al. [66] has followed the non-variational description of the interface thickness, but this type of models still suffers from numerical instability at high surfactant concentrations and cannot attain the surfactant volume fraction at the interface near 1; whereas, another group of researchers such as Toth and Kvamme [82] have resolved interface-related problems by adopting the variational description of the interface thickness. Similarly to the former group of researchers, the interface thickness becomes unstable when the surfactant volume fraction converges to 1 at the interface [84].

Both descriptions of the interface thickness resolve the interface-related problems and keep the interface thickness stable and constant to some extent for high surfactant concentrations. These descriptions of the interface thickness are formulated because the change in the interface thickness is unphysical from macroscopic point of view. Moreover, the interface thickness should remain constant since the chemical structure of the surfactant molecule is not considered in the free energy functional. This implies that the phase field model is limited to the general non-ionic soluble surfactants. Considering these observations, we would like to pose three questions:

- From the variational and non-variational descriptions of the interface thickness, which one to use to model surfactant-laden systems and obtain physically realistic results that capture experimental observations?

- How can we promote the stability of the model for high surfactant concentrations and avoid the occurrence of perfect miscibility?

- How can we extend the potential of the phase field model to account for the effect of different non-ionic soluble surfactants on surface tension reduction?

In the next section, we will outline the objectives of the present study along with a summary of the subsequent chapters.

## 1.5 Objectives

By addressing the three questions mentioned at the end of Section 1.4, our goal is to propose a phase field model that has a variational description of the interface thickness in a free-energy-based lattice Boltzmann framework that remains numerically stable and provides accurate results at high surfactant concentrations, i.e., when the local surfactant concentration at the interface approaches the maximum allowed value of one, allows controlled reduction of surface tension based on the strength of the nonlocal surfactant coupling or nascent delta function, and can replicate the effect of different surfactants on the reduction of surface tension.

In Chapter 2, we introduce the macroscopic governing equations for the ternary system of two immiscible liquids with non-ionic soluble surfactants. In addition, we provide a derivation of the general phase field model, the phase field models proposed by van der Sman and van der Graaf [65], Engblom et al. [81], Shi et al. [66], and the proposed phase field model followed by the analytical solutions of these models for a benchmark case of the planar interface, the brief description of the surface tension, and the formulation of the free-energy lattice Boltzmann method for solving the governing equations.

In Chapter 3, we validate the ability of the proposed model to simulate two benchmark cases named a planar interface and a spherical drop equilibration. The planar interface between two immiscible liquids in the presence of surfactant was investigated for low as well as high surfactant loads. In addition, the results of the proposed model were compared with the models of van der Sman and van der Graaf [65], Engblom et al. [81], and Shi et al. [66] at high surfactant concentrations. Similarly, the proposed model was applied to study the adsorption dynamics of soluble surfactant over the spherical drop interface for low and high surfactant concentrations. Furthermore, we

introduce the methodology to demonstrate the effect of different surfactants on surface tension reduction using the strength of nonlocal coupling between the surfactant and binary liquids. The simulation parameters were also explored to obtain numerically stable simulations for different strengths of the nonlocal surfactant couplings.

In Chapter 4, we summarize the findings of the present study and discuss the scope of future work. In addition, there are two appendices describing the Chapman-Enskog expansions of the lattice Boltzmann equations of particle populations to recover governing equations and the formulation of the chosen collision operator for the particle population representing the density of the binary fluid-surfactant system.

# Chapter 2

# Methodology

In this chapter, the governing equations for an incompressible multiphase system consisting of two immiscible liquids and a non-ionic soluble surfactant are introduced. It is followed by the formulation of the free energy functional describing the thermodynamics of the ternary system. From this, we derive the general model equations for the chemical potentials of binary fluid and the soluble surfactant, as well as the thermodynamic pressure tensor. The equations of the general phase field model are used to recover the equations of the phase field model proposed by van der Sman and van der Graaf [65], Engblom et al. [81], Shi et al. [66]. Following the discussion of these models, we propose the equations of our phase field model. For all models, analytical equations of binary fluid and the soluble surfactant are developed for the case of a planar interface between two immiscible fluids contaminated by a non-ionic soluble surfactant. The EOS is formulated to account for the effect of the soluble surfactant on surface tension reduction in the phase field model. Then, the procedure for solving the governing equations of the ternary system in the free-energy lattice Boltzmann framework is presented.

## 2.1   Governing equations

The system of two immiscible liquids and a non-ionic soluble surfactant is represented by the order parameter $\phi$ that describes the immiscible liquids and the order param-

eter $\psi$ that captures the concentration of soluble surfactant. The parameter $\phi$ is the difference between the densities of two immiscible liquids [20] and the parameter $\psi$ is the volume fraction of the surfactant [65].

Four equations govern the hydrodynamics of the surfactant-laden system: the continuity equation, the momentum equation, and two Cahn-Hilliard equations describing the transport of $\phi$ and $\psi$:

$$\partial_t \rho + \partial_\alpha (\rho u_\alpha) = 0 \tag{2.1a}$$

$$\partial_t (\rho u_\alpha) + \partial_\beta (\rho u_\alpha u_\beta) = -\partial_\beta P_{\alpha\beta}^{th} + \partial_\beta \nu (\rho \partial_\alpha u_\beta + \rho \partial_\beta u_\alpha) \tag{2.1b}$$

$$\partial_t \phi + \partial_\alpha (\phi u_\alpha) = M_\phi \partial_{\alpha\alpha}^2 \mu_\phi \tag{2.1c}$$

$$\partial_t \psi + \partial_\alpha (\psi u_\alpha) = M_\psi \partial_{\alpha\alpha}^2 \mu_\psi \tag{2.1d}$$

The equations are written in the Einstein notation, where $\alpha$ and $\beta$ represent the spatial coordinates $x$, $y$, and $z$; $t$ stands for time; $\rho$ and $\nu$ are the fluid density and kinematic viscosity, respectively; $u_\alpha$ is the fluid velocity; $M_\phi$ and $M_\psi$ represent the mobility of $\phi$ and $\psi$, respectively; $P_{\alpha\beta}^{th}$ is the thermodynamic pressure tensor; $\mu_\phi$ and $\mu_\psi$ are the chemical potentials for $\phi$ and $\psi$, respectively.

## 2.2 Free energy functional

The Ginzburg-Landau free energy functional, $F_{total}$, describing the thermodynamics of the ternary system, is represented as follows [42]:

$$F_{total}(\rho, \phi, \psi) = \int \mathcal{F}_{total} dV = \int \left[ \mathcal{F}_\phi + \mathcal{F}_\psi + \mathcal{F}_0 + \mathcal{F}_{ex} - E\phi\psi + \rho T \ln\rho \right] dV \tag{2.2}$$

where

- $\mathcal{F}_\phi$ is the Ginzburg-Landau free energy density functional describing the Cahn-Hilliard theory of a binary fluid mixture [38]. It is defined as follows:

$$\mathcal{F}_\phi = \frac{A}{2}\phi^2 + \frac{B}{4}\phi^4 + \frac{\kappa_{int}}{2}(\partial_\beta \phi)^2 \tag{2.3}$$

The first two terms represent the double-well potential with two minima for two pure bulk phases: $\phi_0 = \pm\sqrt{-A/B}$. Here, $A$ is negative and $\kappa_{int}$ & $B$ are positive constants. Assuming that $-A = B$ gives $\phi_0 = \pm 1$, where $\phi_0 = +1$ and $\phi_0 = -1$ refer to the dispersed and continuous phases, respectively. From hereafter, we assume $-A = B$. The last term accounts for the free energy density excess of the interfacial region [38] and is interpreted as the interfacial free energy density between liquids due to the diffuse interface approximation.

- $\mathcal{F}_\psi$ is the free energy density associated with the surfactant expressed as follows:

$$\mathcal{F}_\psi = k_B T[\psi\ln(\psi) + (1-\psi)\ln(1-\psi)] - \frac{C}{2}\psi^2 \qquad (2.4)$$

The term in square brackets represents the ideal entropy of mixing of surfactant with the immiscible binary fluid mixture [65]. This term restricts the value of $\psi$ to be in the $[0, 1]$ range. The coefficient $k_B T$ represents the thermal energy. The second term accounts for the free energy density related to the self-interaction strength between neighbouring surfactant molecules, $C$ [75].

- $\mathcal{F}_0$ is the free energy density contribution due to the adsorption of the surfactant at the interface. $\mathcal{F}_0$ suggested by Toth and Kvamme [82] is adopted, which is the combination of the squared-gradient nascent delta function, $\hat{\delta}_{SQ}(x)$, proposed in [65] and the gradient-free nascent delta function, $\hat{\delta}_{E3}(x)$, (Model 3 in ref. [81]). It reads as follows:

$$\mathcal{F}_0 = -\frac{D}{2}\psi\left[\lambda_1\hat{\delta}_{SQ}(x) + \lambda_2\hat{\delta}_{E3}(x)\right] \qquad (2.5)$$

Here, $\hat{\delta}(x)$, is the nascent delta function or the approximation of the Dirac delta function, $\delta(x)$, used in the sharp interface models suggested by Diamant and Andelman [75] and Diamant et al. [79]; $\lambda_1$ and $\lambda_2$ are coefficients incorporating the different combinations of $\hat{\delta}(x)$. The squared-gradient and the gradient-free nascent delta functions are defined as follows:

$$\hat{\delta}_{SQ}(x) = (\partial_\beta\phi)^2 \qquad \hat{\delta}_{E3}(x) = \frac{1}{\xi_0^2}\frac{(\phi_0^2 - \phi^2)^2}{\phi_0^2} \qquad (2.6)$$

where the interface thickness of the pure system [85] reads:

$$\xi_0 = \sqrt{\frac{-2\kappa_{int}}{A}} \tag{2.7}$$

After substituting Eqs. (2.6) in Eq. 2.5, assuming $D = \kappa_{int}$, and taking $\phi_0^2 = 1$, the simplified form of $\mathcal{F}_0$ is obtained:

$$\mathcal{F}_0 = -\psi \left[ \lambda_1 \left( \frac{D}{2} (\partial_\beta \phi)^2 \right) - \lambda_2 \left( \frac{A}{4} (1 - \phi^2)^2 \right) \right] \tag{2.8}$$

- The term $\mathcal{F}_{ex}$ penalizes the presence of free surfactant in bulk phases [81]. The expression for $\mathcal{F}_{ex}$ proposed by Theissen and Gompper [20] is used in the present study:

$$\mathcal{F}_{ex} = \frac{W}{2} \psi \phi^2 \tag{2.9}$$

Furthermore, the solubility of surfactant in the bulk phases can be controlled by dimensionless number $Ex$:

$$Ex = \frac{D}{W\xi_0^2} \tag{2.10}$$

We set the value of $Ex$ and then calculate the corresponding value of $W$.

- The term $-E\phi\psi$ accounts for the different solubility of the surfactant in the bulk phases [42] and the parameter $E$ describes the difference in the solubility strength of the surfactant in two bulk phases.

- The term $\rho T \ln \rho$ ensures the incompressibility of the fluid in the lattice Boltzmann (LB) algorithm and $T = \frac{1}{3}$ is recommended to reduce compressibility errors within the acceptable numerical tolerances [85]. This term does not influence the phase behaviour. [20].

## 2.3 Derivation of chemical potentials and thermodynamic pressure tensor

The key quantities, $P_{\alpha\beta}^{th}$, $\mu_\phi$, and $\mu_\psi$ are derived from the total free energy density functional of the binary fluid-surfactant system.

The chemical potentials $\mu_\phi$ and $\mu_\psi$ are derived by taking the functional derivative of the total free energy density functional, $\mathcal{F}_{total}$, the integrand of Eq. (2.2), with respect to $\phi$ and $\psi$ as follows:

$$\mu_\phi = \frac{\delta \mathcal{F}_{total}}{\delta \phi} = A(\phi - \phi^3)(1 - \lambda_2 \psi) - (\kappa_{int} - D\lambda_1 \psi)\partial^2_{\beta\beta}\phi + D\lambda_1(\partial_\beta \phi)(\partial_\beta \psi)$$
$$+ W\phi\psi - E\psi \tag{2.11a}$$

$$\mu_\psi = \frac{\delta \mathcal{F}_{total}}{\delta \psi} = k_B T \ln\left(\frac{\psi}{1 - \psi}\right) - C\psi - \frac{D}{2}\lambda_1(\partial_\beta \phi)^2 + \frac{A}{4}\lambda_2(1 - \phi^2)^2 + \frac{W}{2}\phi^2 - E\phi \tag{2.11b}$$

In addition to the chemical potentials of the order parameters, the expression for the thermodynamic pressure tensor $P^{th}_{\alpha\beta}$ is necessary to solve the system (2.1). The challenge is that there is no explicit expression for $P^{th}_{\alpha\beta}$ that follows directly from the total free energy density functional. However, the divergence of this tensor must satisfy the mechanical equilibrium [20] represented by the Gibbs-Duhem relation at a constant temperature:

$$\partial_\beta P^{th}_{\alpha\beta} = [\rho(\partial_\beta \mu_\rho) + \phi(\partial_\beta \mu_\phi) + \psi(\partial_\beta \mu_\psi)]\delta_{\alpha\beta} \tag{2.12}$$

Following the explanation of the meaning of $\partial_\beta P^{th}_{\alpha\beta}$ given by Kendon et al. [85] for the pure system, it can be said that the divergence of thermodynamic pressure tensor for the surfactant-laden systems represents the thermodynamic force density acting at each point in the binary fluid-surfactant mixture which is caused by the non-uniform compositions of binary liquids and surfactant in terms of excess chemical potential gradients. After inserting Eq. (2.11a) and Eq. (2.11b) in Eq. (2.12), the expression

for $\partial_\beta P_{\alpha\beta}^{th}$ can be simplified as follows:

$$\partial_\beta P_{\alpha\beta}^{th} = [\rho(\partial_\beta \mu_\rho) + \phi(\partial_\beta \mu_\phi) + \psi(\partial_\beta \mu_\psi)]\delta_{\alpha\beta}$$

$$= \phi(\partial_\alpha \mu_\phi) + \psi(\partial_\alpha \mu_\psi)$$

$$= \phi\Bigg(A[(\phi - \phi^3)(-\lambda_2 \partial_\alpha \psi) + (\partial_\alpha \phi - 3\phi^2 \partial_\alpha \phi)(1 - \lambda_2 \psi)] - \kappa_{int}\partial_\alpha(\partial_{\beta\beta}^2 \phi)$$

$$+ D\lambda_1 \psi \partial_\alpha(\partial_{\beta\beta}^2 \phi) + D\lambda_1(\partial_\alpha \psi)\partial_{\beta\beta}^2 \phi + D\lambda_1 \partial_\alpha(\partial_\beta \phi)(\partial_\beta \psi)$$

$$+ D\lambda_1 \partial_\alpha(\partial_\beta \psi)(\partial_\beta \phi) + W(\partial_\alpha \phi)\psi + W\phi(\partial_\alpha \psi) - E(\partial_\alpha \psi)\Bigg)$$

$$+ \psi\Bigg((\partial_\alpha \psi)\frac{k_B T}{\psi(1 - \psi)} - C(\partial_\alpha \psi) - D\lambda_1(\partial_\beta \phi)\partial_\alpha(\partial_\beta \phi) - A\lambda_2 \phi(1 - \phi^2)(\partial_\alpha \phi)$$

$$+ W\phi(\partial_\alpha \phi) - E(\partial_\alpha \phi)\Bigg)$$

$$= A\phi(\partial_\alpha \phi) - 3A\phi^3(\partial_\alpha \phi) - 2A\lambda_2 \psi(\phi - 2\phi^3)(\partial_\alpha \phi) - A\lambda_2 \phi(\phi - \phi^3)(\partial_\alpha \psi)$$

$$- \kappa_{int}\phi\partial_\alpha(\partial_{\beta\beta}^2 \phi) + D\lambda_1 \phi\psi\partial_\alpha(\partial_{\beta\beta}^2 \phi) + D\lambda_1 \phi(\partial_\alpha \psi)\partial_{\beta\beta}^2 \phi + D\lambda_1 \phi\partial_\alpha(\partial_\beta \phi)(\partial_\beta \psi)$$

$$+ D\lambda_1 \phi\partial_\alpha(\partial_\beta \psi)(\partial_\beta \phi) + W\phi\psi(\partial_\alpha \phi) + W\phi^2(\partial_\alpha \psi) - E\phi(\partial_\alpha \psi)$$

$$+ (\partial_\alpha \psi)\frac{k_B T}{(1 - \psi)} - C\psi(\partial_\alpha \psi) - D\lambda_1 \psi(\partial_\beta \phi)\partial_\alpha(\partial_\beta \phi) + W\phi\psi(\partial_\alpha \phi)$$

$$- E\psi(\partial_\alpha \phi) \qquad (2.13)$$

To develop an expression for $P_{\alpha\beta}^{th}$, we will follow the suggestion of Theissen and Gompper [20] and decompose this tensor into the isotropic and non-isotropic parts as follows:

$$P_{\alpha\beta}^{th} = p\delta_{\alpha\beta} + P_{\alpha\beta}^{chem} \qquad (2.14)$$

Taking the divergence of Eq. (2.14) gives:

$$\partial_\beta P_{\alpha\beta}^{th} = \partial_\beta(p\delta_{\alpha\beta}) + \partial_\beta P_{\alpha\beta}^{chem} \qquad (2.15)$$

The thermodynamic pressure $p$ is the scalar part of the thermodynamic pressure tensor that can be derived using the following thermodynamic relation [20]:

$$p = \rho\mu_\rho + \phi\mu_\phi + \psi\mu_\psi - \mathcal{F}_{total} \qquad (2.16)$$

Using Eq. (2.11a), Eq. (2.11b), and Eq. (2.2), the simplified expression for $p$ can be

23

written as:

$$p = \rho T + \frac{A}{2}\phi^2 - \frac{3A}{4}\phi^4 - A\lambda_2\psi(\phi^2 - \phi^4) - \kappa_{int}\phi(\partial^2_{\beta\beta}\phi) + D\lambda_1\phi\psi(\partial^2_{\beta\beta}\phi)$$
$$+ D\lambda_1\phi(\partial_\beta\phi)(\partial_\beta\psi) - k_BT\ln(1 - \psi) - \frac{C}{2}\psi^2 - \frac{\kappa_{int}}{2}(\partial_\beta\phi)^2 + W\psi\phi^2 - E\phi\psi \quad (2.17)$$

From Eq. (2.17), the divergence of $p\delta_{\alpha\beta}$ can be obtained as follows:

$$\partial_\beta(p\delta_{\alpha\beta}) = A\phi(\partial_\alpha\phi) - 3A\phi^3(\partial_\alpha\phi) - 2A\lambda_2\psi(\phi - 2\phi^3)(\partial_\alpha\phi) - A\lambda_2\phi(\phi - \phi^3)(\partial_\alpha\psi)$$
$$- \kappa_{int}(\partial_\alpha\phi)\partial^2_{\beta\beta}\phi - \kappa_{int}\phi\partial_\alpha(\partial^2_{\beta\beta}\phi) + D\lambda_1(\partial_\alpha\phi)\psi\partial^2_{\beta\beta}\phi + D\lambda_1\phi(\partial_\alpha\psi)\partial^2_{\beta\beta}\phi$$
$$+ D\lambda_1\phi\psi\partial_\alpha(\partial^2_{\beta\beta}\phi) + D\lambda_1(\partial_\alpha\phi)(\partial_\beta\phi)(\partial_\beta\psi) + D\lambda_1\phi\partial_\alpha(\partial_\beta\phi)(\partial_\beta\psi)$$
$$+ D\lambda_1\phi(\partial_\beta\phi)\partial_\alpha(\partial_\beta\psi) + (\partial_\alpha\psi)\frac{k_BT}{(1 - \psi)} - C\psi(\partial_\alpha\psi) - \kappa_{int}(\partial_\beta\phi)\partial_\alpha(\partial_\beta\phi)$$
$$+ W(\partial_\alpha\psi)\phi^2 + 2W\phi(\partial_\alpha\phi)\psi - E(\partial_\alpha\phi)\psi - E\phi(\partial_\alpha\psi) \quad (2.18)$$

Now we have the expression for the divergence of $P^{th}_{\alpha\beta}$ which is Eq. (2.13) and we know the expression for $\partial_\beta(p\delta_{\alpha\beta})$ which is Eq. (2.18). What remains is the unknown expression for $\partial_\beta P^{chem}_{\alpha\beta}$. We will adopt the similar form of $P^{chem}_{\alpha\beta}$ that has been used in references [65], [42], and [66] which satisfies the Gibbs-Duhem equation (2.12) and reads as follows:

$$P^{chem}_{\alpha\beta} = (\kappa_{int} - D\lambda_1\psi)(\partial_\alpha\phi)(\partial_\beta\phi) \quad (2.19)$$

The divergence of Eq. (2.19) gives:

$$\partial_\beta P^{chem}_{\alpha\beta} = \partial_\beta[(\kappa_{int} - D\lambda_1\psi)(\partial_\alpha\phi)(\partial_\beta\phi)]$$
$$= \kappa_{int}\partial_\beta(\partial_\alpha\phi)(\partial_\beta\phi) + \kappa_{int}(\partial_\alpha\phi)\partial^2_{\beta\beta}\phi - D\lambda_1(\partial_\beta\psi)(\partial_\alpha\phi)(\partial_\beta\phi)$$
$$- D\lambda_1\psi\partial_\beta(\partial_\alpha\phi)(\partial_\beta\phi) - D\lambda_1\psi(\partial_\alpha\phi)\partial^2_{\beta\beta}\phi \quad (2.20)$$

Combining Eq. (2.18) and Eq. (2.20) gives us exact terms as in Eq. (2.13) confirming the correctness of the choice to represent the thermodynamic pressure tensor $P^{th}_{\alpha\beta}$.

We will call this derived set of equations *mathematically consistent*, meaning that the expressions for the chemical potentials and the divergence of the thermodynamic

pressure tensor are obtained directly from the free energy functional, the divergence of the pressure tensor satisfies the Gibbs-Duhem relation, and no terms are neglected.

The last quantity that we need is the expression for the bulk pressure in the phases. It can be obtained from Eq. (2.17) assuming there are no gradients of the order parameters:

$$p_b = \rho T + \frac{A}{2}\phi^2 - \frac{3A}{4}\phi^4 - k_B T \ln(1-\psi) - \frac{C}{2}\psi^2 - A\lambda_2\psi(\phi^2 - \phi^4) + W\psi\phi^2 - E\phi\psi \tag{2.21}$$

We will estimate the Laplace pressure using Eq. (2.21).

The equations (2.11a), (2.11b), (2.17), (2.19), and (2.21) represent the key equations of the general model to simulate a system of two immiscible liquids with soluble non-ionic surfactant.

## 2.4    Variations of the free energy models

In this section, we describe four phase field models that capture the behaviour of binary fluid systems with soluble surfactant: the squared-gradient model [65], the gradient-free model [81], the non-variational squared-gradient model [66] and the proposed model.

From the general model described in Section 2.1, we can recover the equations of chemical potentials, the scalar part of the thermodynamic pressure tensor, the chemical pressure tensor, and the bulk pressure that represent the models developed by van der Sman and van der Graaf [65], Engblom et al. [81], and Shi et al. [66].

**Case A: Squared-gradient model** [65]

Setting $\lambda_1 = 1$ & $\lambda_2 = 0$ in equations (2.8) – (2.21) gives the model equations based on the squared-gradient approximation of $\hat{\delta}(x)$ in $\mathcal{F}_0$ proposed by van der Sman and

van der Graaf [65]. Then, the model equations read:

$$\mu_\phi = A(\phi - \phi^3) - (\kappa_{int} - D\psi)\partial^2_{\beta\beta}\phi + D(\partial_\beta\phi)(\partial_\beta\psi) + W\phi\psi - E\psi \tag{2.22a}$$

$$\mu_\psi = k_B T \ln\left(\frac{\psi}{1-\psi}\right) - C\psi - \frac{D}{2}(\partial_\beta\phi)^2 + \frac{W}{2}\phi^2 - E\phi \tag{2.22b}$$

$$p = \rho T + \frac{A}{2}\phi^2 - \frac{3A}{4}\phi^4 - \kappa_{int}\phi(\partial^2_{\beta\beta}\phi) + D\phi\psi(\partial^2_{\beta\beta}\phi) + D\phi(\partial_\beta\phi)(\partial_\beta\psi)$$
$$- k_B T \ln(1-\psi) - \frac{C}{2}\psi^2 - \frac{\kappa_{int}}{2}(\partial_\beta\phi)^2 + W\psi\phi^2 - E\phi\psi \tag{2.22c}$$

$$P^{chem}_{\alpha\beta} = (\kappa_{int} - D\psi)(\partial_\alpha\phi)(\partial_\beta\phi) \tag{2.22d}$$

$$p_b = \rho T + \frac{A}{2}\phi^2 - \frac{3A}{4}\phi^4 - k_B T \ln(1-\psi) - \frac{C}{2}\psi^2 + W\psi\phi^2 - E\phi\psi \tag{2.22e}$$

This model is mathematically consistent. The drawback of the model reported by Yun et al. [80] is that the thickness of the interface decreases with increasing surfactant load at high surfactant concentrations. As indicated by Yun et al. [80], this numerical effect occurs due to the presence of the term $\mathcal{I} = D\lambda_1\psi\partial^2_{\beta\beta}\phi + D\lambda_1(\partial_\beta\phi)(\partial_\beta\psi) + W\phi\psi$ in the expression for the chemical potential $\mu_\phi$. In addition, Engblom et al. [81] noted the ill-posedness of this model, meaning that physical solutions do not exist under a large set of model parameters and raised questions related to the model stability.

**Case B: Gradient-free model** (Model 3 in [81])

The model equations based on the gradient-free approximation of $\hat{\delta}(x)$ in $\mathcal{F}_0$ proposed by Engblom et al. [81] are recovered by setting $\lambda_1 = 0$ & $\lambda_2 = 1$:

$$\mu_\phi = A(\phi - \phi^3)(1 - \psi) - \kappa_{int}\partial^2_{\beta\beta}\phi + W\phi\psi - E\psi \tag{2.23a}$$

$$\mu_\psi = k_B T \ln\left(\frac{\psi}{1-\psi}\right) - C\psi + \frac{A}{4}(1-\phi^2)^2 + \frac{W}{2}\phi^2 - E\phi \tag{2.23b}$$

$$p = \rho T + \frac{A}{2}\phi^2 - \frac{3A}{4}\phi^4 - A\psi(\phi^2 - \phi^4) - \kappa_{int}\phi(\partial^2_{\beta\beta}\phi) - k_B T \ln(1-\psi) - \frac{C}{2}\psi^2$$
$$- \frac{\kappa_{int}}{2}(\partial_\beta\phi)^2 + W\psi\phi^2 - E\phi\psi \tag{2.23c}$$

$$P^{chem}_{\alpha\beta} = \kappa_{int}(\partial_\alpha\phi)(\partial_\beta\phi) \tag{2.23d}$$

$$p_b = \rho T + \frac{A}{2}\phi^2 - \frac{3A}{4}\phi^4 - k_B T \ln(1-\psi) - \frac{C}{2}\psi^2 - A\psi(\phi^2 - \phi^4) + W\psi\phi^2 - E\phi\psi \tag{2.23e}$$

This model is also mathematically consistent. The gradient-free nascent delta function suggested by Engblom et al. [81] solves the instability problem. However, it

brings another effect: the interface thickness increases with the increase in the surfactant concentration, as observed by Toth and Kvamme [82] and van der Sman and Meinders [83].

**Case C: Non-variational squared-gradient model [66]**

Following the suggestion of removing the term $\mathcal{I} = D\lambda_1\psi\partial^2_{\beta\beta}\phi + D\lambda_1(\partial_\beta\phi)(\partial_\beta\psi) + W\phi\psi$ from $\mu_\phi$ [80] and setting $\lambda_1 = 1$ & $\lambda_2 = 0$, the model equations studied by Shi et al. [66] are obtained:

$$\mu_\phi = A(\phi - \phi^3) - \kappa_{int}\partial^2_{\beta\beta}\phi - E\psi \tag{2.24a}$$

$$\mu_\psi = k_BT\ln\left(\frac{\psi}{1-\psi}\right) - C\psi - \frac{D}{2}(\partial_\beta\phi)^2 + \frac{W}{2}\phi^2 - E\phi \tag{2.24b}$$

$$p = \rho T + \frac{A}{2}\phi^2 - \frac{3A}{4}\phi^4 - \kappa_{int}\phi(\partial^2_{\beta\beta}\phi) - k_BT\ln(1-\psi) - \frac{C}{2}\psi^2$$
$$\quad - \frac{\kappa_{int}}{2}(\partial_\beta\phi)^2 - E\phi\psi \tag{2.24c}$$

$$P^{chem}_{\alpha\beta} = (\kappa_{int} - D\psi)(\partial_\alpha\phi)(\partial_\beta\phi) \tag{2.24d}$$

$$p_b = \rho T + \frac{A}{2}\phi^2 - \frac{3A}{4}\phi^4 - k_BT\ln(1-\psi) - \frac{C}{2}\psi^2 - E\phi\psi \tag{2.24e}$$

Here, the modified $\mu_\phi$, Eq. (2.24a), is used to simplify the isotropic pressure $p$, but the expression of $P^{chem}_{\alpha\beta}$ is still the same as implemented in refs. [65] and [42]. This modification in $\mu_\phi$ introduces the non-variational description of the interface thickness, i.e., no effect of the coupling between the surfactant and the binary fluid in $\mu_\phi$, ensuring no change in the interface thickness regardless of the surfactant concentration. However, this modification of the equations makes the model mathematically inconsistent. Furthermore, the simulations become unstable for high surfactant concentrations, as mentioned by Shi et al. [66] and Zong et al. [60].

**Proposed model**

Before we introduce the proposed model, we want to stress the importance of the effects related to the change in the thickness of the interface when the surfactant is adsorbed. Van der Sman and Meinders [83] raised the question about the physical significance of the interface broadening phenomenon; however, there is still no clarity

if the thickness of the interface should depend on the surfactant load. In their models, Yun et al. [80], Shi et al. [66], Soligo et al. [21], and Zong et al. [60] assume that the adsorption of the surfactant at the interface does not affect the thickness of the interface. At the same time, MD) [86] and DPD simulations [87] of surfactant-laden systems indicate that certain surfactants adsorbed at the liquid-liquid interface increase the interface thickness due to the chemical structure or orientation of the surfactant. If so, then the thickness of the interface must be a function of the surfactant concentration.

Considering that we apply a diffuse interface method, meaning that the thickness of the interface is substantially enlarged compared to the physical interface thickness, we believe that the interface thickness should not noticeably change as the surfactant is adsorbed; however, to follow the observations of MD and DPD simulations, we want to retain the ability of the interface thickness to depend on the surfactant load. Therefore, we make the interface thickness a function of the surfactant concentration, as done in refs. [81], [82], and [83]. In addition to this assumption, we make the following modifications to the general model described in Section 2.1 with the primary intention of improving the numerical stability of the model and accuracy of the results at high surfactant concentrations:

- We neglect the term $D\lambda_1(\partial_\beta\phi)(\partial_\beta\psi)$ in $\mu_\phi$, Eq. (2.11a), to improve the stability of numerical simulations for high surfactant concentrations. The discretization error in the calculation of the gradient of $\psi$ increases with the increase in surfactant concentration [42] and the presence of this term in $\mu_\phi$ causes unphysical behaviour (i.e., decrease in the interface thickness) in $\phi$-profile [80] or leads to instability.

- We neglect the term $W\phi\psi$ in $\mu_\phi$, Eq. (2.11a). This term introduces the concept of perfect miscibility of the binary fluid mixture as the surfactant concentration reaches the critical surfactant concentration [82]. Since we aim to model

immiscible fluids only, we remove this term.

- Even though two terms are neglected from $\mu_\phi$, the expression for $P_{\alpha\beta}^{chem}$ remains unchanged (as these two terms have not been neglected), following the strategy adopted by Shi et al. [66].

Following these considerations, our proposed model equations read as follows:

$$\mu_\phi = A(\phi - \phi^3)(1 - \lambda_2\psi) - (\kappa_{int} - D\lambda_1\psi)\partial_{\beta\beta}^2\phi - E\psi \tag{2.25a}$$

$$\mu_\psi = k_BT\ln\left(\frac{\psi}{1-\psi}\right) - C\psi - \frac{D}{2}\lambda_1(\partial_\beta\phi)^2 + \frac{A}{4}\lambda_2(1-\phi^2)^2 + \frac{W}{2}\phi^2 - E\phi \tag{2.25b}$$

$$p = \rho T + \frac{A}{2}\phi^2 - \frac{3A}{4}\phi^4 - A\lambda_2\psi(\phi^2 - \phi^4) - \kappa_{int}\phi(\partial_{\beta\beta}^2\phi) + D\lambda_1\phi\psi(\partial_{\beta\beta}^2\phi)$$
$$- k_BT\ln(1-\psi) - \frac{C}{2}\psi^2 - \frac{\kappa_{int}}{2}(\partial_\beta\phi)^2 - E\phi\psi \tag{2.25c}$$

$$P_{\alpha\beta}^{chem} = (\kappa_{int} - D\lambda_1\psi)(\partial_\alpha\phi)(\partial_\beta\phi) \tag{2.25d}$$

$$p_b = \rho T + \frac{A}{2}\phi^2 - \frac{3A}{4}\phi^4 - k_BT\ln(1-\psi) - \frac{C}{2}\psi^2 - A\lambda_2\psi(\phi^2 - \phi^4) - E\phi\psi \tag{2.25e}$$

The proposed model is mathematically inconsistent. We gave up mathematical consistency to gain the essential advantage of keeping the interface thickness constant while still letting it be a function of the surfactant load for high surfactant concentrations.

## 2.5 Analytical solutions for a planar interface and stability of the models

In this section, we derive analytical solutions for $\phi$ and $\psi$ profiles in the case of a planar interface for the general model described in Section 2.1, three models outlined in Section 2.4 (Cases A-C), and the proposed model. The derivation is accompanied by a discussion of the stability conditions for each model, the choice of the numerical parameters, and the physical quantities. We consider a planar interface between two immiscible fluids contaminated by a non-ionic surfactant with the same solubility in both fluids ($E = 0$).

**Analytical solution for the order parameter representing binary fluid**

In thermodynamic equilibrium, the chemical potential of $\phi$ is the same at every point in the system. Comparing $\mu_\phi$, Eq. (2.25a), at any arbitrary location '$x$' with the same at the interface '$x = 0$' and keeping $\psi$ constant at the bulk surfactant concentration $\psi_b$ (i.e., constant surfactant field approximation), we have:

$$\mu_{\phi,x} = \mu_{\phi,0}$$

$$A(\phi - \phi^3)(1 - \lambda_2\psi_b) - \kappa_{int}(1 - \lambda_1\psi_b)d_{xx}^2\phi + W\phi\psi_b = 0 \tag{2.26}$$

Assuming $D = \kappa_{int}$, using the definition of $Ex$ that characterizes the surfactant solubility, Eq. (2.10), replacing $W$ with $A$ and $Ex$ in Eq. (2.26) and dividing it by $-A(1 - \lambda_2\psi_b)$, we get the following equation:

$$-\phi_b^2\phi + \phi^3 + \frac{\kappa_{int}}{A}\frac{(1 - \lambda_1\psi_b)}{(1 - \lambda_2\psi_b)}d_{xx}^2\phi = 0 \tag{2.27}$$

where the coefficient of the first term in Eq. (2.27) represents the bulk phase order parameter in the presence of surfactant (i.e., $\phi_b$) which is:

$$\phi_b^2 = \phi_0^2\frac{\left[1 - \left(\lambda_2 + \frac{1}{2Ex}\right)\psi_b\right]}{(1 - \lambda_2\psi_b)} \tag{2.28}$$

After factoring out $\phi_b^3$ from Eq. (2.27) and using Eq. (2.28), we obtain a differential equation that should be integrated to obtain the analytical expression for $\phi$:

$$\int d_{xx}^2\left(\frac{\phi}{\phi_b}\right)dx = -\frac{A\phi_0^2\left[1 - \left(\lambda_2 + \frac{1}{2Ex}\right)\psi_b\right]}{\kappa_{int}(1 - \lambda_1\psi_b)}\int\left[\left(\frac{\phi}{\phi_b}\right)^3 - \frac{\phi}{\phi_b}\right]dx \tag{2.29}$$

We can rewrite the term on the right side of Eq. (2.29) as follows:

$$d_{xx}^2\left(\frac{\phi}{\phi_b}\right) = d_x\left(\frac{1}{2}\left[d_x\left(\frac{\phi}{\phi_b}\right)\right]^2\right) \tag{2.30}$$

After inserting Eq. (2.30) in Eq. (2.29) and assuming $\left(\frac{\phi}{\phi_b}\right) = \omega$ to simplify this derivation, Eq. (2.29) can be rewritten as:

$$\int d_x\left(\frac{1}{2}[d_x(\omega)]^2\right)dx = -\frac{A\phi_0^2\left[1 - \left(\lambda_2 + \frac{1}{2Ex}\right)\psi_b\right]}{\kappa_{int}(1 - \lambda_1\psi_b)}\int[\omega^3 - \omega]dx \tag{2.31}$$

Taking the integration on both sides of Eq. (2.31) gives the following expression:

$$\left(\frac{1}{2}[d_x(\omega)]^2\right) + c_1 = -\frac{A\phi_0^2\left[1 - \left(\lambda_2 + \frac{1}{2Ex}\right)\psi_b\right]}{\kappa_{int}(1 - \lambda_1\psi_b)}\left[\left(\frac{\omega^4}{4}\right) - \left(\frac{\omega^2}{2}\right)\right] + c_2$$

$$\left(\frac{1}{2}[d_x(\omega)]^2\right) = -\frac{A\phi_0^2\left[1 - \left(\lambda_2 + \frac{1}{2Ex}\right)\psi_b\right]}{\kappa_{int}(1 - \lambda_1\psi_b)}\left[\left(\frac{\omega^4}{4}\right) - \left(\frac{\omega^2}{2}\right)\right] + c \qquad (2.32)$$

Here, the constants of integration $c_1$ and $c_2$ are combined as a single constant of integration $c = c_2 - c_1$ in Eq. (2.32). As we know behavior of $\phi$ in the interfacial region and bulk phases, we can determine $c$ by evaluating Eq. (2.32) at a very far distance from the origin such as $x = \pm\infty$ (i.e., the bulk phases), where $\omega(\pm\infty) = \pm 1$ and $\partial_x(w)_{(x=\pm\infty)} = 0$. After evaluating Eq. (2.32) at $x = \pm\infty$, the value of $c$ can be obtained as:

$$\left(\frac{1}{2}[d_x(\omega)]^2\right)_{x=\pm\infty} = -\frac{A\phi_0^2\left[1 - \left(\lambda_2 + \frac{1}{2Ex}\right)\psi_b\right]}{\kappa_{int}(1 - \lambda_1\psi_b)}\left[\left(\frac{\omega^4}{4}\right) - \left(\frac{\omega^2}{2}\right)\right]_{x=\pm\infty} + c$$

$$0 = -\frac{A\phi_0^2\left[1 - \left(\lambda_2 + \frac{1}{2Ex}\right)\psi_b\right]}{\kappa_{int}(1 - \lambda_1\psi_b)}\left[\left(\frac{1}{4}\right) - \left(\frac{1}{2}\right)\right] + c$$

$$c = -\frac{A\phi_0^2\left[1 - \left(\lambda_2 + \frac{1}{2Ex}\right)\psi_b\right]}{\kappa_{int}(1 - \lambda_1\psi_b)} \qquad (2.33)$$

Eq. (2.32) can be simplified after putting the value of $c$ back into it as follows:

$$\left(\frac{1}{2}[d_x(\omega)]^2\right) = -\frac{A\phi_0^2\left[1 - \left(\lambda_2 + \frac{1}{2Ex}\right)\psi_b\right]}{\kappa_{int}(1 - \lambda_1\psi_b)}\left[\left(\frac{\omega^4}{4}\right) - \left(\frac{\omega^2}{2}\right)\right] - \frac{A\phi_0^2\left[1 - \left(\lambda_2 + \frac{1}{2Ex}\right)\psi_b\right]}{\kappa_{int}(1 - \lambda_1\psi_b)}$$

$$\left(\frac{1}{2}[d_x(\omega)]^2\right) = -\frac{A\phi_0^2\left[1 - \left(\lambda_2 + \frac{1}{2Ex}\right)\psi_b\right]}{4\kappa_{int}(1 - \lambda_1\psi_b)}[\omega^4 - 2\omega^2 + 1]$$

$$[d_x(\omega)]^2 = \frac{(\omega^2 - 1)^2}{\xi^2} \qquad (2.34)$$

Here, $\xi$ represents the interface thickness in the presence of surfactant and it is expressed in terms of $\xi_0$ as:

$$\xi = \xi_0 \sqrt{\frac{(1 - \lambda_1 \psi_b)}{\left[1 - \left(\lambda_2 + \frac{1}{2Ex}\right)\psi_b\right]}} \tag{2.35}$$

We know that $\phi$ varies from $-1$ to $+1$ and using this argument, it can be stated that the term $(\omega^2 - 1)$ is negative throughout the interfacial region except in the bulk phases, where it is zero. Now, taking the square root on both sides of Eq. (2.34), it can be represented as follows:

$$d_x(\omega) = -\frac{(\omega^2 - 1)}{\xi} \tag{2.36}$$

Integrating Eq. (2.36) by the method of separation of variables as:

$$\int \frac{d\omega}{(1 - \omega^2)} = \int \frac{dx}{\xi} \tag{2.37}$$

The term on the left side of Eq. (2.36) can be decomposed into partial fractions for the integration as follows:

$$\frac{1}{(1 - \omega^2)} = \frac{A}{(1 + \omega)} + \frac{B}{(1 - \omega)} \tag{2.38}$$

Now, we need to find the values of $A$ and $B$ such that Eq. (2.36) holds true for any $\omega$. This can be done by equating the numerators on both sides of Eq. (2.36) as:

$$1 = A(1 - \omega) + B(1 + \omega) \tag{2.39}$$

For $\omega = -1$, $A = \frac{1}{2}$ and for $\omega = 1$, $B = \frac{1}{2}$. With these values, we can integrate Eq. (2.36) as follows:

$$\frac{1}{2} \int \frac{1}{(1 + \omega)} d\omega + \frac{1}{2} \int \frac{1}{(1 - \omega)} d\omega = \int \frac{1}{\xi} dx$$
$$\frac{1}{2}\ln|(1 + \omega)| - \frac{1}{2}\ln|(1 - \omega)| + c_1 = \frac{x}{\xi} + c_2$$
$$\frac{1}{2}\ln\left|\frac{(1 + \omega)}{(1 - \omega)}\right| = \frac{x}{\xi} + c \tag{2.40}$$

By evaluating Eq. (2.40) at the interface $x = 0$, where $\omega(0) = 0$, gives the constant of integration $c = 0$. After that, the analytical solution for $\phi$ is obtained by simplifying Eq. (2.40) as follows:

$$\frac{1}{2}\ln\left|\frac{(1+\omega)}{(1-\omega)}\right| = \frac{x}{\xi}$$

$$\frac{(\omega+1)}{(\omega-1)} = \frac{-\exp\left(\frac{2x}{\xi}\right)}{1}$$

$$\frac{(\omega+1)+(\omega-1)}{(\omega+1)-(\omega-1)} = \frac{-\exp\left(\frac{2x}{\xi}\right)+1}{-\exp\left(\frac{2x}{\xi}\right)-1}$$

$$\omega = \frac{-\cancel{\exp\left(\frac{x}{\xi}\right)}\left[\exp\left(\frac{x}{\xi}\right)-\exp\left(\frac{-x}{\xi}\right)\right]}{-\cancel{\exp\left(\frac{x}{\xi}\right)}\left[\exp\left(\frac{x}{\xi}\right)+\exp\left(\frac{-x}{\xi}\right)\right]}$$

$$\frac{\phi(x)}{\phi_b} = \omega = \tanh\left(\frac{x}{\xi}\right) \tag{2.41}$$

For Eqs. (2.28) and (2.35), the following necessary conditions proposed by [82] must be satisfied to keep constant $\xi$ and $\phi_b^2 \approx 1$ for the general model:

$$\lambda_2 \gg \frac{1}{2Ex} \tag{2.42a}$$

$$\lambda_1 = \lambda_2 + \frac{1}{2Ex} \tag{2.42b}$$

We discuss the numerical challenges these conditions impose on selecting $Ex$ and $\lambda_2$ values later in the section 3.1.

We also present analytical solutions for the $\phi$ profiles for other models using the general analytical solution for a planar interface. Note that the expression for $\phi$ described by Eq. (2.41) is the same for all models; only the definitions of $\phi_b$ and $\xi$ are different.

**Case A: Squared-gradient model**

Assuming $\lambda_1 = 1$ and $\lambda_2 = 0$ in equations (2.28) and (2.35) gives the bulk order parameter and the interface thickness for the model proposed by van der Sman and

33

van der Graaf [65] as follows:

$$\phi_b^2 = \phi_0^2 \left( 1 - \frac{1}{2Ex} \psi_b \right) \tag{2.43a}$$

$$\xi = \xi_0 \sqrt{\frac{(1 - \psi_b)}{\left( 1 - \frac{1}{2Ex} \psi_b \right)}} \tag{2.43b}$$

Van der Sman and van der Graaf [65] assumed $\psi_b \ll 1$, which means $\phi_b^2$ and $\xi$ become independent of $\psi_b$ & $Ex$. As a result, this model gives stable and accurate results for low $\psi_b$ values, as shown by Liu and Zhang [42]. When the assumption of $\psi_b \ll 1$ is not made, the condition $Ex \gg 0.5$ ensures that $Ex$ has a negligible effect on $\phi_b^2$ and $\xi$. However, the thickness of the interface $\xi$ decreases with increasing $\psi_b$. In addition, a combination of $Ex \leq 0.5$ and high $\psi_b$ values leads to physically unrealistic results.

**Case B: Gradient-free model**

The equations of $\phi_b^2$ and $\xi$ for the model suggested by Engblom et al. [81] can be obtained by setting $\lambda_1 = 0$ and $\lambda_2 = 1$ in equations (2.28) and (2.35) as follows:

$$\phi_b^2 = \phi_0^2 \frac{\left[ 1 - \left( 1 + \frac{1}{2Ex} \right) \psi_b \right]}{(1 - \psi_b)} \tag{2.44a}$$

$$\xi = \xi_0 \sqrt{\frac{1}{\left[ 1 - \left( 1 + \frac{1}{2Ex} \right) \psi_b \right]}} \tag{2.44b}$$

Similarly, setting $Ex \gg 0.5$ is required to keep $\phi_b^2 \approx 1$. Then, the thickness of the interface depends only on $\psi_b$, and increases with increasing $\psi_b$.

**Case C: Non-variational squared-gradient model**

After removing the term $\mathcal{I} = D\lambda_1 \psi \partial_{\beta\beta}^2 \phi + D\lambda_1 (\partial_\beta \phi)(\partial_\beta \psi) + W\phi\psi$ from $\mu_\phi$, Eq. (2.11a), and setting $\lambda_1 = 1$ & $\lambda_2 = 0$, the equations of $\phi_b^2$ and $\xi$ of the model proposed by Shi et al. [66] are obtained:

$$\phi_b^2 = \phi_0^2 \tag{2.45a}$$

$$\xi = \xi_0 \tag{2.45b}$$

34

Here, $\phi_b^2$ and $\xi$ are independent of the surfactant concentration and $Ex$. This model is still susceptible to numerical instability at high surfactant concentrations, probably due to the use of a squared-gradient delta function, as noticed by Engblom et al. [81].

**Proposed model**

Following the modifications outlined in Section (2.4) and keeping both $\lambda_1$ & $\lambda_2$, the expressions of $\phi_b^2$ and $\xi$ for our model read as follows:

$$\phi_b^2 = \phi_0^2 \frac{(1 - \lambda_2 \psi_b)}{(1 - \lambda_2 \psi_b)} \tag{2.46a}$$

$$\xi = \xi_0 \sqrt{\frac{(1 - \lambda_1 \psi_b)}{(1 - \lambda_2 \psi_b)}} \tag{2.46b}$$

Different combinations of $\lambda_1$ and $\lambda_2$ define the behaviour of the interface thickness, $\xi$, given by Eq. (2.46b) as a function of surfactant concentration. When $\lambda_1 = \lambda_2$ the thickness of the interface remains constant regardless of the value of $\psi_b$; whereas $\lambda_2 > \lambda_1$ and $\lambda_2 < \lambda_1$ refer to the increase and decrease of the thickness with the increase in the bulk surfactant concentration, respectively. For the rest of the discussion and simulations, we consider the case of a constant interface thickness setting $\lambda_1 = \lambda_2$.

Neither $\phi_b$ nor $\xi$ depend on $Ex$ values. In Eq. (2.46a), we did not cancel the numerator and denominator even though they are the same to explicitly show the case when $\phi_b^2$ becomes indeterminate, i.e., $(1 - \lambda_2 \psi_b) = 0$ and leads to numerical instability. To derive the additional condition of numerical stability, we examine the thermodynamic equilibrium where the chemical potential for $\phi$ is defined by Eq. (2.25a) reads as follows:

$$\mu_\phi = (1 - \lambda_2 \psi)[A(\phi - \phi^3) - \kappa_{int}\partial_{\alpha\alpha}^2 \phi] = 0 \tag{2.47}$$

The term $(1 - \lambda_2 \psi)$ should not be zero because it makes the definition of interface thickness $\xi$ and bulk order parameter $\phi_b$ indeterminate. To promote numerical stability, we must have the term $(1 - \lambda_2 \psi)$ positive, which means that the following

35

condition must be satisfied:

$$\lambda_2 < \frac{1}{\psi} \tag{2.48}$$

To get a quantitative limit for $\lambda_2$, we need to approximate $\psi$ at either bulk value, $\psi = \psi_b$ or $\psi = \psi_0 = \psi(0)$, i.e., the surfactant concentration at the interface. Following the literature, the constant surfactant field (i.e., bulk value) is typically used to approximate $\psi$; however, $\lambda_2$ should be chosen based on $\psi_0$, which is the maximum value of $\psi$ in equilibrium, ensuring that the term $(1 - \lambda_2\psi)$ never becomes zero. Hence, the condition of numerical stability can be rewritten as follows:

$$\lambda_2 < \frac{1}{\psi_0} \tag{2.49}$$

Considering that $\psi_0$ must be in the range between 0 and 1, $\lambda_2$ must be equal to or greater than 1 ($\lambda_2 \geq 1$) to achieve physically realistic results.

**Analytical solution for the order parameter representing surfactant**

At the thermodynamic equilibrium, a steady state profile of $\psi(x)$ for the general model can be obtained by comparing $\mu_\psi$ (2.11b) at any arbitrary location, $x$, with the value at the bulk phase location, $b$, as follows:

$$\mu_{\psi,x} = \mu_{\psi,b}$$

$$k_B T \ln\left(\frac{\psi}{1-\psi}\right) - C\psi - \frac{\kappa_{int}}{2}\lambda_1(d_x\phi)^2 + \frac{A}{4}\lambda_2(1-\phi^2)^2 + \frac{W}{2}\phi^2 = k_B T \ln\left(\frac{\psi_b}{1-\psi_b}\right)$$
$$- C\psi_b + \frac{A}{4}\lambda_2(1-\phi_b^2)^2 + \frac{W}{2}\phi_b^2 \tag{2.50}$$

After dividing Eq. (2.50) by $k_B T$ and then taking the exponential on both sides, the equilibrium profile of $\psi$ reads as follows:

$$\psi(x) = \frac{\psi_b}{\psi_b + (1-\psi_b)\Psi_c(x)} \tag{2.51}$$

Where, $\Psi_c(x)$ is given by:

$$\Psi_c(x) = \exp\left(-\frac{1}{k_B T}\left[C(\psi - \psi_b) - \frac{A}{4}\lambda_2[(1-\phi^2)^2 - (1-\phi_b^2)^2] + \frac{\kappa_{int}}{2}\lambda_1(d_x\phi)^2 - \frac{W}{2}(\phi^2 - \phi_b^2)\right]\right)$$
$$\tag{2.52}$$

The surfactant concentration at the interface (i.e., $x = 0$) can be defined from Eq. (2.51) as:

$$\psi_0 = \psi(0) = \frac{\psi_b}{\psi_b + (1 - \psi_b)\Psi_c(0)} \tag{2.53}$$

$\Psi_c(0)$ is the adsorption constant that depends on the model parameters. At the interface $x = 0$, $\Psi_c(0)$ is obtained by using the definition of $\xi_0$ & $Ex$ and Eq. (2.41) giving $\phi(0) = 0$ & $(\partial_x \phi)_{x=0} = \frac{\phi_b}{\xi}$ as follows:

$$\Psi_c(0) = \exp\left(-\frac{1}{k_B T}\left[\frac{A}{4}\phi_b^2\left(\lambda_2[\phi_b^2 - 2] - \frac{\xi_0^2}{\xi^2}\lambda_1 - \frac{1}{Ex}\right)\right]\right)\exp\left(-\frac{1}{k_B T}[C(\psi_0 - \psi_b)]\right)$$
$$= \psi_c(0)\exp\left(-\frac{1}{k_B T}[C(\psi_0 - \psi_b)]\right) \tag{2.54}$$

Here, $\psi_c(0)$ is the adsorption constant for the Langmuir isotherm and $\Psi_c(0)$ becomes $\psi_c(0)$ at $C = 0$.

The analytical solutions for $\psi$ for different models differ in the $\Psi_c(x)$ expression. The equation of $\Psi_c(x)$ is the same for the models proposed by van der Sman and van der Graaf [65] and Shi et al. [66]. It is obtained by setting $\lambda_1 = 1$ & $\lambda_2 = 0$ in Eq. (2.52). For the model proposed by Engblom et al. [81], the expression of $\Psi_c(x)$ is recovered by setting $\lambda_1 = 0$ & $\lambda_2 = 1$ in Eq. (2.52). For our model, the equation of $\Psi_c(x)$ is exactly the same as Eq. (2.52) because of the way we modified $\mu_\phi$ not $\mu_\psi$. Note that the analytical equations for the pure system (i.e., no surfactant) can be recovered from equations (2.41) and (2.51) by putting $\psi_b = 0$.

In addition, we define the limiting value of $\psi_0$ from the condition of numerical stability (2.49) as follows:

$$(\psi_0)_{lim} = \frac{1}{\lambda_2} \tag{2.55}$$

For a given $\lambda_2$ and $\psi_c(0)$, this relation is used to determine the limiting value of $\psi_0$, which is the value of $\psi_0$ at which $\phi_b$ and $\xi$ become indeterminate for the case of constant thickness. From $(\psi_0)_{lim}$, $(\psi_b)_{lim}$ is calculated analytically for the Langmuir isotherm ($C = 0$) or numerically for the Frumkin isotherm ($C \neq 0$) using Eq. (2.53)

to devise a range of $\psi_b$ values until $(\psi_b)_{lim}$ (i.e., $\psi_b < (\psi_b)_{lim}$). This range of $\psi_b$ values satisfies the stability condition, Eq. (2.49), and ensures the stability of numerical simulations.

## 2.6 Surface tension

There are two approaches to account for the surface tension in the diffuse interface models: geometric and thermodynamic. In the geometric approach, the surface tension force is based on the interface curvature and is represented as a sum of the normal and tangential (i.e., Marangoni) components [88], where the EOS describing the effect of surfactant on surface tension is explicitly present in the surface tension force. This approach is used in refs. [88], [80], [21], and [60].

In the thermodynamic approach, the surface tension force is implemented as the divergence of the thermodynamic pressure tensor, $P_{\alpha\beta}^{th}$, using the Gibbs-Duhem relation, where the EOS is implicit and is derived from the Gibbs adsorption equation that relates the surface tension to the surface excess quantity and chemical potential of $\psi$. Following the references [65], [42], and [66], we adopt the thermodynamic approach to incorporate the surface tension force into the system, Eq. (2.1).

Using the Gibbs adsorption equation at constant temperature, the variation of surface tension is expressed in terms of surface excess quantities [89] as follows:

$$d\sigma = -\psi_{xs}d\mu_\psi \tag{2.56}$$

Here, $\psi_{xs}$ is the excess surfactant concentration accounting for the local variation of $\psi$ in the interfacial region (i.e., diffuse interface) and the integration of $\psi$ (i.e., Eq. (2.51)) over the diffuse interface can not be analytically obtained. As suggested in [65] and [42], we assume that the excess surfactant concentration $\psi_{xs}$ is proportional to $\psi_0$ (i.e., $\psi_{xs} = \alpha\psi_0$) with the proportionality coefficient $\alpha$. Then, taking $\mu_\psi = \mu_{\psi_0}$ (i.e., $\mu_\psi$ at the interface obtained using equations (2.51) and (2.41)) at the equilibrium

in Eq. (2.56) and integrating it with respect to $\psi_0$ give the EOS as follows:

$$d\sigma = -\psi_{xs}d\mu_\psi$$

$$= -\alpha\psi_0 d\mu_{\psi_0}$$

$$\int d\sigma = -\alpha \int \psi_0 d\left[k_B T\ln\left(\frac{\psi_0}{1-\psi}\right) - C\psi_0 - \frac{\kappa_{int}}{2}\lambda_1\frac{\phi_b^2}{\xi^2} + \frac{A}{4}\lambda_2\right]$$

$$\sigma(\psi_0) - \sigma_0 = \alpha\left[k_B T\ln(1-\psi_0) + \frac{C}{2}\psi_0^2\right] \qquad (2.57)$$

Where, $\sigma_0 = 4\kappa_{int}\phi_0^2/3\xi_0$ represents the surface tension of the pure system. After specifying the thickness of the interface $\xi$, the fitting coefficient $\alpha$ depends on $\lambda_2$ and $Ex$. In addition, $k_B T$ increases with an increase in $\lambda_2$ or a decrease in $Ex$, resulting in a reduction in $\sigma$. The coefficient $\alpha$ is less than or greater than unity depending on the combination of $\lambda_2$ and $Ex$.

## 2.7 Free-energy lattice Boltzmann method

The set of governing equations (2.1) representing the binary fluid-surfactant system is solved numerically using a free-energy LBM proposed by Swift et al. [61]. This method is extended to accommodate the presence of surfactant following the work of Theissen and Gompper [20] and Lamura et al. [90]. Three particle distribution functions $f_q(x_\alpha, t)$, $g_q(x_\alpha, t)$, and $h_q(x_\alpha, t)$ are used to solve continuity, the Navier-Stokes equations, and two Cahn-Hilliard equations for $\phi$ and $\psi$. The total number of discrete velocity directions (i.e., $Q$) required to represent the continuous particle velocity space depends on the consistent approximations of the governing equations with minimum computational resources. In the present study, the D3Q19 velocity set is selected for the three populations $f$, $g$, and $h$.

The lattice structure of the D3Q19 velocity set is represented in Figure 2.1. The lattice velocity directions of the D3Q19 velocity set are split into two groups. The
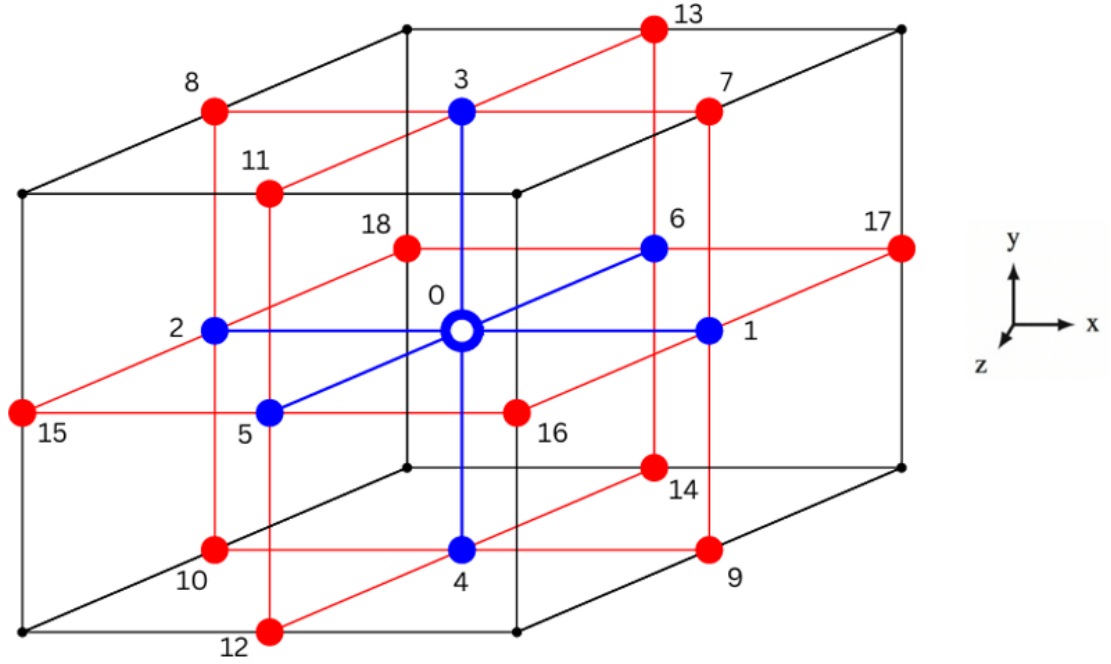
Figure 2.1: Lattice structure of the D3Q19 velocity set

directions $\vec{c}_{1-6}$ point in the nearest neighbour directions:

$$
\begin{bmatrix} c_{x1-6} \\ c_{y1-6} \\ c_{z1-6} \end{bmatrix} = \begin{bmatrix} 1 & -1 & 0 & 0 & 0 & 0 \\ 0 & 0 & 1 & -1 & 0 & 0 \\ 0 & 0 & 0 & 0 & 1 & -1 \end{bmatrix} \tag{2.58}
$$

and $\vec{c}_{7-18}$ point into 12 square diagonal directions

$$
\begin{bmatrix} c_{x7-18} \\ c_{y7-18} \\ c_{z7-18} \end{bmatrix} = \begin{bmatrix} 1 & -1 & 1 & -1 & 0 & 0 & 0 & 0 & 1 & -1 & 1 & -1 \\ 1 & 1 & -1 & -1 & 1 & -1 & 1 & -1 & 0 & 0 & 0 & 0 \\ 0 & 0 & 0 & 0 & 1 & 1 & -1 & -1 & 1 & 1 & -1 & -1 \end{bmatrix} \tag{2.59}
$$

The weights suggested in [91] are considered for the D3Q19 velocity set:

$$w_{1-6} = \frac{1}{6}, \quad w_{7-18} = \frac{1}{12},$$

$$w^{xx}_{1-2} = w^{yy}_{3-4} = w^{zz}_{5-6} = \frac{5}{12}, \quad w^{xx}_{3-6} = w^{yy}_{1-2,5-6} = w^{zz}_{1-4} = -\frac{1}{3},$$

$$w^{xx}_{7-10} = w^{xx}_{15-18} = w^{yy}_{7-14} = w^{zz}_{11-18} = -\frac{1}{24},$$

$$w^{xx}_{11-14} = w^{yy}_{15-18} = w^{zz}_{7-10} = \frac{1}{12}, \tag{2.60a}$$

$$w^{xy}_{1-6} = w^{yz}_{1-6} = w^{zx}_{1-6} = 0, \quad w^{xy}_{7,10} = w^{yz}_{11,14} = w^{zx}_{15,18} = \frac{1}{4},$$

$$w^{xy}_{8,9} = w^{yz}_{12,13} = w^{zx}_{16,17} = -\frac{1}{4}, \quad w^{xy}_{11-18} = w^{yz}_{7-10} = w^{zx}_{7-14} = 0$$

The discretized Boltzmann equations describe the evolution of particle distribution functions with respect to time, space, and velocity as follows:

$$f_q(x_\alpha + c_{q\alpha}\Delta t, t + \Delta t) = f_q(x_\alpha, t) + \Omega^f_q(x_\alpha, t) \tag{2.61a}$$

$$g_q(x_\alpha + c_{q\alpha}\Delta t, t + \Delta t) = g_q(x_\alpha, t) + \Omega^f_q(x_\alpha, t) \tag{2.61b}$$

$$h_q(x_\alpha + c_{q\alpha}\Delta t, t + \Delta t) = h_q(x_\alpha, t) + \Omega^f_q(x_\alpha, t) \tag{2.61c}$$

Where $x_\alpha$ and $c_{q\alpha}$ represent the position and the discrete velocity vectors, respectively, and $q$ represents the discrete velocity number. These equations describe the discrete particle populations travelling from the initial lattice position $x_\alpha$ to the neighbouring lattice position $x_\alpha + c_{q\alpha}\Delta t$ with a velocity $c_{q\alpha} = (c_{qx}, c_{qy}, c_{qz})$ during the time step $\Delta t$. This leads to particle collision, which is incorporated by a collision operator $\Omega_q$, i.e., the last term on the right side of the equations. The grid spacing $\Delta x$ and the time step $\Delta t$ are scaled in lattice units so that $\Delta x = 1$ and $\Delta t = 1$. The conversion from lattice units to SI base units is achieved by scaling the physical parameters, analyzing relevant dimensionless numbers, and using the law of similarity (see [92] for more details). The system of governing equations (2.1) can be obtained from the set of equations (2.61) by the Chapman-Enskog expansion. The Chapman-Enskog expansions of the lattice Boltzmann equations (LBE) for particle populations $f$, $g$, and $h$ are provided in Appendix A.

41

The collision operator $\Omega_q$ accounts for the relaxation of the particle populations towards the equilibrium distributions after collisions between them. The selection of a collision operator affects the stability and accuracy of numerical results. In the present study, the Bhatnagar-Gross-Crook (BGK) collision operator (i.e. single-relaxation-time (SRT) collision operator) [93] is considered for the particle populations $g$ and $h$. The collision operators $\Omega_q^g$ and $\Omega_q^h$ in eq. (2.61b) and eq. (2.61c) can be written as follows:

$$\Omega_q^g = -\frac{g_q - g_q^{eq}}{\tau_g}\Delta t \tag{2.62a}$$

$$\Omega_q^h = -\frac{h_q - h_q^{eq}}{\tau_h}\Delta t \tag{2.62b}$$

where $\tau_g$ and $\tau_h$ are the relaxation times representing the time which the particle populations $g$ and $h$ take to reach their equilibrium distributions $g_q^{eq}$ and $h_q^{eq}$, respectively.

For the particle population $f$, the multiple-relaxation-time (MRT) collision operator is used, improving the accuracy and stability of the solution of the Navier-Stokes equations [94]. The MRT collision operator relaxes the collision of particles in the moment space instead of the population space with individual collision rates for $q = 0{:}18$. The collision operator $\Omega_q^f$ in eq. (2.61a) can be represented as follows:

$$\Omega_q^f = -\mathbf{M}^{-1}\mathbf{S}\mathbf{M}(f_q - f_q^{eq})\Delta t \tag{2.63}$$

where $f_q^{eq}$ represents the equilibrium distribution of particle population $f$. The transformation from the population space to moment space and implementation of different relaxation rates are performed by the transformation matrix $\mathbf{M}$ and relaxation matrix $\mathbf{S}$, respectively. Then, the multiplication by $\mathbf{M}^{-1}$ refers to the mapping from moment to population space after relaxation. These matrices are constructed for the D3Q19 velocity set from the guidelines suggested in ref. [94]. The MRT collision operator is incorporated into the free-energy-based LB algorithm using Ref. [95]. The matrix representation of the transformation and relaxation matrices are provided in

42

Appendix B.

Local macroscopic variables such as density, momentum density, and order parameters at any lattice site are calculated by the moments of the particle distribution functions. The moments are defined as the summation or weighted summation of particle populations over the discretized velocity space:

$$\sum_q f_q = \rho \qquad \sum_q f_q c_{q\alpha} = \rho u_\alpha \tag{2.64a}$$

$$\sum_q g_q = \phi \qquad \sum_q h_q = \psi \tag{2.64b}$$

The moments of the equilibrium distribution functions $f_q^{eq}$, $g_q^{eq}$, and $h_q^{eq}$ represent the set of equations which is the same as the set (2.64). In addition, the higher-order moments of these functions are related to the thermodynamic pressure tensor, the coefficient of mobilities, and the chemical potentials according to the free-energy LBM schemes suggested in refs. [61], [90], and [20] as follows:

$$\sum_q f_q^{eq} c_{q\alpha} c_{q\beta} = P_{\alpha\beta}^{th} + \rho u_\alpha u_\beta \tag{2.65a}$$

$$\sum_q g_q^{eq} c_{q\alpha} c_{q\beta} = \Gamma_\phi \mu_\phi \delta_{\alpha\beta} + \phi u_\alpha u_\beta \tag{2.65b}$$

$$\sum_q h_q^{eq} c_{q\alpha} c_{q\beta} = \Gamma_\psi \mu_\psi \delta_{\alpha\beta} + \psi u_\alpha u_\beta \tag{2.65c}$$

The equilibrium distributions of particle populations $f_q^{eq}$, $g_q^{eq}$, and $h_q^{eq}$ for directions $q = (1 - 18)$ are calculated as follows [96]:

$$f_q^{eq} = w_q \left( p_b - \kappa_{int}\phi(\partial_{xx}^2\phi + \partial_{yy}^2\phi + \partial_{zz}^2\phi) + c_{q\alpha}\rho u_\alpha + \frac{3}{2}\left[c_{q\alpha}c_{q\beta} - \frac{1}{3}\delta_{\alpha\beta}\right]\rho u_\alpha u_\beta \right)$$

$$+ (\kappa_{int} - D\lambda_1\psi)\left( w_q^{xx}\partial_x\phi\partial_x\phi + w_q^{yy}\partial_y\phi\partial_y\phi + w_q^{zz}\partial_z\phi\partial_z\phi + w_q^{xy}\partial_x\phi\partial_y\phi \right.$$

$$\left. + w_q^{xz}\partial_x\phi\partial_z\phi + w_q^{yz}\partial_y\phi\partial_z\phi \right) \tag{2.66}$$

$$g_q^{eq} = w_q \left( \Gamma_\phi\mu_\phi + c_{q\alpha}\phi u_\alpha + \frac{3}{2}\left[c_{q\alpha}c_{q\beta} - \frac{1}{3}\delta_{\alpha\beta}\right]\phi u_\alpha u_\beta \right) \tag{2.67}$$

$$h_q^{eq} = w_q \left( \Gamma_\psi \mu_\psi + c_{q\alpha} \psi u_\alpha + \frac{3}{2} \left[ c_{q\alpha} c_{q\beta} - \frac{1}{3} \delta_{\alpha\beta} \right] \psi u_\alpha u_\beta \right) \tag{2.68}$$

The populations for $q = 0$ are calculated as

$$f_0^{eq} = \rho - \sum_{q=1}^{18} f_q^{eq} \tag{2.69a}$$

$$g_0^{eq} = \phi - \sum_{q=1}^{18} g_q^{eq} \tag{2.69b}$$

$$h_0^{eq} = \psi - \sum_{q=1}^{18} h_q^{eq} \tag{2.69c}$$

Note that the expressions of $f_q^{eq}$, $g_q^{eq}$, and $h_q^{eq}$ for the free energy models discussed in Section 2.4 differ from each other based on the selection of $\lambda_1$ and $\lambda_2$ values mentioned in Section 2.4.

The stencils for the calculation of gradients and Laplacian in the pressure tensor and chemical potential are given by Pooley and Furtado [91]

$$\partial_x = \frac{1}{12} \left[ \begin{pmatrix} 0 & 0 & 0 \\ -1 & 0 & 1 \\ 0 & 0 & 0 \end{pmatrix}, \begin{pmatrix} -1 & 0 & 1 \\ -2 & 0 & 2 \\ -1 & 0 & 1 \end{pmatrix}, \begin{pmatrix} 0 & 0 & 0 \\ -1 & 0 & 1 \\ 0 & 0 & 0 \end{pmatrix} \right] \tag{2.70}$$

$$\nabla^2 = \frac{1}{6} \left[ \begin{pmatrix} 0 & 1 & 0 \\ 1 & 2 & 1 \\ 0 & 1 & 0 \end{pmatrix}, \begin{pmatrix} 1 & 2 & 1 \\ 2 & -24 & 2 \\ 1 & 2 & 1 \end{pmatrix}, \begin{pmatrix} 0 & 1 & 0 \\ 1 & 2 & 1 \\ 0 & 1 & 0 \end{pmatrix} \right] \tag{2.71}$$

where left, middle, and right matrices show slices of the stencil when $c_{zq} = 1$, 0, and $-1$, respectively.

Macroscopic properties, such as the kinematic viscosity and mobility, are described in terms of the speed of sound and the relaxation time via the Chapman-Enskog expansion. The kinematic viscosity $\nu$ of the system is defined as:

$$\nu = c_s^2 \left( \tau_f - \frac{1}{2} \right) \Delta t \tag{2.72}$$

where $\tau_f$ is the relaxation time of particle population $f$. The mobilities $M_\phi$ and $M_\psi$ are calculated as follows:

$$M_\phi = \Gamma_\phi \left( \tau_g - \frac{1}{2} \right) \Delta t \tag{2.73a}$$

$$M_\psi = \Gamma_\psi \left( \tau_h - \frac{1}{2} \right) \Delta t \tag{2.73b}$$

Here, $\Gamma_\phi$ and $\Gamma_\psi$ represent the mobility coefficients of $\phi$ and $\psi$, respectively.

For all the simulations conducted in the present study, the periodic boundary condition (BC) is implemented. In the periodic BC, the unknown incoming populations entering the domain on the one side are given by those leaving the domain on the opposite side. We consider the opposing periodic edges of the flow domain as if they were attached together. The periodic BCs are implemented during the streaming process, where post-streaming populations that enter the domain on one side are replaced by post-collision populations that leave the domain on the opposite side. The detailed procedure of the periodic BC implementation is provided in Ref. [51].

In the present study, a computer code is developed using Fortran 90 to implement the free-energy-based LB algorithm. We have developed serial and parallel versions of the code. Parallelization of the code is important to save simulation time and allow us to study larger simulation domains. The message-passing interface (MPI) is used for parallelization. In the parallel version of the code, we decompose the simulation domain into equal-sized sub-domains in three directions $x$, $y$, and $z$. Each CPU is assigned one sub-domain. The communication between the sub-domains is based on a receive-sent scheme, and it is established using a command MPI_SENDRECV.

The steps of the free-energy-based LB algorithm are described as follows:

1. We assign the values of model parameters such as $\kappa_{int}$ and $Ex$ and then the fields of macroscopic quantities, for example, $\rho$, $\phi$, $\psi$, and $u_\alpha$ are initialized for a validation case at each lattice site. Note that $\rho = 1$ and $u_\alpha = \{u_x, u_y, u_z\} = \{0, 0, 0\}$ are considered for all simulations.

2. The equilibrium distribution functions $f_q^{eq}$, $g_q^{eq}$, and $h_q^{eq}$ at each lattice site are calculated using the following equations from the initialized values of macroscopic quantities as follows:

$$f_q^{eq} = \rho w_q \left( c_s^2 + c_{q\alpha} u_\alpha + \frac{3}{2} \left[ c_{q\alpha} c_{q\beta} - \frac{1}{3} \delta_{\alpha\beta} \right] u_\alpha u_\beta \right) \tag{2.74a}$$

$$g_q^{eq} = \phi w_q \left( c_{q\alpha} u_\alpha + \frac{3}{2} \left[ c_{q\alpha} c_{q\beta} - \frac{1}{3} \delta_{\alpha\beta} \right] u_\alpha u_\beta \right) \tag{2.74b}$$

$$h_q^{eq} = \psi w_q \left( c_{q\alpha} u_\alpha + \frac{3}{2} \left[ c_{q\alpha} c_{q\beta} - \frac{1}{3} \delta_{\alpha\beta} \right] u_\alpha u_\beta \right) \tag{2.74c}$$

After that, the particle populations $f$, $g$, and $h$ are initialized as their respective equilibrium distribution functions.

3. Using the moments (2.64), $\rho$, $\phi$, $\psi$, and $u_\alpha$ are calculated at each lattice site.

4. The gradient and Laplace operators are calculated using Eqs. (2.70) and (2.71) to determine the bulk pressure $p_b$ and chemical potentials $\mu_\phi$ & $\mu_\psi$. Then, we calculate the equilibrium distributions $f_q^{eq}$, $g_q^{eq}$, and $h_q^{eq}$ by using Eqs. (2.66), (2.67), (2.68) for directions $q = (1 - 18)$ and the set of equations (2.69) for $q = 0$.

5. The collision operators for $f$, $g$, and $h$ are calculated using Eqs. (2.63), (2.62a), and (2.62a), respectively. For example, the discretized Boltzmann equation for the particle population $g$ is represented as:

$$g_q^*(x_\alpha, t) = g_q(x_\alpha, t) - \frac{g_q(x_\alpha, t) - g_q^{eq}(x_\alpha, t)}{\tau_g} \Delta t \tag{2.75}$$

Here, $g_q^*(x_\alpha, t)$ is the state of the particle distribution function after the collision process.

6. The post-collision distribution functions are then propagated to neighbouring lattice sites. For example, the streaming process for the particle population $g$ from the initial position of $x_\alpha$ to the neighbouring position $x_\alpha + c_{q\alpha} \Delta t$ is

represented as:

$$g_q(x_\alpha + c_{q\alpha}\Delta t, t + \Delta t) = g_q^*(x_\alpha, t) \tag{2.76}$$

During one time step, both collision and streaming processes are completed.

7. Based on the particle populations obtained after the streaming process, $\rho$, $\phi$, $\psi$, and $u_\alpha$ are updated using the moments (2.64).

8. The cycle from step 4 to step 7 resumes for the next time step, and it continues untill the last time step or the system reaches equilibrium.

# Chapter 3

# Results and discussion

To demonstrate the capability of the proposed model and compare its performance with the models of van der Sman and van der Graaf [65], Engblom et al. [81], Shi et al. [66], and the general model, we apply these models to simulate two benchmark problems: a surfactant-laden planar interface between two immiscible liquids and the equilibration of a spherical drop in a quiescent medium. First, we show our model performance at low and high surfactant concentrations for a planar interface for Langmuir and Frumkin isotherms. We compare the numerical profiles of the order parameters obtained with different models, confirming the enhanced capability of the proposed model to accurately capture the stable profiles of the order parameters for high surfactant concentrations.

Then, we apply the proposed model to study the equilibration of a spherical drop. We discuss the equilibrium fields and profiles of $\phi$ & $\psi$, the effect of the surfactant mobility $M_\psi$ on the stability of numerical results, the reduction of surface tension, and the spurious velocity for different $\lambda_2$ values.

For all simulations, several numerical parameters were fixed. The relaxation times of the particle populations $g$ and $h$ are set $\tau_g = \tau_h = 1/(3 - \sqrt{3})$ following the suggestion in Ref. [97] to obtain accurate and stable numerical results for the convection-diffusion type equations of $\phi$ and $\psi$. The constant mobilities $M_\phi$ & $M_\psi$ and the coefficient $D = \kappa_{int}$ are assumed for convenience. Note that all the quantities defined

for the simulations are in lattice units [lu].

When selecting numerical parameters and physical quantities, it is necessary to satisfy the condition of numerical stability, Eq. (2.49). We use the following procedure to set the simulations. First, the value of $\psi_c(0)$ is selected from the typical range $\psi_c(0) = [0.002 - 0.2]$. Subsequently, we fix $\lambda_2$ from the range $[0.5 - 10]$ to calculate $(\psi_0)_{lim}$ using Eq. (2.55). Then, using Eq. (2.53), we calculate $(\psi_b)_{lim}$ analytically for the Langmuir isotherm $(C = 0)$ or numerically for the Frumkin isotherm $(C \neq 0)$ to construct a range of $\psi_b$ values until $(\psi_b)_{lim}$ that lead to stable numerical simulations. Finally, we select a single value of $\psi_b$ representing a low or high bulk surfactant concentration to run the desired simulation.
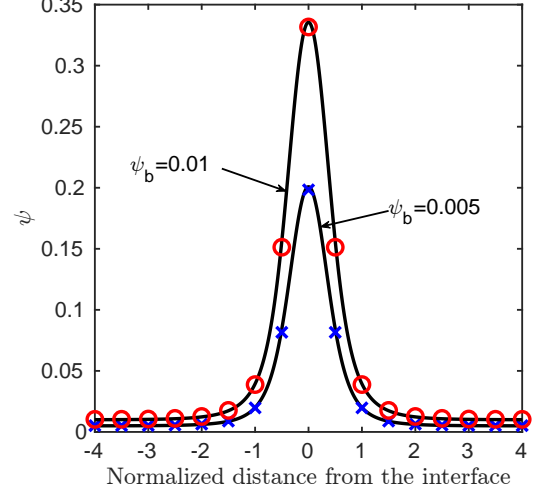
## 3.1 Planar interface

We begin by presenting the results of the planar interface obtained with the proposed numerical model governed by a set of equations (2.25) where $C = 0$ is set for the Langmuir and $C = 2k_BT$ for the Frumkin isotherms, respectively. Simulations are carried out in the fully periodic domain of size $130 \times 130 \times 130$ [lu], where the dispersed phase is initially positioned at $34 \leq x \leq 97$ [lu], and the interface locations are fixed at $x_{01} = 33$ [lu] and $x_{02} = 98$ [lu]. The simulation parameters were selected as follows: interfacial tension $\sigma_0 = 0.02$ [lu], dimensionless initial thickness of the interface $\xi_0/\Delta x = 2$ [lu], mobility for $\phi$ parameter $M_\phi = 0.2$, mobility for $\psi$ parameter $M_\psi = 0.02$, bulk surfactant concentration $\psi_b = \{0.005, 0.01\}$, Langmuir adsorption constant $\psi_c(0) = 0.02$, $Ex = 0.17$, $\lambda_2 = 1$, and $\lambda_1 = \lambda_2$. Note that the profiles of $\phi$ and $\psi$ in all planar interface simulations were initialized using the analytical solutions presented in Section (2.5).

The equilibrium profiles of $\phi$ and $\psi$ at low surfactant concentrations $\psi_b = \{0.005, 0.01\}$ for Langmuir and Frumkin isotherms are shown in Figure 3.1. The numerical profiles of $\phi$ and $\psi$ accurately follow the analytical solutions (2.41) and (2.51). In addition, the comparison of $\psi$-profiles (Figure 3.1(b) and (d)) between Langmuir and Frumkin
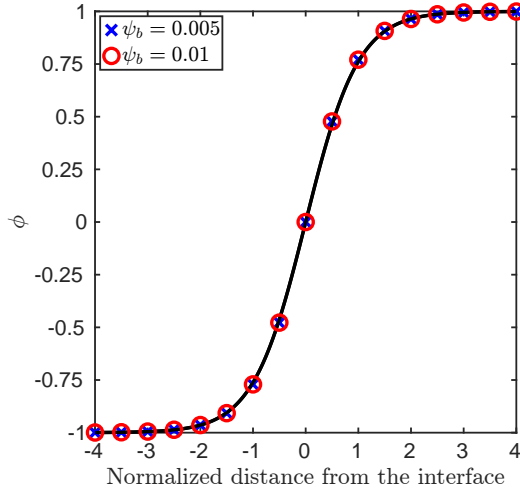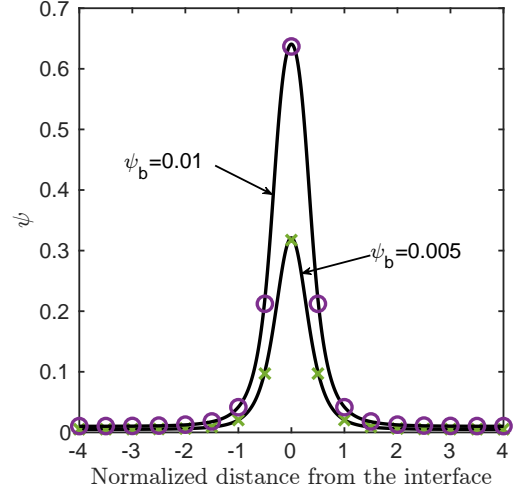
(a) $\phi$-profile for Langmuir isotherm



(b) $\psi$-profile for Langmuir isotherm
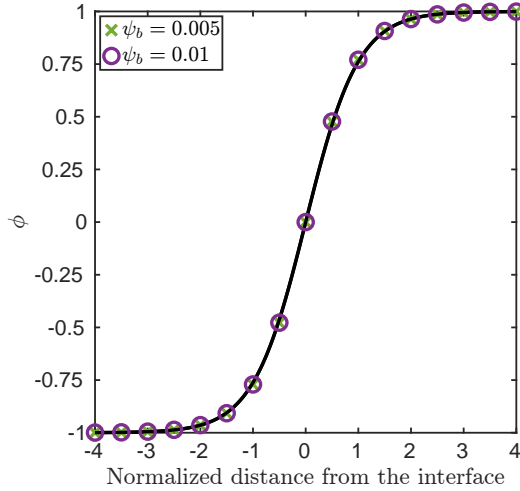


(c) $\phi$-profile for Frumkin isotherm



(d) $\psi$-profile for Frumkin isotherm

Figure 3.1: Planar interface results of the different isotherms for low surfactant concentrations, $\psi_b = \{0.005, 0.01\}$, $Ex = 0.17$, $\lambda_1 = \lambda_2 = 1$. The solid lines and markers represent the analytical and numerical solutions, respectively.

isotherms shows the significant difference in the value of surfactant concentration at the interface for a given bulk surfactant concentration.

Next, we show the results of the proposed model when applied to high concentrations of surfactants. Bulk surfactant concentrations were set as $\psi_b = 0.5$ and $\psi_b = 0.2$ for the Langmuir ($C = 0$) and Frumkin ($C = 2k_BT$) isotherms, respectively. The rest of the settings are the same as for the case of low surfactant concentration. The

50

profiles of $\phi$ and $\psi$ are given in Figures 3.2(a) and (b), respectively. Our results show that following proper selection of $\lambda_2$ from the stability condition (2.49), the proposed model gives physical results for high values of $\psi_b$. The key outcome here is that the $\phi$ profile is not affected by the high surfactant load at the interface and follows the analytical prediction for both isotherms.
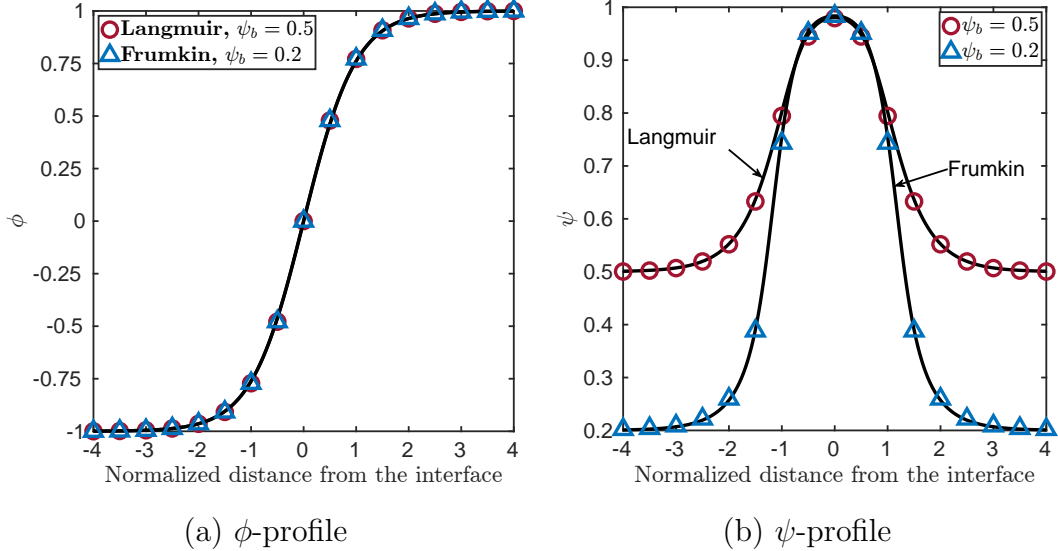


Figure 3.2: Planar interface results for high surfactant concentrations: Langmuir isotherm $(C = 0)$ & $\psi_b = 0.5$ and Frumkin isotherm $(C = 2k_BT)$ & $\psi_b = 0.2$, $Ex = 0.17$, $\lambda_1 = \lambda_2 = 1$. The solid curves and markers represent the analytical and numerical solutions, respectively.

To compare the performance of our model with the performance of the models proposed in Refs. [65], [81] & [66], we set $\lambda_2 = 0.5$ in our model. This case makes the comparison of the surfactant profile consistent by ensuring the same mathematical expression of $\Psi_c(x)$ for all models. Following Eq. (2.55), $\lambda_2 = 0.5$ gives $(\psi_0)_{lim} = 2$ (i.e., $(\psi_0)_{lim} > 1$), indicating that this choice of $\lambda_2$ does not affect the stability of simulations for high concentrations of surfactants.

We consider the Langmuir isotherm with the bulk surfactant concentration $\psi_b = 0.03$. The rest of the settings are selected as follows: $\sigma_0 = 0.02$ [lu], $\xi_0/\Delta x = 2$ [lu], $M_\phi = 0.2$, $M_\psi = 0.03$, $\psi_c(0) = 0.02$, and $Ex = 1$. The $\phi$ and $\psi$ profiles obtained using different models are represented in Figures 3.3(a) and (b), respectively. From Figure

3.3(a), we see that the interface thickness decreases and increases with increasing surfactant concentration for the models proposed by van der Sman and van der Graaf [65] and Engblom et al. [81], respectively. The interface thickness behaves as expected from the definition of $\xi$ for these models after ensuring $\phi_b^2 \approx 1$. Change in $\xi$ due to surfactant concentration is considered a numerical artifact because the chemical structure or orientation of the surfactant is not considered in diffuse interface models. As a result, most research groups have removed the presence of $\psi$-terms from $\mu_\phi$ to keep $\xi$ constant. This is the case for the model proposed by Shi et al. [66], which demonstrates no change in $\xi$ at high surfactant loads. In Figure 3.3(b), the significant difference in the prediction of the surfactant concentration at the interface between the model of van der Sman and van der Graaf [65] and other models is mainly due to the discretization error in the calculation of $(\partial_\beta \psi)$. Removal of the term $D(\partial_\beta \phi)(\partial_\beta \psi)$ from $\mu_\phi$, Eq. (2.22a), resolves the issue of overpredicting $\psi_0$ but the remaining term $D\psi\partial_{\beta\beta}^2\phi$ still leads to the interface sharpening phenomenon as shown in Ref. [83].

It is also necessary to discuss the numerical stability of different models. Models based on squared-gradients, including the models of van der Sman and van der Graaf [65] and Liu and Zhang [42], are susceptible to instability at high concentrations of surfactant and restrict the choice of simulation parameters [81]. The model of Engblom et al. [81] is more stable than the models of van der Sman and van der Graaf [65] and Shi et al. [66] for a wide range of simulation parameters due to the use of the gradient-free nascent delta function. Considering the same set of parameters as above, we confirmed that the results of the van der Sman and van der Graaf [65] and Shi et al. [66] become unstable for $Ex = 1$ and high $\psi_b$ values. The model of Shi et al. [66] gives accurate and physical results for high values of $\psi_b$ ($\psi_b = 0.3$) and low values of $Ex$ ($Ex = 0.17$). The advantage of our model is that it retains the $\psi$ terms in $\mu_\phi$ as opposed to the suggestion of Yun et al. [80] to neglect these terms, and it gives a stable interfacial profile without exhibiting the interface sharpening phenomenon as observed in the model of van der Sman and van der Graaf [65] and

the interface broadening phenomenon as observed in the model of Engblom et al. [81] for high surfactant concentrations.
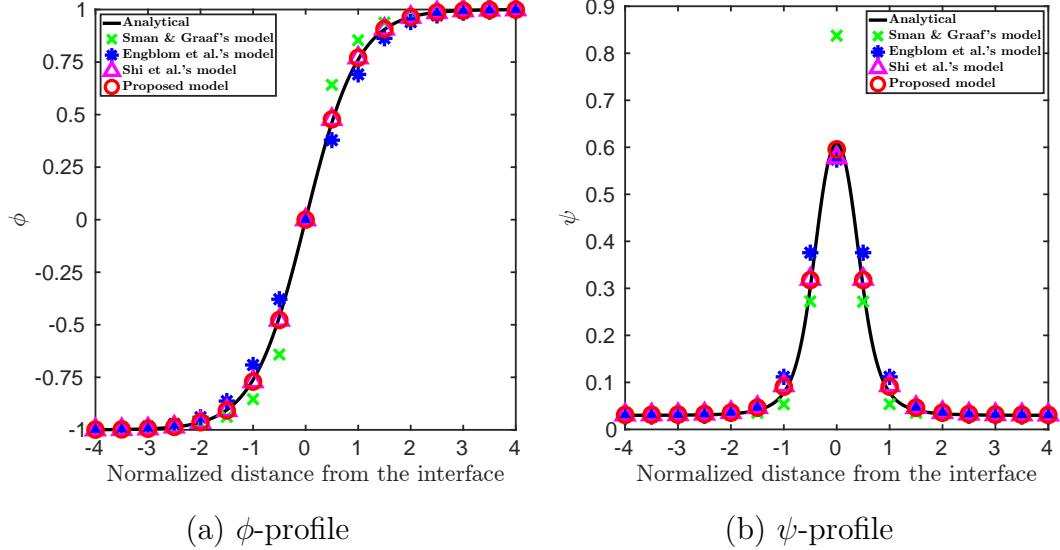


(a) $\phi$-profile

(b) $\psi$-profile

Figure 3.3: Planar interface results of the different models discussed in Section 2.4 considering the Langmuir isotherm for $\psi_b = 0.03$ with the common parameter set: $\sigma_0 = 0.02$ [lu], $\xi_0/\Delta x = 2$ [lu], $M_\phi = 0.2$, $M_\psi = 0.03$, $\psi_c(0) = 0.02$ & $Ex = 1$.

Finally, we discuss the performance of the general model for high concentrations of surfactants with $\lambda_2 = \{1, 5\}$, $Ex = 0.17$, and the remaining set of parameters as the same as for the previous case. The necessary conditions proposed by Toth and Kvamme [82] to keep $\phi_b^2 \approx 1$ and $\xi$ constant as mentioned in Section 2.5 are also satisfied. The presence of the term $D\lambda_1(\partial_\beta\phi)(\partial_\beta\psi)$ in $\mu_\phi$, Eq. (2.11a), causes instability or unphysical results due to discretization errors in the gradient calculations for high $\psi_b$ values. Simulations of low surfactant concentrations are also carried out for $\lambda_2 = 0.5$ and $Ex = 1$, which means that the presence of $\psi$ terms should not affect $\mu_\phi$. However, we obtained inaccurate results and noticed the interface-sharpening phenomenon. For more accurate results, we recommend improving the finite difference stencils used for the Laplacian and gradient calculations and/or increasing the initial interface thickness ($\xi_0/\Delta x$).

Overall, the removal of the $\psi$-terms from $\mu_\phi$ suggested by Yun et al. [80], the conditions of Toth and Kvamme [82] for a general model, and the case of constant

thickness of our model, all lead to constant thickness of the interface for high values of $\psi_b$. The advantage of our model is that it inherits a physically consistent definition of $\xi$ as a function of the surfactant concentration. In addition, the conditions of our model to keep $\xi$ constant and $\phi_b^2 = 1$ are not as stringent as the conditions suggested by Toth and Kvamme [82] for the general model. Furthermore, our model produces stable and accurate results for high concentrations of surfactants at the interface (that is, $\psi_0 \approx 1$).

## 3.2 Drop in equilibrium

We proceed with the results of a single spherical drop equilibration in a quiescent immiscible liquid obtained with the proposed model. The drop of radius $R = 32$ [lu] is placed in the centre of a fully periodic domain of $128 \times 128 \times 128$ [lu]. Similar to a planar interface initialization, we use analytical solutions to initialize the profiles of $\phi$ and $\psi$ for drop simulations. We consider the following set of simulation parameters: $\sigma_0 = 0.02$ [lu], $\xi_0/\Delta x = 2$ [lu], $M_\phi = 0.2$, $M_\psi = 0.03$, $\psi_c(0) = 0.02$, $Ex = 0.17$, $C = 0$ (that is, Langmuir isotherm), $\lambda_2 = 1$ and $\lambda_1 = \lambda_2$.

The equilibrium fields of $\phi$ and $\psi$ for $\psi_b = \{0.005, 0.5\}$ on a two-dimensional cross-section $xy$ plane at $z = 64$ [lu] are presented in Figure 3.4. The $\phi$-fields, as shown in Figure 3.4(a) and (c) are stable and do not exhibit any interface-related problems for both low and high surfactant concentrations. The surfactant distribution over the interface is more uniform for higher bulk surfactant concentration $\psi_b = 0.5$ (Figure 3.4(d)) vs Figure 3.4(b)).

To quantify the accuracy of the results, we plot the order parameter profiles for the Langmuir isotherm with $\psi_b = \{0.005, 0.5\}$ and for the Frumkin isotherm ($C = 2k_BT$) with $\psi_b = \{0.005, 0.2\}$ along a line segment starting from $x = 24$ [lu] to $x = 40$ [lu] for the fixed planes $y = 64$ & $z = 64$ [lu]. Profiles of $\phi$ and $\psi$ for the Langmuir and Frumkin isotherms are shown in Figure 3.5.

As seen in Figures 3.5(a) and (c), the profiles of $\phi$ at $\psi_b = 0.005$ are shifted
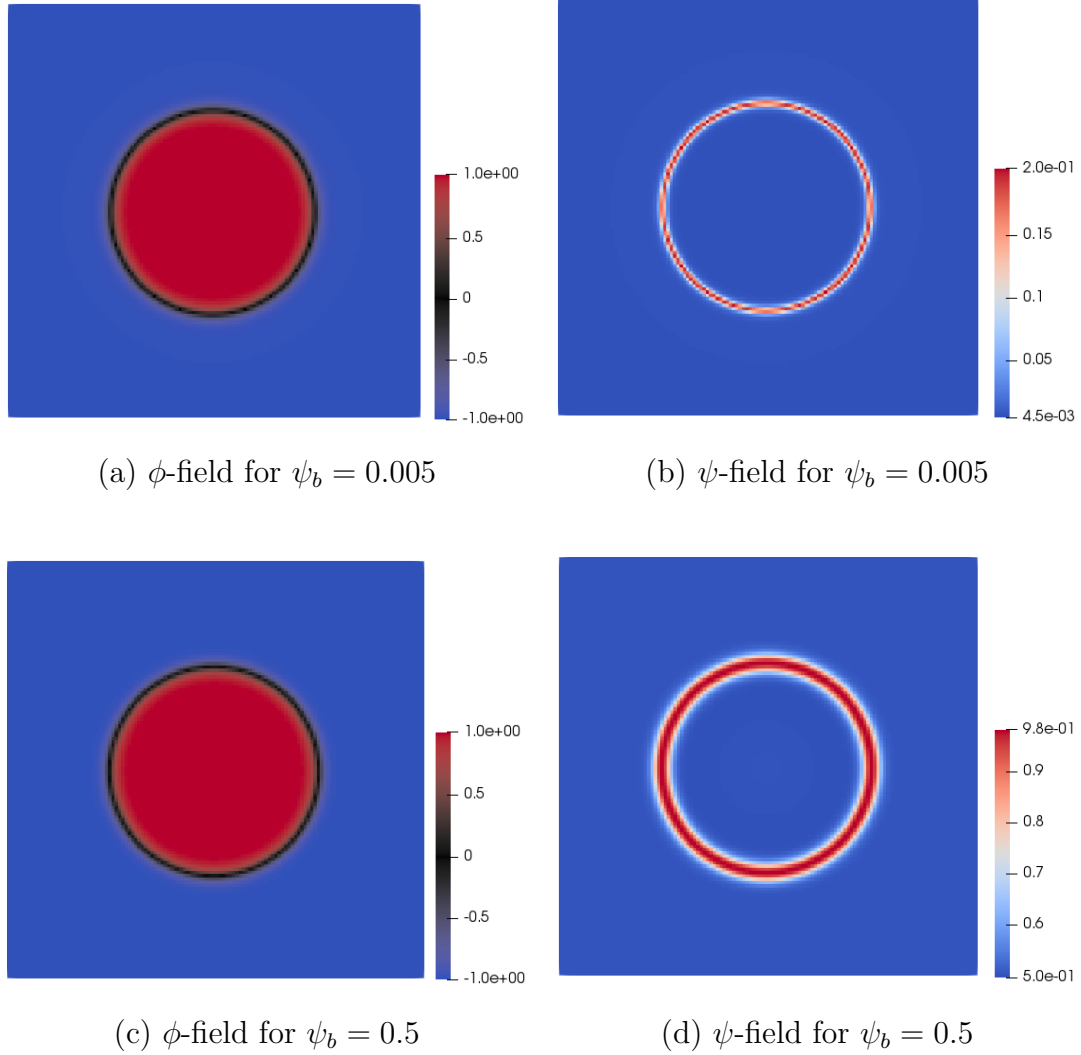
(a) $\phi$-field for $\psi_b = 0.005$

(b) $\psi$-field for $\psi_b = 0.005$

(c) $\phi$-field for $\psi_b = 0.5$

(d) $\psi$-field for $\psi_b = 0.5$

Figure 3.4: Fields of the solvent composition and surfactant concentration considering the Langmuir isotherm on the $xy$-plane for $\psi_b = \{0.005, 0.5\}$.

from the expected location of $x = 32$ [lu] due to the shrinkage of the drop volume caused by the use of the double well potential [98]. The presence of surfactant at low concentrations does not inhibit this phenomenon. However, at high surfactant concentrations, $\phi$ profiles are not significantly affected by the shrinkage effect and the location of the interface is close to $x = 32$ [lu]. In addition, the numerically predicted profiles of $\phi$ for high surfactant concentrations agree well with analytical solutions compared. To mitigate the drop dissolution effect, we recommend incorporating the penalty flux in the Cahn-Hilliard equation for $\phi$, as suggested by Li et al. [99].
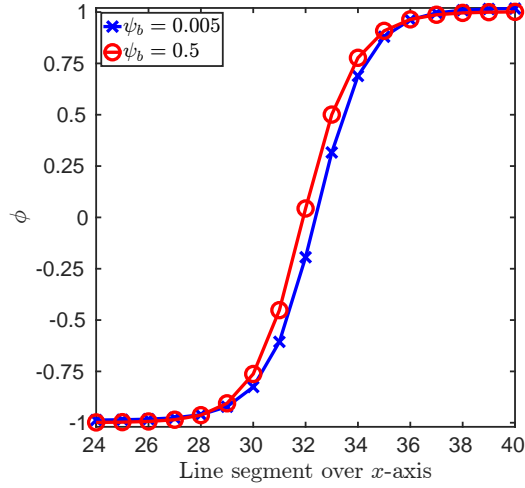
(a) $\phi$-profile for Langmuir isotherm
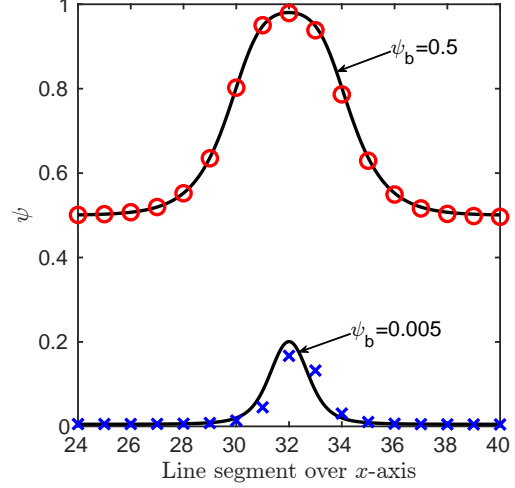
(b) $\psi$-profile for Langmuir isotherm
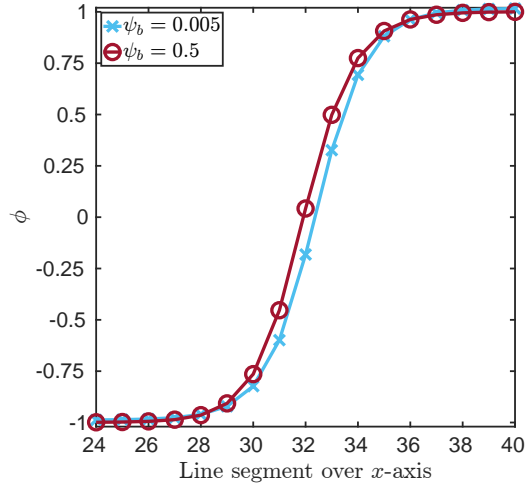
(c) $\phi$-profile for Frumkin isotherm
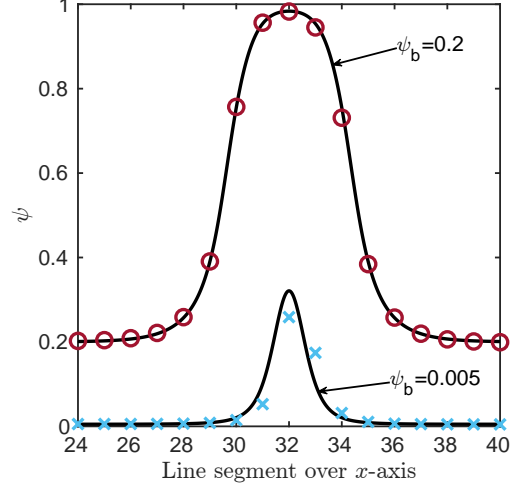
(d) $\psi$-profile for Frumkin isotherm

Figure 3.5: Profiles of the solvent composition and surfactant concentration on the line segment considering Langmuir and Frumkin isotherms for $\psi_b = \{0.005, 0.5\}$. The black solid lines and markers represent the analytical and numerical solutions, respectively.

In addition, the discretization errors in the $\psi$ profiles for $\psi_b = 0.005$ as shown in Figures 3.5 (b) and (d) are more apparent due to $\psi_b \ll \psi_c(0)$, which makes the approximation of $\psi$ values in the interfacial region for low surfactant concentrations less accurate with $\xi_0/\Delta x = 2$ [lu]. Consequently, the surfactant value at the interface and $\psi$ profile over different line segments for the low surfactant concentrations vary

more than the high surfactant concentrations.

To explore the equilibrium drop shape and uniformity of the drop coverage by surfactant, we calculated the mean and standard deviation of the order parameters and their gradients for the Langmuir isotherm at the different radii values starting from the droplet centre in the same way as suggested by Kendon et al. [85]. The mean and standard deviation of $\phi$ & $\nabla\phi$ and $\psi$ & $\nabla\psi$ at different radii values are represented in Figure 3.6.

The gap between the profiles of $\phi$ and $\nabla\phi$ for $\psi_b = \{0.005, 0.5\}$ (Figure 3.6(a) and (b)) indicates the apparent decrease in drop volume for $\psi_b = 0.005$ compared to $\psi_b = 0.5$. Furthermore, the error bars, that is, standard deviations, are higher for $\psi_b = 0.005$ in the profiles of $\psi$ and $\nabla\psi$ that denote the high discretization errors in the interfacial region for low surfactant concentrations (Figure 3.6 (b) and (d)). The discretization errors in the profile of $\psi$ for low surfactant concentrations can be decreased by taking the large values of $\xi_0/\Delta x$.

Understanding the effect of $\lambda_2$ on the surfactant concentration profile is important and discussed here. Simulations are performed for $\lambda_2 = \{1, 2, 5\}$ and $\psi_b = 0.003$ with the remaining parameters the same as above for the Langmuir isotherm. Note that $\psi_b = 0.003$ is taken for $\lambda_2 = \{1, 2, 5\}$ using the stability criterion (2.49). The profiles of $\phi$ and $\psi$ along the line segment starting from $x = 24$ [lu] to $x = 40$ [lu] for fixed planes $y = 64$ & $z = 64$ are shown in Figure 3.7(a) and Figure 3.7(b), respectively. Here, the analytical solutions of $\phi$ and $\psi$ are not shown in the comparison, as the purpose of this discussion is to demonstrate the significance of $\lambda_2$ on the results. Due to the shrinkage effect, the shift in $\phi$ profiles for $\lambda_2 = \{1, 2, 5\}$ occurs as seen in Figure 3.7(a); otherwise, the profile of $\phi$ is not affected by the presence of $\lambda_2$ because of the condition $\lambda_1 = \lambda_2$. In Figure 3.7(b), the visible difference in the profile of surfactant for different $\lambda_2$ values can be correlated with the packing of surfactant molecules along the interfacial region, and the packing or arrangement of surfactant molecules varies based on the chemical structure of the surfactant. The large value of
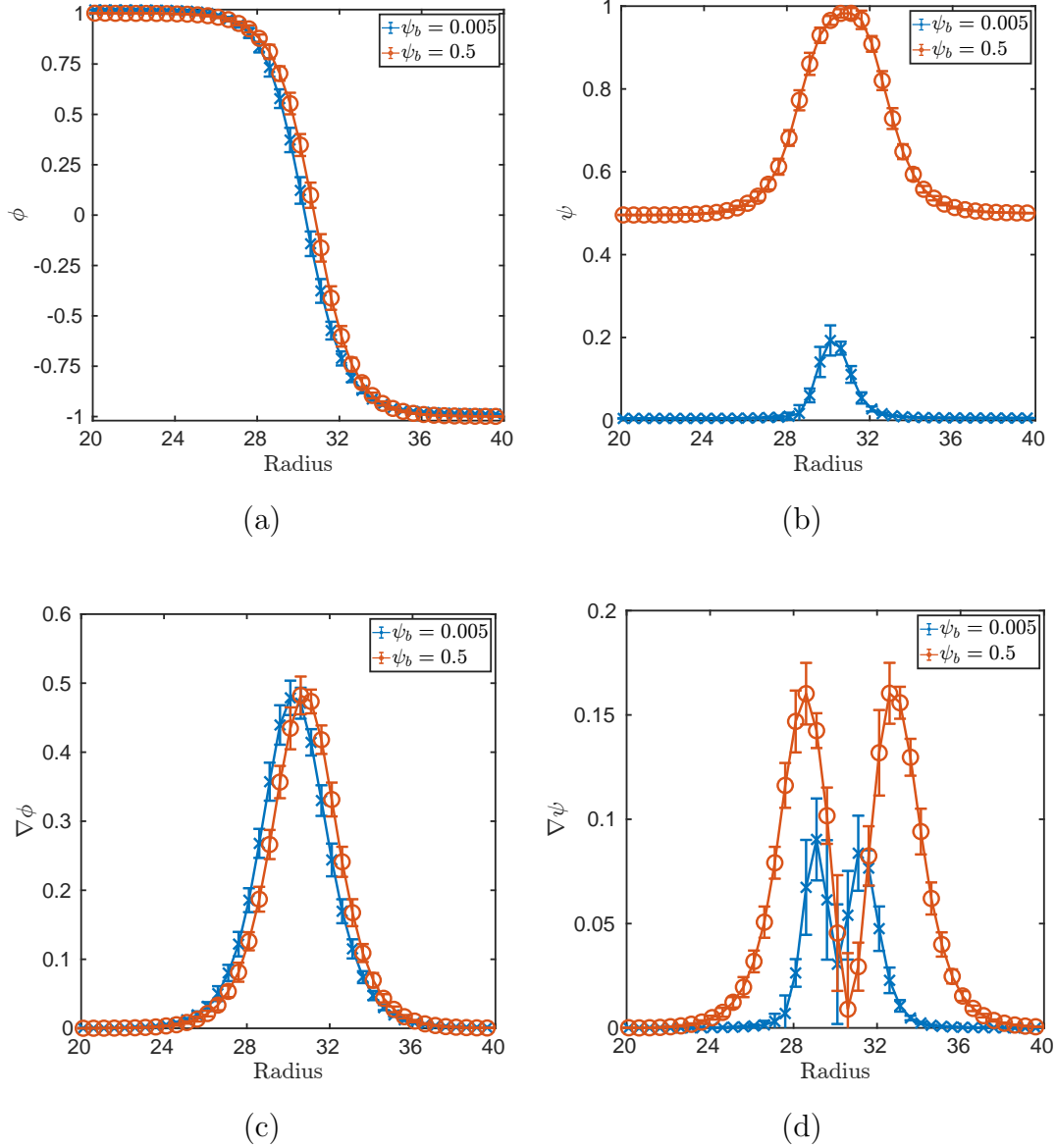
Figure 3.6: Mean and standard deviation of order parameters and their gradients at different radii values considering Langmuir isotherm for $\psi_b = \{0.005, 0.5\}$. Mean and standard deviation values are depicted as markers and error bars, respectively.

$\lambda_2$ can be considered to mimic the type of surfactant with dense packing of surfactant molecules compared to the small value of $\lambda_2$ exhibiting the loosely packed arrangement of surfactant molecules. It is demonstrated in Figure 3.7(b) describing the narrow thickness, which means the compact packing for $\lambda_2 = 5$ compared to the same for $\lambda_2 = \{1, 2\}$. Note that the difference in the $\psi$ profile for different $\lambda_2$ values is not due to numerical errors. The interpretation of $\lambda_2$ is different from $Ex$, i.e., $W$, because
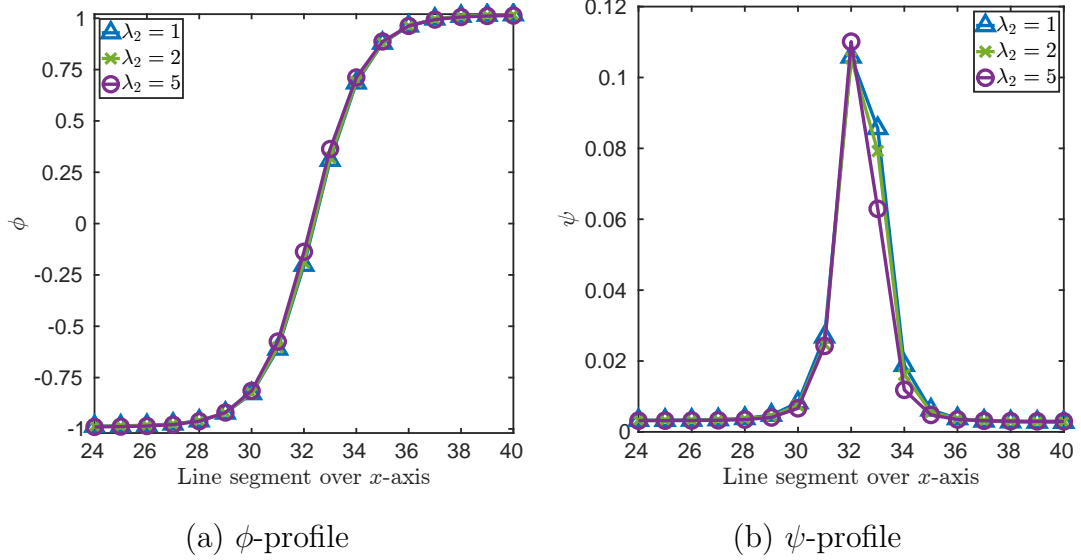
(a) $\phi$-profile          (b) $\psi$-profile

Figure 3.7: Profiles of the solvent composition and surfactant concentration on the line segment considering the Langmuir isotherm for $\lambda_2 = \{1, 2, 5\}$ & $\psi_b = 0.003$.

$Ex$ is introduced in the free energy functional to numerically stabilize the diffuse-interface models [20]; whereas $\lambda_2$ has the potential to represent the nature of different surfactants and their effects on the surface tension reduction for the case of constant thickness.

## 3.3 Surface tension

In this section, we assess the proposed model's capability to capture a surface tension reduction. We compare the numerical predictions of the surface tension reduction to the analytical solution derived based on the thermodynamic approach as mentioned in Section 2.6. The numerical results of the surface tension are calculated using the Laplace pressure:

$$\Delta p_b = \frac{2\sigma}{R} \tag{3.1}$$

Here, $p_b$ is the bulk pressure defined by Eq. (2.25e), and $\sigma$ is the surface tension. The numerical results of the surface tension obtained from Eq. (3.1) are compared to the results of the analytical equation (2.57) by fitting the value of the parameter $\alpha$.

We set $\psi_c(0) = 0.02$ for the Langmuir ($C = 0$) and Frumkin ($C = 2k_BT$) isotherms. The values of $\lambda_2$ for the Langmuir and Frumkin isotherms are $\lambda_2 = \{1, 2, 5, 10\}$ and $\lambda_2 = \{1, 2, 5\}$, respectively. From Eq. (2.55), the limiting values of $\psi_0$ for $\lambda_2 = \{1, 2, 5, 10\}$ are $(\psi_0)_{lim} = \{1, 0.5, 0.2, 0.1\}$. For both isotherms, the ranges of $\psi_b$ values are determined based on their corresponding $(\psi_b)_{lim}$ values obtained using Eq. (2.53).

The next step is to specify the values of the surfactant mobility $M_\psi$ and the surfactant solubility $Ex$ that give stable simulations and accurate results for selected $\lambda_2$ values. We deem simulations accurate when the relative error in the numerical prediction of $\psi_0$ compared to the analytical estimate, $(\psi_0)_{RE} = |((\psi_0)_a - (\psi_0)_n)/(\psi_0)_a| \cdot 100\%$, is less than 5%, and the maximum magnitude of spurious velocity, $u_{max}$, is at the order of or less than $10^{-4}$.

To identify the appropriate values of $M_\psi$ and $Ex$, we performed the sensitivity analysis of drop equilibration with respect to $M_\psi = \{0.001, 0.005, 0.01, 0.02, 0.03, 0.05, 0.1\}$ and $Ex = \{0.05, 0.1, 0.17, 0.25\}$. We simulated a drop of radius $R = 32$ [lu] with $\sigma_0 = 0.02$ [lu], $\xi_0/\Delta x = 2$ [lu], $M_\phi = 0.2$, and $\psi_c(0) = 0.02$ in the domain size of $128 \times 128 \times 128$ [lu]. We found that low $M_\psi$ values ($M_\psi < 0.01$) give stable results for low surfactant concentrations ($\psi_b < 0.002$) for a given combination of $\lambda_2$ and $Ex \geq 0.1$ but our criterion of accuracy is not satisfied. The relative error, $(\psi_0)_{RE}$, exceeds 5% because $\psi_b \ll \psi_c(0)$ leads to high discretization errors in gradient calculation that are amplified even more with increasing $\lambda_2$. At the same time, the decrease in $Ex$ promotes the diffusion of surfactants that smooths the gradients of surfactant concentration and, as a result, improves the accuracy of numerical results for high $\lambda_2$ values. Furthermore, the simulations become unstable for high surfactant concentrations ($\psi_b > 0.3$) with low $M_\psi$ values. Based on this analysis, we selected $M_\psi = 0.005$ for $\lambda_2 = \{1, 2, 5\}$ and $M_\psi = 0.001$ for $\lambda_2 = 10$ with a fixed value of $Ex = 0.05$ for considered $\lambda_2$ values.

With the selected surfactant mobility and solubility values, we estimate the reduc-

tion of surface tension as the surfactant accumulates at the interface of the equilibrating drop. The relation between the reduction of the surface tension compared to the surface tension of the pure system, $\sigma_0$, $\left(\text{i.e. } \dfrac{\Delta\sigma}{\sigma_0} = \dfrac{\sigma(\psi_0) - \sigma_0}{\sigma_0}\right)$ and $\psi_0$ for the Langmuir and Frumkin isotherms are represented in Figure 3.8.



(a) Langmuir isotherm
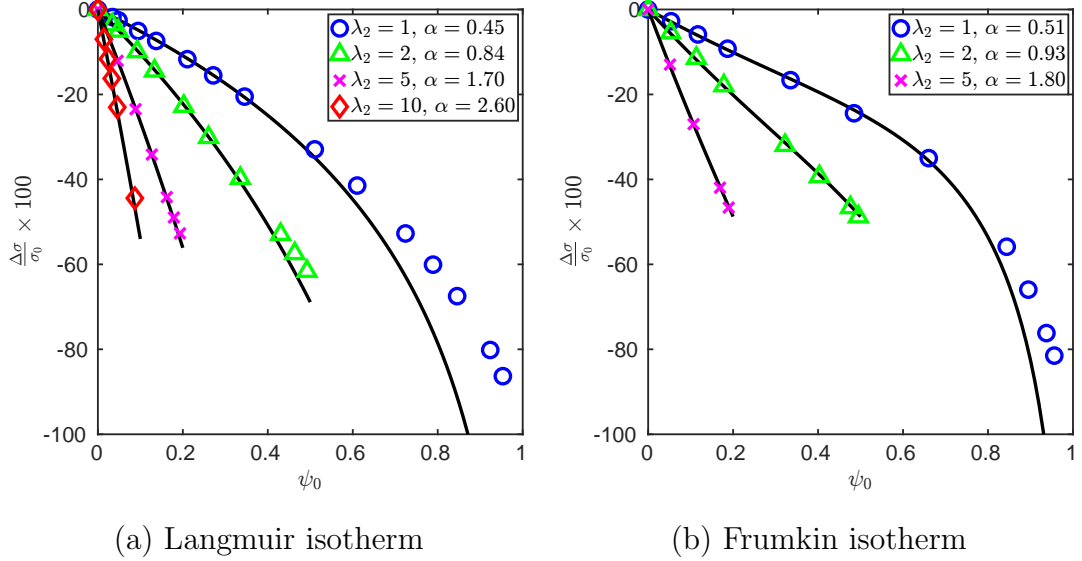
(b) Frumkin isotherm

Figure 3.8: The reduction of surface tension as a function of $\psi_0$ for different values of $\lambda_2$ for the Langmuir (a) and Frumkin (b) isotherms. The solid curves and markers represent the analytical and numerical solutions, respectively.

The numerical results are compared to the analytical solutions until $(\psi_0)_{lim}$-values because exceeding $(\psi_0)_{lim}$ for a given $\lambda_2$ results in the unstable simulations according to Eq. (2.49). The quantitative comparison is achieved by calculating the relative deviation between the numerically predicted value of the surface tension reduction and the corresponding value calculated using the equation of state Eq. (2.57): $(\sigma)_{RE} = \left| \dfrac{\Delta\sigma - (\Delta\sigma)_{EOS}}{(\Delta\sigma)_{EOS}} \right| \cdot 100\%.$

As shown in Figure 3.8(a) for the Langmuir isotherm, the numerical results for $\lambda_2 = \{1, 2, 5, 10\}$ agree with their analytical solutions with $(\sigma)_{RE} < 10\%$ up to $\psi_0 = \{0.5, 0.49, 0.19, 0.09\}$, respectively. As expected, the numerical results at $\lambda_2 = 1$ do not follow the analytical solutions for high surfactant concentrations (i.e., $\psi_0 > 0.5$). This confirms that this isotherm should not be used for high surfactant concentrations.

Compared to most existing free energy models, our model demonstrates a higher surface tension reduction at lower surfactant concentrations, which is highly desirable for comparing the surface tension results with the experimental findings. The surface tension reduction for the Langmuir isotherm follows the experimental results observed in Refs. [100] and [101], where the range of surface tension reduction for the liquid-liquid system is between $30 - 60\%$ of $\sigma_0$. Furthermore, by varying $\lambda_2$, our model replicates the effect of different surfactants on the reduction of surface tension without accounting for their chemical structures.

For the Frumkin isotherm, the numerical results for $\lambda_2 = 1$ follow the analytical solutions for the high concentrations of surfactants, and it is consistent up to $\psi_0 \leq 0.8$ as shown in Figure 3.8(b). For low surfactant concentrations, the Frumkin isotherm reduces to the Langmuir isotherm, as the numerical results of both isotherms at low surfactant concentrations (i.e. $\psi_0 \leq 0.15$) become similar.

The proposed model decreases surface tension by increasing the strength of non-linear surfactant couplings, i.e., $\lambda_2$ & $\lambda_1$, and enhancing the diffusion of surfactant, i.e., increasing $W$ or decreasing $Ex$. In most existing models, decreasing $Ex$ is the only way to reduce surface tension, which may be the reason behind the inability of these models to obtain a significant reduction in $\sigma$ at low surfactant concentrations.

In the free energy models discussed in this study, the relation between $Ex$ and the change in $\alpha$ is investigated for several cases and it can be concluded that the surface tension reduction increases with the decrease in $Ex$ but these models do not have $\lambda_1$ and $\lambda_2$ terms. So, it is important to explain the change in $\alpha$ due to $\lambda_2$ for a given value of $Ex$. $\alpha$ varies depending on the increase in $k_B T$ caused by the combination $Ex$ and $\lambda_2$. The analytical prediction of surface tension reduction is significant compared to the numerical reduction for low $Ex$ values (i.e., $Ex = 0.05$) that makes $\alpha < 1$ for small values of $\lambda_2$. However, this disparity between the analytical and numerical results can be compensated by increasing the value of $\lambda_2$ for a given $Ex$. For this case, the analytical as well as numerical results of surface tension are substantial at

low surfactant concentrations making $\alpha > 1$ for large values of $\lambda_2$.

Overall, the increase in $\lambda_2$ decreases the surface tension more significantly than the reduction of the same due to the decrease in $Ex$. Moreover, the increase in the value of $\alpha$ due to the increase in $Ex$ is higher for large values of $\lambda_2$ compared to small values of $\lambda_2$.

Taking into account the simulation results of the Langmuir isotherm shown in Figure 3.8(a), the comparison of analytical & numerical values of $\psi_0$ and the variation in the maximum magnitude of the spurious velocity $u_{max}$ over a range of $\psi_0$ for $\lambda_2 = \{1, 2, 5, 10\}$ are represented in Figure 3.9(a) and (b), respectively. Similar to
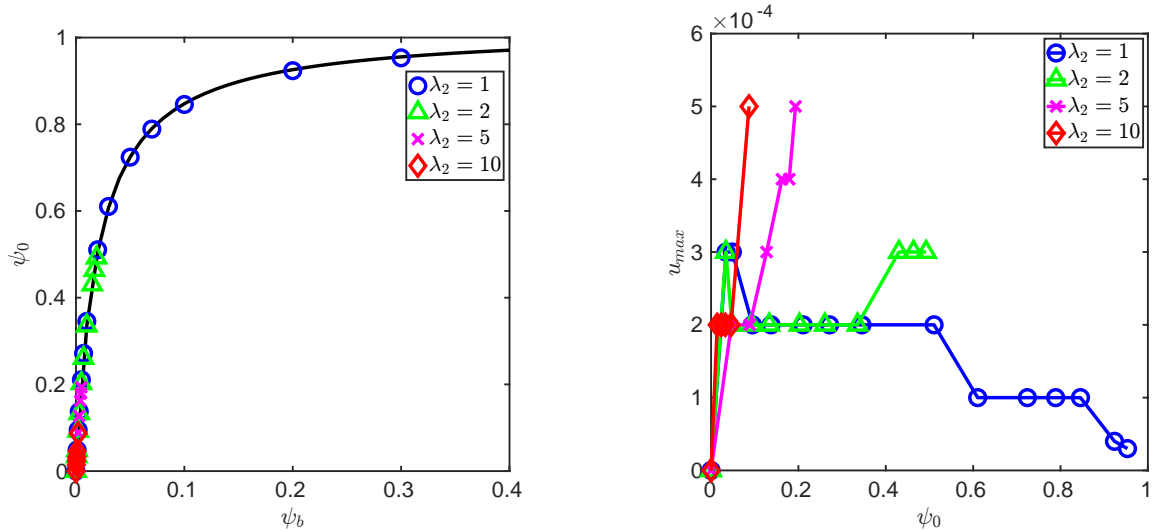


(a) Surfactant concentration at the interface   (b) Magnitude of maximum spurious velocity

Figure 3.9: (a) Analytical & numerical results of $\psi_0$ as a function of $\psi_b$ and (b) the magnitude of maximum spurious velocity as a function $\psi_0$ for the Langmuir isotherm, $\lambda_2 = \{1, 2, 5, 10\}$, and $Ex = 0.05$. The solid curves and markers correspond to the analytical and numerical solutions, respectively.

$Ex$, $\lambda_2$ does not affect the surfactant concentration at the interface. The numerical results of $\psi_0$ accurately follow the analytical solutions for low and high surfactant concentrations as shown in Figure 3.9(a), despite the considerable discretization error in the results of low surfactant concentrations due to $\psi_b \ll \psi_c(0)$ that magnifies the value of $u_{max}$ as shown in Figure 3.9(b).

As $\psi_0 \geq (\psi_0)_{lim}$, the simulation becomes unstable due to the stability criterion (2.49) that triggers the sudden increase in $u_{max}$ for $\lambda_2 = \{2, 5, 10\}$. The increase in $u_{max}$ for high values of $\lambda_2$ is due to $\psi_0 \approx (\psi_0)_{lim}$ and the discretization errors caused by low $\psi_b$ values. For these extreme cases, the numerical results of the order parameters are stable and physical. Increasing the thickness of the clear interface thickness $(\xi_0/\Delta x)$ or improving the finite difference stencils for gradient calculations can decrease the magnitude of spurious velocities.

# Chapter 4

# Conclusions and future work

## 4.1 Conclusions

We proposed a diffuse interface free energy model based on a modification of the Ginzburg-Landau free energy functional to simulate the system of immiscible liquids with non-ionic soluble surfactants. We made the free energy density contribution due to the adsorption of the surfactant at the interface to be a combination of the nonlocal squared-gradient and gradient-free surfactant couplings controlled by two coefficients, $\lambda_1$ and $\lambda_2$, respectively.

In the present study, we set $\lambda_1 = \lambda_2$ which means that the thickness of the interface, while being a function of the surfactant concentration, remains constant as the surfactant load increases: no interface-sharpening or interface-broadening is observed. We also neglected two terms in the expression of the chemical potential of the phase field order parameter to improve numerical stability at high surfactant concentrations and avoid perfect miscibility.

We implemented the proposed model in the free-energy-based lattice Boltzmann framework where the Navier-Stokes equations were coupled with the solution of two Cahn-Hilliard transport equations to capture the behaviour of two order parameters representing the immiscible liquids and surfactant concentration. We also derived the conditions to ensure the numerical stability of the model at high surfactant loads and outlined the procedure for selecting numerical parameters and physical quantities.

The free-energy-based LB algorithm developed in Fortran 90 was used to verify and validate the proposed model for the Langmuir and Frumkin isotherms. Two benchmark problems were simulated at low and high surfactant concentrations: a planar interface and the equilibration of a spherical drop in a quiescent medium.

The proposed model accurately predicts the order parameter profiles at high surfactant concentrations (i.e., $\psi_0 > 0.5$) with the relative deviation in capturing the maximum surfactant concentration at the interface less than 1.1%. The maximum magnitude of spurious velocity is at the order of $10^{-4}$ in the case of the spherical drop in equilibrium.

The typical way to promote the reduction of surface tension as the surfactant accumulates at the interface is by decreasing the surfactant solubility $Ex$. In our model, the increase of $\lambda_2$ & $\lambda_1$ introduces an alternative robust way to reduce the surface tension. Consequently, the reduction of surface tension based on the simultaneous decrease of $Ex$ and increase of $\lambda_2$ enables the proposed model to achieve a significant reduction of surface tension (i.e., $45 - 50\%$) at low surfactant concentrations ($0.085 < \psi_0 < 0.2$). Furthermore, varying the parameter $\lambda_2$ paves the way to mimic the effect of different types of surfactant molecules on the reduction of surface tension.

The surfactant solubility $Ex$ plays a pivotal role in establishing the numerical accuracy. We recommend selecting $Ex$ within the range of $0.05 \leq Ex \leq 0.25$ for $\lambda_2 = \{0.5, 1, 2\}$. For high $\lambda_2$ values such as $\lambda_2 = \{5, 10\}$, it is recommended to set low $Ex$ values (i.e., $Ex = 0.05$) to enhance accuracy. In addition, it is necessary to carefully select the value of the surfactant mobility $M_\psi$. We recommend $0.001 \leq M_\psi \leq 0.005$ for $\lambda_2 = \{5, 10\}$ and $0.001 \leq M_\psi \leq 0.03$ for $\lambda_2 = \{0.5, 1, 2\}$.

## 4.2   Future work

Taking into account the advantages mentioned above and the availability of the proposed model, the following studies can be conducted to extend the usability and potential of the proposed model:

- The assumption of a constant $M_\psi$ does not always provide a regular diffusional equation for $\psi$ in the bulk phase [82] that sometimes leads to unrealistic results of the surfactant profile. The implementation of variable surfactant mobility $M_\psi = \psi(1 - \psi)$ as a function $\psi$ ensures rigorous solutions of $\psi$ between 0 and 1 [81]. The procedure to incorporate the variable surfactant mobility into the free-energy LBM is needed to recover the Cahn-Hilliard equation for $\psi$ with the variable $M_\psi$.

- The penalty flux term needs to be included in the Cahn-Hilliard equation for $\phi$ to conserve the interfacial profile and to overcome the drop dissolution effect leading to the shift of the equilibrium profile of $\phi$ from its expected location as shown in Figures 3.5(a) and 3.5(b).

- Only the case of constant interface thickness is analyzed, but the phenomenon of interface-broadening based on the chemical structure of the surfactant as observed in MD [86] and DPD [87] simulations is not explored in the present study. It is crucial to first address the question regarding the physical relevance of showing this behaviour from a macroscopic point of view. Second, a methodology needs to be constructed to correlate the parameters $\lambda_1$ and $\lambda_2$ regulating the behaviour of the interface thickness with the chemical structure of different surfactant molecules in the free-energy lattice Boltzmann framework for the comparison with the results of MD [86] and DPD [87] simulations. The suggested modification could help to demonstrate the constant behaviour of surface tension after the formation of micelles by correlating $(\psi_0)_{lim}$ with CMC.

- The study of the surfactant-laden drop in shear flows is needed to further validate the usability of the proposed model and to analyze the effect of viscosity and surfactant concentration on topological changes such as drop deformation and drop breakage.

# Bibliography

[1] J. L. Burguera and M. Burguera, "Analytical applications of emulsions and microemulsions," *Talanta*, vol. 96, pp. 11–20, 2012.

[2] D. J. McClements, "Nanoemulsions versus microemulsions: Terminology, differences, and similarities," *Soft Matter*, vol. 8, pp. 1719–1729, 2012.

[3] I. Capek, "Degradation of kinetically-stable o/w emulsions," *Advances in Colloid and Interface Science*, vol. 107, pp. 125–155, 2004.

[4] H. Manikantan and T. M. Squires, "Surfactant dynamics: hidden variables controlling fluid flows," *Journal of Fluid Mechanics*, vol. 892, P1, 2020.

[5] B. Babajanzadeh, S. Sherizadeh, and H. Ranji, "Detergents and surfactants: a brief review," *Open Access Journal of Science*, vol. 3, pp. 94–99, 2019.

[6] J. C. Baret, "Surfactants in droplet-based microfluidics," *Lab on a Chip*, vol. 12, pp. 422–433, 2012.

[7] D. Myers, "An Overview of Surfactant Science and Technology," in *Surfactant Science and Technology*. John Wiley & Sons, Ltd, 2005, ch. 1, pp. 1–28.

[8] A. Pattanaik and R. Venugopal, "Role of Surfactants in Mineral Processing: An Overview," in *Surfactants and Detergents*, A. K. Dutta, Ed., IntechOpen, 2019, ch. 2, pp. 1–17.

[9] O. Massarweh and A. S. Abushaikha, "The use of surfactants in enhanced oil recovery: A review of recent advances," *Energy Reports*, vol. 6, pp. 3150–3178, 2020.

[10] A. Rashidi-Khaniabadi, E. Rashidi-Khaniabadi, B. Amiri-Ramsheh, M. R. Mohammadi, and A. Hemmati-Sarapardeh, "Modeling interfacial tension of surfactant–hydrocarbon systems using robust tree-based machine learning algorithms," *Scientific Reports*, vol. 13, no. 026705, pp. 1–19, 2023.

[11] B.-B. Lee, P. Ravindra, and E.-S. Chan, "A critical review: Surface and d interfacial tension measurement by the drop weight method," *Chemical Engineering Communications*, vol. 195, no. 8, pp. 889–924, 2008.

[12] O. E. Yildirim, Q. Xu, and O. A. Basaran, "Analysis of the drop weight method," *Physics of Fluids*, vol. 17, pp. 1–13, 2005.

[13] J. P. Garandet, B. Vinet, and P. Gros, "Considerations on the Pendant Drop Method: A New Look at Tate's Law and Harkins' Correction Factor," *Journal of Colloid and Interface Science*, vol. 165, pp. 351–354, 1994.

[14] Y. Touhami, G. H. Neale, V. Hornof, and H. Khalfalah, "A modified pendant drop method for transient and dynamic interfacial tension measurement," *Colloids and Surfaces A: Physicochemical and Engineering Aspects*, vol. 112, pp. 31–41, 1996.

[15] J. D. Berry, M. J. Neeson, R. R. Dagastine, D. Y. Chan, and R. F. Tabor, "Measurement of surface and interfacial tension using pendant drop tensiometry," *Journal of Colloid and Interface Science*, vol. 454, pp. 226–237, 2015.

[16] J. L. Cayias, R. S. Schechter, and W. H. Wade, "The Measurement of Low Interfacial Tension via the Spinning Drop Technique," *ACS Symposium Series*, vol. 8, pp. 234–247, 1975.

[17] D. Joseph, M. Arney, G. Gillberg, *et al.*, "A Spinning Drop Tensioextensiometer," *Journal of Rheology*, vol. 36, pp. 621–662, 1992.

[18] J. Viades-Trejo and J. Gracia-Fadrique, "Spinning drop method: From Young–Laplace to Vonnegut," *Colloids and Surfaces A: Physicochemical and Engineering Aspects*, vol. 302, pp. 549–552, 2007.

[19] V. V. Ginzburg, K. Chang, P. K. Jog, A. B. Argenton, and L. Rakesh, "Modeling the Interfacial Tension in Oil-Water-Nonionic Surfactant Mixtures Using Dissipative Particle Dynamics and Self-Consistent Field Theory," *The Journal of Physical Chemistry B*, vol. 115, pp. 4654–4661, 2011.

[20] O. Theissen and G. Gompper, "Lattice-Boltzmann study of spontaneous emulsification," *European Physical Journal B*, vol. 11, pp. 91–100, 1999.

[21] G. Soligo, A. Roccon, and A. Soldati, "Breakage, coalescence and size distribution of surfactant-laden droplets in turbulent flow," *Journal of Fluid Mechanics*, vol. 881, pp. 244–282, 2019.

[22] D. M. Anderson, G. B. McFadden, and A. A. Wheeler, "DIFFUSE-INTERFACE METHODS IN FLUID MECHANICS," *Annual Review of Fluid Mechanics*, vol. 30, pp. 139–165, 1998.

[23] H. Lamb, in *Hydrodynamics*. Cambridge University Press, 1932.

[24] G. K. Batchelor, in *An Introduction to Fluid Dynamics*. Cambridge University Press, 1967.

[25] J. Lighthill, in *Waves in Fluids*. Cambridge University Press, 1978.

[26] P. G. Drazin and W. H. Reid, in *Hydrodynamic Stability*. Cambridge University Press, 1981.

[27] S. H. Davis, "Contact-Line Problems in Fluid Mechanics," *Journal of Applied Mechanics*, vol. 50, pp. 977–982, 1983.

[28] H. Montazeri, S. H. Zandavi, and A. Bazylak, "Sharp interface models for two-phase flows: Insights towards new approaches," *Computer Methods in Applied Mechanics and Engineering*, vol. 322, pp. 238–261, 2017.

[29] S. O. Unverdi and G. Tryggvason, "A front-tracking method for viscous, incompressible, multi-fluid flows," *Journal of Computational Physics*, vol. 100, pp. 25–37, 1992.

[30] S. McKee, M. Tomé, V. Ferreira, *et al.*, "The MAC method," *Computers & Fluids*, vol. 37, pp. 907–930, 2008.

[31] C. Hirt and B. Nichols, "Volume of fluid (VOF) method for the dynamics of free boundaries," *Journal of Computational Physics*, vol. 39, pp. 201–225, 1981.

[32] J. A. Sethian and P. Smereka, "LEVEL SET METHODS FOR FLUID INTERFACES," *Annual Review of Fluid Mechanics*, vol. 35, pp. 341–372, 2003.

[33] M. Sussman, K. Smith, M. Hussaini, M. Ohta, and R. Zhi-Wei, "A sharp interface method for incompressible two-phase flows," *Journal of Computational Physics*, vol. 221, pp. 469–505, 2007.

[34] M. Kang, R. P. Fedkiw, and X.-D. Liu, "A Boundary Condition Capturing Method for Multiphase Incompressible Flow," *Journal of Scientific Computing*, vol. 15, pp. 323–360, 2000.

[35] L. Rayleigh, "On the theory of surface forces—II. Compressible fluids," *The London, Edinburgh, and Dublin Philosophical Magazine and Journal of Science*, vol. 33, pp. 209–220, 1892.

[36] J. D. van der Waals, "The thermodynamic theory of capillarity under the hypothesis of a continuous density variation," trans. by J. S. R. in 1979, *Journal of Statistical Physics*, vol. 20, pp. 197–244, 1893.

[37] D. J. Korteweg, "Sur la forme que prennent les equations du mouvements des fluides si l'on tient compte des forces capillairees causees par des variations de densite considerables mais continues et sur la theorie de capillarite dans l'hypothese d'une variation continue de la densite," *Arch Neerl. Sci. Exactes Nat. Ser. II*, vol. 6, pp. 1–24, 1901.

[38] J. W. Cahn and J. E. Hilliard, "Free energy of a nonuniform system. I. Interfacial free energy," *The Journal of Chemical Physics*, vol. 28, pp. 258–267, 1958.

[39] J. U. Brackbill, D. B. Kothe, and C. Zemach, "A continuum method for modeling surface tension," *Journal of Computational Physics*, vol. 100, pp. 335–354, 1992.

[40] D. M. Anderson and G. B. McFadden, "A diffuse-interface description of internal waves in a near-critical fluid," *Physics of Fluids*, vol. 9, pp. 1870–1879, 1997.

[41] D. Jacqmin, "Calculation of Two-Phase Navier–Stokes Flows Using Phase-Field Modeling," *Journal of Computational Physics*, vol. 155, pp. 96–127, 1999.

[42] H. Liu and Y. Zhang, "Phase-field modeling droplet dynamics with soluble surfactants," *Journal of Computational Physics*, vol. 229, pp. 9166–9187, 2010.

[43] M. Laradji, H. Guo, M. Grant, and M. J. Zuckermann, "The effect of surfactants on the dynamics of phase separation," *Journal of Physics: Condensed Matter*, vol. 4, pp. 6715–6728, 1992.

[44] S. Mirjalili, S. S. L. Jain, and M. S. Dodd, "Interface-capturing methods for two-phase flows : An overview and recent developments," in *Center for Turbulence Research Annual Research Briefs*, 2017, pp. 117–135.

[45] V. Khatavkar, P. Anderson, and H. Meijer, "On scaling of diffuse–interface models," *Chemical Engineering Science*, vol. 61, pp. 2364–2378, 2006.

[46] J. Shaikh, A. Sharma, and R. Bhardwaj, "On comparison of the sharp-interface and diffuse-interface level set methods for 2D capillary or/and gravity induced flows," *Chemical Engineering Science*, vol. 176, pp. 77–95, 2018.

[47] H. E. Stanley, in *Introduction to Phase Transitions and Critical Phenomena*. Oxford University Press, 1971.

[48] L. S. Pan, J. Lou, H. Y. Li, and C. W. Kang, "A diffuse interface model for two-phase flows with phase transition," *Physics of Fluids*, vol. 31, pp. 1–12, 9 2019.

[49] G. Zhu and A. Li, "Interfacial dynamics with soluble surfactants: A phase-field two-phase flow model with variable densities," *Advances in Geo-Energy Research*, vol. 4, pp. 86–98, 2020.

[50] O. Shardt, S. K. Mitra, and J. J. Derksen, "The Critical Conditions for Coalescence in Phase Field Simulations of Colliding Droplets in Shear," *Langmuir*, vol. 30, pp. 14 416–14 426, 2014.

[51] T. Krüger, H. Kusumaatmaja, A. Kuzmin, O. Shardt, G. Silva, and E. M. Viggen, "Numerical Methods for Fluids," in *The Lattice Boltzmann Method: Principles and Practice*. Springer International Publishing, 2017, ch. 2, pp. 31–56.

[52] M. Muradoglu and G. Tryggvason, "A front-tracking method for computation of interfacial flows with soluble surfactants," *Journal of Computational Physics*, vol. 227, pp. 2238–2262, 2008.

[53] I. B. Bazhlekov, P. D. Anderson, and H. E. H. Meijer, "Boundary integral method for deformable interfaces in the presence of insoluble surfactants," in *Large-Scale Scientific Computing*, I. Lirkov, S. Margenov, J. Waśniewski, and P. Yalamov, Eds., Springer Berlin Heidelberg, 2004, pp. 355–362.

[54] I. B. Bazhlekov, P. D. Anderson, and H. E. Meijer, "Numerical investigation of the effect of insoluble surfactants on drop deformation and breakup in simple shear flow," *Journal of Colloid and Interface Science*, vol. 298, pp. 369–394, 2006.

[55] K. Feigl, D. Megias-Alguacil, P. Fischer, and E. J. Windhab, "Simulation and experiments of droplet deformation and orientation in simple shear flow with surfactants," *Chemical Engineering Science*, vol. 62, pp. 3242–3258, 2007.

[56] G. Falcucci, S. Ubertini, C. Biscarini, *et al.*, "Lattice Boltzmann Methods for Multiphase Flow Simulations across Scales," *Communications in Computational Physics*, vol. 9, pp. 269–296, 2011.

[57] Q. Li, K. Luo, Q. Kang, Y. He, Q. Chen, and Q. Liu, "Lattice Boltzmann methods for multiphase flow and phase-change heat transfer," *Progress in Energy and Combustion Science*, vol. 52, pp. 62–105, 2016.

[58] S. Chen and G. D. Doolen, "LATTICE BOLTZMANN METHOD FOR FLUID FLOWS," *Annual Review of Fluid Mechanics*, vol. 30, pp. 329–364, 1998.

[59] H. L. Wang, Z. H. Chai, B. C. Shi, and H. Liang, "Comparative study of the lattice Boltzmann models for Allen-Cahn and Cahn-Hilliard equations," *Physical Review E*, vol. 94, no. 033304, pp. 1–7, 2016.

[60] Y. Zong, C. Zhang, H. Liang, L. Wang, and J. Xu, "Modeling surfactant-laden droplet dynamics by lattice Boltzmann method," *Physics of Fluids*, vol. 32, no. 122105, pp. 1–17, 2020.

[61] M. R. Swift, E. Orlandini, W. R. Osborn, and J. M. Yeomans, "Lattice Boltzmann simulations of liquid-gas and binary fluid systems," *Physical Review E*, vol. 54, pp. 5041–5052, 1996.

[62] T. Inamuro, T. Ogata, S. Tajima, and N. Konishi, "A lattice Boltzmann method for incompressible two-phase flows with large density differences," *Journal of Computational Physics*, vol. 198, pp. 628–644, 2004.

[63] T. Lee and C.-L. Lin, "A stable discretization of the lattice Boltzmann equation for simulation of incompressible two-phase flows at high density ratio," *Journal of Computational Physics*, vol. 206, pp. 16–47, 2005.

[64] R. van der Sman and S. van der Graaf, "Emulsion droplet deformation and breakup with Lattice Boltzmann model," *Computer Physics Communications*, vol. 178, pp. 492–504, 2008.

[65] R. van der Sman and S. van der Graaf, "Diffuse interface model of surfactant adsorption onto flat and droplet interfaces," *Rheologica Acta*, vol. 46, pp. 3–11, 2006.

[66] Y. Shi, G. H. Tang, L. H. Cheng, and H. Q. Shuang, "An improved phase-field-based lattice Boltzmann model for droplet dynamics with soluble surfactant," *Computers and Fluids*, vol. 179, pp. 508–520, 2019.

[67] H. A. Stone and L. G. Leal, "The effects of surfactants on drop deformation and breakup," *Journal of Fluid Mechanics*, vol. 220, pp. 161–186, 1990.

[68] W. J. Milliken and L. G. Leal, "The Influence of Surfactant on the Deformation and Breakup of a Viscous Drop: The Effect of Surfactant Solubility," *Journal of Colloid and Interface Science*, vol. 166, pp. 275–285, 1994.

[69] J. Zhang, D. Eckmann, and P. Ayyaswamy, "A front tracking method for a deformable intravascular bubble in a tube with soluble surfactant transport," *Journal of Computational Physics*, vol. 214, pp. 366–396, 2006.

[70] M. Muradoglu and G. Tryggvason, "Simulations of soluble surfactants in 3D multiphase flow," *Journal of Computational Physics*, vol. 274, pp. 737–757, 2014.

[71] F. Jin and K. J. Stebe, "The effects of a diffusion controlled surfactant on a viscous drop injected into a viscous medium," *Physics of Fluids*, vol. 19, pp. 1–8, 11 2007.

[72] K.-Y. Chen and M.-C. Lai, "A conservative scheme for solving coupled surface-bulk convection–diffusion equations with an application to interfacial flows with soluble surfactant," *Journal of Computational Physics*, vol. 257, pp. 1–18, 2014.

[73] A. Alke and D. Bothe, "3D Numerical Modeling of Soluble Surfactant at Fluidic Interfaces Based on the Volume-of-Fluid Method," *Fluid Dynamics & Materials Processing*, vol. 5, pp. 345–372, 2009.

[74] M. R. Booty and M. Siegel, "A hybrid numerical method for interfacial fluid flow with soluble surfactant," *Journal of Computational Physics*, vol. 229, pp. 3864–3883, 2010.

[75] H. Diamant and D. Andelman, "Kinetics of surfactant adsorption at fluid/fluid interfaces: non-ionic surfactants," *Europhysics Letters*, vol. 34, pp. 575–580, 1996.

[76] T. Teramoto and F. Yonezawa, "Droplet growth dynamics in a water/oil/surfactant system," *Journal of Colloid and Interface Science*, vol. 235, pp. 329–333, 2001.

[77] C.-H. Teng, I.-L. Chern, and M.-C. Lai, "Simulating binary fluid-surfactant dynamics by a phase field model," *Discrete and Continuous Dynamical Systems - Series B*, vol. 17, pp. 1289–1307, 2012.

[78] Y. Li and J. Kim, "A comparison study of phase-field models for an immiscible binary mixture with surfactant," *European Physical Journal B*, vol. 85, no. 340, pp. 1–9, 2012.

[79] H. Diamant, G. Ariel, and D. Andelman, "Kinetics of surfactant adsorption: the free energy approach," *Colloids and Surfaces A: Physicochemical and Engineering Aspects*, vol. 183–185, pp. 259–276, 2001.

[80] A. Yun, Y. Li, and J. Kim, "A new phase-field model for a water-oil-surfactant system," *Applied Mathematics and Computation*, vol. 229, pp. 422–432, 2014.

[81] S. Engblom, M. Do-Quang, G. Amberg, and A. K. Tornberg, "On diffuse interface modeling and simulation of surfactants in two-phase fluid flow," *Communications in Computational Physics*, vol. 14, pp. 879–915, 2013.

[82] G. I. Tóth and B. Kvamme, "Analysis of Ginzburg-Landau-type models of surfactant-assisted liquid phase separation," *Physical Review E - Statistical, Nonlinear, and Soft Matter Physics*, vol. 91, no. 032404, pp. 1–14, 2015.

[83] R. van der Sman and M. Meinders, "Analysis of improved Lattice Boltzmann phase field method for soluble surfactants," *Computer Physics Communications*, vol. 199, pp. 12–21, 2016.

[84] G. I. Tóth and B. Kvamme, "Phase field modelling of spinodal decomposition in the oil/water/asphaltene system," *Physical Chemistry Chemical Physics*, vol. 17, pp. 20 259–20 273, 2015.

[85] V. M. Kendon, M. E. Cates, I. Pagonabarraga, J. C. Desplat, and P. Bladon, "Inertial effects in three-dimensional spinodal decomposition of a symmetric binary fluid mixture: A lattice Boltzmann study," *Journal of Fluid Mechanics*, vol. 440, pp. 147–203, 2001.

[86] C. Xue, G. Qu, Y. Han, S. Li, X. Gao, and W. Ding, "Molecular Dynamics Simulations of Sulfobetaine-Type Zwitterionic Surfactant at the Decane/Water Interface," *Journal of Dispersion Science and Technology*, vol. 37, pp. 1480–1485, 2016.

[87] Y. Li, X. J. He, X. L. Cao, Y. H. Shao, Z. Q. Li, and F. L. Dong, "Mesoscopic simulation study on the efficiency of surfactants adsorbed at the liquid/liquid interface," *Molecular Simulation*, vol. 31, pp. 1027–1033, 2005.

[88] K. Erik Teigen, P. Song, J. Lowengrub, and A. Voigt, "A diffuse-interface method for two-phase flows with soluble surfactants," *Journal of Computational Physics*, vol. 230, pp. 375–393, 2011.

[89] G. B. McFadden and A. A. Wheeler, "On the Gibbs adsorption equation and diffuse interface models," *Proceedings of the Royal Society A: Mathematical, Physical and Engineering Sciences*, vol. 458, pp. 1129–1149, 2002.

[90] A. Lamura, G. Gonnella, and J. M. Yeomans, "A lattice Boltzmann model of ternary fluid mixtures," *Europhysics Letters*, vol. 45, pp. 314–320, 1999.

[91] C. M. Pooley and K. Furtado, "Eliminating spurious velocities in the free-energy lattice Boltzmann method," *Physical Review E - Statistical, Nonlinear, and Soft Matter Physics*, vol. 77, no. 046702, pp. 1–9, 2008.

[92] A. E. Komrakova, D. Eskin, and J. J. Derksen, "Lattice Boltzmann simulations of a single n-butanol drop rising in water," *Physics of Fluids*, vol. 25, no. 042102, pp. 1–29, 2013.

[93] P. L. Bhatnagar, E. P. Gross, and M. Krook, "A Model for Collision Processes in Gases. I. Small Amplitude Processes in Charged and Neutral One-Component Systems," *Physical Review*, vol. 94, pp. 511–525, 1954.

[94] D. D'Humieres, I. Ginzburg, M. Krafczyk, P. Lallemand, and L. S. Luo, "Multiple-relaxation-time lattice Boltzmann," *Philosophical Transactions of the Royal Society London A*, vol. 360, pp. 437–451, 2002.

[95] H. Yu, L.-S. Luo, and S. S. Girimaji, "LES of turbulent square jet flow using an MRT lattice Boltzmann model," *Computers & Fluids*, vol. 35, pp. 957–965, 2006.

[96] C. M. Pooley, H. Kusumaatmaja, and J. M. Yeomans, "Contact line dynamics in binary lattice Boltzmann simulations," *Physical Review E*, vol. 78, no. 056709, pp. 1–9, 2008.

[97] R. van der Sman, "Galilean invariant lattice Boltzmann scheme for natural convection on square and rectangular lattices," *Physical Review E - Statistical, Nonlinear, and Soft Matter Physics*, vol. 74, no. 026705, pp. 1–17, 2006.

[98] P. Yue, C. Zhou, and J. J. Feng, "Spontaneous shrinkage of drops and mass conservation in phase-field simulations," *Journal of Computational Physics*, vol. 223, pp. 1–9, 2007.

[99] Y. Li, J.-I. Choi, and J. Kim, "A phase-field fluid modeling and computation with interfacial profile correction term," *Communications in Nonlinear Science and Numerical Simulation*, vol. 30, pp. 84–100, 2016.

[100] D. López-Díaz, I. García-Mateos, and M. M. Velázquez, "Surface properties of mixed monolayers of sulfobetaines and ionic surfactants," *Journal of Colloid and Interface Science*, vol. 299, pp. 858–866, 2006.

[101] H. Ju, Y. Jiang, T. Geng, Y. Wang, and C. Zhang, "Equilibrium and dynamic surface tension of quaternary ammonium salts with different hydrocarbon chain length of counterions," *Journal of Molecular Liquids*, vol. 225, pp. 606–612, 2017.

[102] P. Lallemand and L.-S. Luo, "Theory of the lattice Boltzmann method: Dispersion, dissipation, isotropy, Galilean invariance, and stability," *Physical Review E*, vol. 6, pp. 6546–6562, 2000.

# Appendix A: Chapman-Enskog expansions of the LBEs to recover governing equations

The Chapman-Enskong analysis is the perturbation analysis of a particle distribution function around its equilibrium distribution with Knudsen number (i.e. Kn) in terms of $\epsilon$ as the expansion parameter to find the non-equilibrium part of the particle distribution function that is necessary to recover macroscopic equations beyond the Euler equations.

Note that all equations in this chapter are written in the Einstein notation, where $\alpha$, $\beta$, and $\gamma$ represent the spatial coordinates $x$, $y$, and $z$.

## A.1 The Chapman-Enskong expansions of the LBEs for the order parameters representing two immiscible liquids and soluble surfactant

First, we will recover the Cahn-Hilliard equation for $\phi$ from the Chapman-Enskog expansion of the LBE of the particle population $g$. The Cahn-Hilliard equation for $\phi$ (i.e., Eq. (2.1c)) can be written as follows:

$$\partial_t \phi + \partial_\alpha (\phi u_\alpha) = M_\phi \partial^2_{\alpha\alpha} \mu_\phi \tag{A.1}$$

The Lattice Boltzmann equation (i.e. LBE) for the population $g$ representing $\phi$ can be expressed as:

$$g_q(x_\alpha + g_{q\alpha}\Delta t, t + \Delta t) - g_q(x_\alpha, t) = -\left( \frac{g_q(x_\alpha, t) - g_q^{eq}(x_\alpha, t)}{\tau_g} \right) \tag{A.2}$$

Where $x_\alpha$ and $c_{q\alpha}$ represent the position and the discrete velocity vectors; respectively; $t$ and $\Delta t$ refer to time and time-step; respectively; $g_q$ and $g_q^{eq}$ represent the particle distribution and the equilibrium distribution functions, respectively; $\tau_g$ is the dimensionless relaxation time of the particle distribution function $g_q$. $\Omega_q^g = -\left(\dfrac{g_q - g_q^{eq}}{\tau_g}\right)$ is the BGK collision operator [93]. From hereafter, we use the convention $g_q$ and $g_q^{eq}$ instead of $g_q(x_\alpha, t)$ and $g_q^{eq}(x_\alpha, t)$, respectively.

The equilibrium distribution function and the source term can be represented as:

$$g_q^{eq} = \begin{cases} w_q\left(\Gamma_\phi \mu_\phi + \phi c_{q\alpha} u_\alpha + \frac{3}{2}\left[c_{q\alpha}c_{q\beta} - \frac{1}{3}\delta_{\alpha\beta}\right]\phi u_\alpha u_\beta\right), & \text{for } q \neq 0 \\ \phi - \sum_{q=1}^{q=Q-1} g_q^{eq}, & \text{for } q = 0 \end{cases} \tag{A.3}$$

Here, $w_q$ refers to the weights associated with the chosen discrete velocity set; $c_s$ is the speed of sound and it is represented as $c_s^2 = (1/3)\Delta x^2/\Delta t^2$; $u_\alpha$ is the fluid velocity; $\Gamma_\phi$ is the mobility coefficient of $\phi$ controlling $M_\phi$. Eq. (A.3) must satisfy the moments of $g_q^{eq}$ defined as follows:

$$\sum_q g_q^{eq} = \phi \tag{A.4a}$$

$$\sum_q c_{q\alpha} g_q^{eq} = \phi u_\alpha \tag{A.4b}$$

$$\sum_q c_{q\alpha} c_{q\beta} g_q^{eq} = \Gamma_\phi \mu_\phi \delta_{\alpha\beta} + \phi u_\alpha u_\beta \tag{A.4c}$$

After Taylor expansion of the left side of Eq. (A.2) up to a second order (i.e. the derivatives of order higher than three do not significantly affect the macroscopic behaviour [51]), the LBE for the population $g$ (A.2) can be written as follows:

$$\Delta t(\partial_t + c_{q\alpha}\partial_\alpha)g_q + \frac{(\Delta t)^2}{2}(\partial_t + c_{q\alpha}\partial_\alpha)^2 g_q = -\left(\frac{g_q - g_q^{eq}}{\tau_g}\right) \tag{A.5}$$

After cancelling $\Delta t$ from both sides of the above equation, eq. (A.5) can be rewritten as:

$$(\partial_t + c_{q\alpha}\partial_\alpha)g_q + \frac{\Delta t}{2}(\partial_t + c_{q\alpha}\partial_\alpha)^2 g_q = -\left(\frac{g_q - g_q^{eq}}{\tau_g \Delta t}\right) \tag{A.6}$$

The expansions of $g_q$ around $g_q^{(0)}$ (i.e. $g_q^{eq}$), $\partial_t$, and $\partial_\alpha$ in terms of $\epsilon$ as the expansion

parameter can be represented as:

$$g_q = g_q^{(0)} + \epsilon g_q^{(1)} + \epsilon^2 g_q^{(2)} \tag{A.7a}$$

$$\partial_t = \epsilon \partial_t^{(1)} + \epsilon^2 \partial_t^{(2)} \tag{A.7b}$$

$$\partial_\alpha = \epsilon \partial_\alpha^{(1)} \tag{A.7c}$$

Please note that the expansions of $g_q$ and $\partial_t$ are considered only up to a second order in $\epsilon$, as we are interested in the second order analysis (i.e. $\mathcal{O}(\epsilon^2)$) of the LBE (A.6) to recover Eq. (2.1c). Considering this simplification, the spatial derivative $\partial_\alpha$ is labelled without any expansion in terms of $\epsilon$ to be consistent with the remaining terms in eq. (A.6) [51]. In Eq. (A.7b), $t^{(1)}$ and $t^{(2)}$ represent the convective and diffusive time scales, respectively.

The solvability conditions obtained based on the conservation of phase field parameter (i.e. $\phi$) can be written as follows:

$$\sum_q g_q^{(n)} = 0 \tag{A.8}$$

Inserting all the expansions represented by the set of equations (A.7) in Eq. (A.6) as follows:

$$(\epsilon \partial_t^{(1)} + \epsilon^2 \partial_t^{(2)} + c_{q\alpha} \epsilon \partial_\alpha^{(1)})(g_q^{(0)} + \epsilon g_q^{(1)} + \epsilon^2 g_q^{(2)})$$
$$+ \frac{\Delta t}{2}(\epsilon \partial_t^{(1)} + \epsilon^2 \partial_t^{(2)} + c_{q\alpha} \epsilon \partial_\alpha^{(1)})^2 (g_q^{(0)} + \epsilon g_q^{(1)} + \epsilon^2 g_q^{(2)})$$
$$= -\left( \frac{(\cancel{g_q^{(0)}} + \epsilon g_q^{(1)} + \epsilon^2 g_q^{(2)}) - \cancel{g_q^{(0)}}}{\tau_g \Delta t} \right) \tag{A.9}$$

From the above equation, compare the coefficients of $\epsilon$ and $\epsilon^2$ on both sides as follows:

$$\mathcal{O}(\epsilon): \quad \partial_t^{(1)}(g_q^{(0)}) + c_{q\alpha} \partial_\alpha^{(1)}(g_q^{(0)}) = -\frac{g_q^{(1)}}{\tau_g \Delta t} \tag{A.10a}$$

$$\mathcal{O}(\epsilon^2): \quad \partial_t^{(2)}(g_q^{(0)}) + \partial_t^{(1)}(g_q^{(1)}) + c_{q\alpha} \partial_\alpha^{(1)}(g_q^{(1)}) + \frac{\Delta t}{2}(\partial_t^{(1)} + c_{q\alpha} \partial_\alpha^{(1)})^2 g_q^{(0)}$$
$$= -\frac{g_q^{(2)}}{\tau_g \Delta t} \tag{A.10b}$$

78

The term $\frac{\Delta t}{2}(\partial_t^{(1)} + c_{q\alpha}\partial_\alpha^{(1)})^2 g_q^{(0)}$ in Eq. (A.10b) can be simplified as:

$$\frac{\Delta t}{2}(\partial_t^{(1)} + c_{q\alpha}\partial_\alpha^{(1)})^2 g_q^{(0)} = \frac{\Delta t}{2}(\partial_t^{(1)} + c_{q\alpha}\partial_\alpha^{(1)})(\partial_t^{(1)} + c_{q\alpha}\partial_\alpha^{(1)})g_q^{(0)}$$

The term $(\partial_t^{(1)} + c_{q\alpha}\partial_\alpha^{(1)})g_q^{(0)}$ in the above equation can be substituted from eq. (A.10a) as follows:

$$\frac{\Delta t}{2}(\partial_t^{(1)} + c_{q\alpha}\partial_\alpha^{(1)})^2 g_q^{(0)} = \frac{\Delta t}{2}(\partial_t^{(1)} + c_{q\alpha}\partial_\alpha^{(1)})\left( -\frac{g_q^{(1)}}{\tau_g \Delta t}\right)$$
$$= -\frac{1}{2\tau_g}(\partial_t^{(1)} + c_{q\alpha}\partial_\alpha^{(1)})g_q^{(1)}$$

Following this simplification, Eq. (A.10b) can be rewritten as follows:

$$\partial_t^{(2)}(g_q^{(0)}) + \left(1 - \frac{1}{2\tau_g}\right)\left[\partial_t^{(1)}(g_q^{(1)}) + c_{q\alpha}\partial_\alpha^{(1)}(g_q^{(1)})\right] = -\frac{g_q^{(2)}}{\tau_g \Delta t} \qquad \text{(A.11)}$$

Taking the zeroth moment (i.e. multiplying by 1 and then summing over $q$) of Eq. (A.10a) and using the solvability conditions (A.8) along with the moments of $g_q^{(0)}$ (A.4), Eq. (A.10a) can be simplified as:

$$\partial_t^{(1)}(\sum_q g_q^{(0)}) + \partial_\alpha^{(1)}(\sum_q c_{q\alpha}g_q^{(0)}) = -\frac{(\sum_q g_q^{(1)})^{\cancel{0}}}{\tau_g \Delta t}$$
$$\partial_t^{(1)}(\phi) + \partial_\alpha^{(1)}(\phi u_\alpha) = 0 \qquad \text{(A.12)}$$

Similarly, Eq. (A.11) can be simplified as follows:

$$\partial_t^{(2)}(\sum_q g_q^{(0)}) + \left(1 - \frac{1}{2\tau_g}\right)\left[\partial_t^{(1)}(\sum_q g_q^{\cancel{(1)}})^{\cancel{0}} + \partial_\alpha^{(1)}(\sum_q c_{q\alpha}g_q^{(1)})\right]$$
$$= -\frac{(\sum_q g_q^{\cancel{(2)}})^{\cancel{0}}}{\tau_g \Delta t}$$
$$\partial_t^{(2)}(\phi) + \left(1 - \frac{1}{2\tau_g}\right)\partial_\alpha^{(1)}(\sum_q c_{q\alpha}g_q^{(1)}) = 0 \qquad \text{(A.13)}$$

The only unknown variable in Eq. (A.13) is $g_q^{(1)}$. $g_q^{(1)}$ can be obtained from Eq. (A.10a) as:

$$g_q^{(1)} = -\tau_g \Delta t\left[\partial_t^{(1)}(g_q^{(0)}) + c_{q\alpha}\partial_\alpha^{(1)}(g_q^{(0)})\right] \qquad \text{(A.14)}$$

Substituting Eq. (A.14) in Eq. (A.13) and again using the moments (A.4), Eq. (A.13) can be further simplified as follows:

$$\partial_t^{(2)}(\phi) + \left(1 - \frac{1}{2\tau_g}\right)(-\tau_g \Delta t)\partial_\alpha^{(1)}\left[\partial_t^{(1)}(\sum_q c_{q\alpha}g_q^{(0)}) + \partial_\beta^{(1)}(\sum_q c_{q\alpha}c_{q\beta}g_q^{(0)})\right] = 0$$

$$\partial_t^{(2)}(\phi) + \left(1 - \frac{1}{2\tau_g}\right)(-\tau_g \Delta t)\partial_\alpha^{(1)}\left[\partial_t^{(1)}(\sum_q c_{q\alpha}g_q^{(0)}) + \partial_\beta^{(1)}(\sum_q c_{q\alpha}c_{q\beta}g_q^{(0)})\right] = 0$$

$$\partial_t^{(2)}(\phi) + \left(1 - \frac{1}{2\tau_g}\right)(-\tau_g \Delta t)\partial_\alpha^{(1)}\left[\partial_t^{(1)}(\phi u_\alpha) + \partial_\beta^{(1)}(\Gamma_\phi \mu_\phi \delta_{\alpha\beta} + \phi u_\alpha u_\beta)\right] = 0 \quad (A.15)$$

In Eq. (A.15), assume $\mathcal{I} = \partial_t^{(1)}(\phi u_\alpha) + \partial_\beta^{(1)}(\phi u_\alpha u_\beta)$ and $\mathcal{II} = \partial_\beta^{(1)}(\Gamma_\phi \mu_\phi \delta_{\alpha\beta})$.

The term $\mathcal{I}$ can be simplified as:

$$\mathcal{I} = u_\alpha \partial_t^{(1)}(\phi) + \phi \partial_t^{(1)}(u_\alpha) + \partial_\beta^{(1)}(\phi u_\alpha u_\beta) \quad (A.16)$$

During the Chapman-Enskog analysis of the Navier-Stokes equation in our case, the coefficient obtained by taking the first moment of $\mathcal{O}(\epsilon)$ terms can be simplified for the incompressible flow as follows [51]:

$$\partial_t^{(1)}(\rho u_\alpha) + \partial_\beta^{(1)}(P_{\alpha\beta}^{th} + \rho u_\alpha u_\beta) = 0$$

$$\rho \partial_t^{(1)}(u_\alpha) + u_\alpha \partial_t^{(1)}(\rho) + \partial_\beta^{(1)}(P_{\alpha\beta}^{th}) + u_\alpha u_\beta \overset{0}{\cancel{\partial_\beta^{(1)}\rho}} + \rho u_\beta \partial_\beta^{(1)} u_\alpha + \rho u_\alpha \overset{0}{\cancel{\partial_\beta^{(1)} u_\beta}} = 0 \quad (A.17)$$

Now, using the coefficient obtained by taking the zeroth moment of $\mathcal{O}(\epsilon)$ terms, the term $\partial_t^{(1)}(\rho)$ in Eq. (A.17) can be simplified as:

$$\partial_t^{(1)}(\rho) = -\partial_\alpha^{(1)}(\rho u_\alpha)$$

$$= \rho \overset{0}{\cancel{\partial_\alpha^{(1)}(u_\alpha)}} + u_\alpha \overset{0}{\cancel{\partial_\alpha^{(1)}(\rho)}}$$

$$= 0 \quad (A.18)$$

Following this simplification, Eq. (A.17) can be further resolved as follows:

$$\partial_t^{(1)}(u_\alpha) = -\left(\frac{\partial_\beta^{(1)}(P_{\alpha\beta}^{th})}{\rho} + u_\beta \partial_\beta^{(1)} u_\alpha\right) \quad (A.19)$$

80

Substituting Eq. (A.19) in Eq. (A.16), the final expression for $\mathcal{I}$ can be obtained as:

$$\mathcal{I} = u_\alpha \partial_t^{(1)}(\phi) - \frac{\phi}{\rho}\partial_\beta^{(1)}(P_{\alpha\beta}^{th}) - \cancel{\phi u_\beta \partial_\beta^{(1)} u_\alpha} + u_\alpha u_\beta \partial_\beta^{(1)}\psi + \cancel{\phi u_\beta \partial_\beta^{(1)} u_\alpha}$$

$$+ \phi u_\alpha \cancelto{0}{\partial_\beta^{(1)} u_\beta} \qquad (A.20)$$

Here, the value of $\partial_t^{(1)}(\phi)$ can be obtained from Eq. (A.12) as follows:

$$\partial_t^{(1)}(\phi) = -\partial_\beta^{(1)}(\phi u_\beta)$$

$$= -(\phi \cancelto{0}{\partial_\beta^{(1)} u_\beta} + u_\beta \partial_\beta^{(1)}\phi)$$

$$= -u_\beta \partial_\beta^{(1)}\phi$$

Using this identity, Eq. (A.20) can be rewritten as:

$$\mathcal{I} = -\cancel{u_\alpha u_\beta \partial_\beta^{(1)}\phi} - \frac{\phi}{\rho}\partial_\beta^{(1)}(P_{\alpha\beta}^{th}) + \cancel{u_\alpha u_\beta \partial_\beta^{(1)}\phi}$$

$$= -\frac{\phi}{\rho}\partial_\beta^{(1)}(P_{\alpha\beta}^{th}) \qquad (A.21)$$

Here, $P_{\alpha\beta}^{th}$ is the thermodynamic pressure tensor and it can be represented as $\partial_\beta P_{\alpha\beta}^{th} = [\rho(\partial_\beta \mu_\rho) + \phi(\partial_\beta \mu_\phi) + \psi(\partial_\beta \mu_\psi)]\delta_{\alpha\beta}$.

We assume that the mobility coefficient of $\phi$ is constant because of the constant $M_\phi$. The simplification of the term $\mathcal{II}$ can be represented as follows:

$$\mathcal{II} = \partial_\beta^{(1)}(\Gamma_\phi \mu_\phi \delta_{\alpha\beta})$$

$$= \partial_\alpha^{(1)}(\Gamma_\phi \mu_\phi)$$

$$= \Gamma_\phi \partial_\alpha^{(1)}(\mu_\phi) \qquad (A.22)$$

Please note that throughout the simplification of terms $\mathcal{I}$ and $\mathcal{II}$, the time derivative expansions of quantities are replaced by the space derivative expansions as these time derivative expansions are not the time derivative itself and the space derivative expansions are used as the space derivative itself because these are simply labelled without any expansion in terms of $\epsilon$ to be consistent with the simplification of terms

in the LBE (A.2). Putting the final expressions Eq. (A.21) and Eq. (A.22) of $\mathcal{I}$ and $\mathcal{II}$ in Eq. (A.15) and then it can be simplified as:

$$\partial_t^{(2)}(\phi) - \left(\tau_g - \frac{1}{2}\right)\Delta t\partial_\alpha^{(1)}\left[-\frac{\phi}{\rho}\partial_\beta^{(1)}(P_{\alpha\beta}^{th}) + \Gamma_\phi\partial_\alpha^{(1)}(\mu_\phi)\right] = 0$$

$$\partial_t^{(2)}(\phi) = \left(\tau_g - \frac{1}{2}\right)\Delta t\left[\partial_\alpha^{(1)}\left(-\frac{\phi}{\rho}\partial_\beta^{(1)}(P_{\alpha\beta}^{th})\right) + \Gamma_\phi\partial_{\alpha\alpha}^{2(1)}(\mu_\phi)\right] \qquad \text{(A.23)}$$

Rewriting the equations (A.12) and (A.23) with the common factors $\epsilon$ and $\epsilon^2$, respectively, as:

$$\epsilon\partial_t^{(1)}(\phi) + \epsilon\partial_\alpha^{(1)}(\phi u_\alpha) = 0 \qquad \text{(A.24)}$$

$$\epsilon^2\partial_t^{(2)}(\phi) = \left(\tau_g - \frac{1}{2}\right)\Delta t\left[\epsilon\partial_\alpha^{(1)}\left(-\frac{\phi}{\rho}\epsilon\partial_\beta^{(1)}(P_{\alpha\beta}^{th})\right) + \Gamma_\phi\epsilon\partial_\alpha^{(1)}(\epsilon\partial_\alpha^{(1)}(\mu_\phi))\right] \qquad \text{(A.25)}$$

Combining Eq. (A.24) and Eq. (A.25) and reversing the derivative expansions represented by Eq. (A.7b) as well as Eq. (A.7c), the Cahn-Hilliard equation for $\phi$ can be recovered as follows:

$$(\epsilon\partial_t^{(1)} + \epsilon^2\partial_t^{(2)})(\phi) + (\epsilon\partial_\alpha^{(1)})(\phi u_\alpha) = \left[\left(\tau_g - \frac{1}{2}\right)\Delta t\epsilon\partial_\alpha^{(1)}\left(-\frac{\phi}{\rho}\epsilon\partial_\beta^{(1)}(P_{\alpha\beta}^{th})\right)\right.$$
$$\left. + \left(\tau_g - \frac{1}{2}\right)\Delta t\Gamma_\phi\epsilon\partial_\alpha^{(1)}(\epsilon\partial_\alpha^{(1)}(\mu_\phi))\right]$$
$$\partial_t(\phi) + \partial_\alpha(\phi u_\alpha) = \left[\left(\tau_g - \frac{1}{2}\right)\Delta t\partial_\alpha\left(-\frac{\phi}{\rho}\partial_\beta(P_{\alpha\beta}^{th})\right)\right.$$
$$\left. + M_\phi\partial_{\alpha\alpha}^2(\mu_\phi)\right] \qquad \text{(A.26)}$$

Where the mobility of $\phi$ can be represented as $M_\phi = \Gamma_\phi\left(\tau_g - \frac{1}{2}\right)\Delta t$.

In Eq. (A.26), the extra term $\partial_\alpha\left(-\frac{\phi}{\rho}\partial_\beta(P_{\alpha\beta}^{th})\right)$ is considered as the spurious term and this term is Galilean-invariant; however it has no relation with the fluid velocity at all [85]. In addition, this term arises due to the way the non-ideality of the fluid is introduced and it has the second order derivative of $P_{\alpha\beta}^{th}$ (i.e. $\partial_\alpha(\partial_\beta(P_{\alpha\beta}^{th}))$) than $\partial_\beta(P_{\alpha\beta}^{th})$, which is in the Navier-Stokes equation. During the linear perturbation analysis of hydrodynamic modes in Fourier space for a quiescent fluid, Kendon et al. [85] showed that the coupling between $\phi$ and $\rho$ can be neglected in the limit of

incompressibility of fluid. Considering this observation, we can ignore the effect of this extra term and write the recovered Cahn-Hilliard equation for $\phi$ as follows:

$$\partial_t(\phi) + \partial_\alpha(\phi u_\alpha) = M_\phi \partial^2_{\alpha\alpha}(\mu_\phi) \tag{A.27}$$

Following the procedure described for the Chapman-Enskog expansion of the LBE for the population $g$ representing $\phi$, we can recover the Cahn-Hilliard equation for $\psi$ (2.1d) by doing the Chapman-Enskog expansion of the LBE for the population $h$ representing $\psi$ within the limit of incompressibility of fluid.

## A.2 The Chapman-Enskong expansion of the LBE for the order parameter representing the density of fluid mixture

Here, we do not represent the derivation of the Champman-Enskog expansion of the LBE of the population $f$ representing $\rho$ to obtain the continuity and the Navier-Stokes equations in the present study, as the reference of this derivation for the BGK collision operator [93] considering the pure system can be found in Chapter 9: Multiphase and Multicomponent Flows [51].

Similarly, one can find the simplification of the Champman-Enskog expansion of the LBE of the population $f$ given by Kendon et al. [85] for the pure system. The differences between the surfactant-laden system in our case and the pure system studied in [85] are the formulation of the divergence of $P^{th}_{\alpha\beta}$ and the use of the MRT collision operator for the population $f$, which do not introduce any new terms and the Chapman-Enskog expansion of the LBE of the population $f$ will recover the similar expression of the Navier-Stokes equations in the present study, as derived by Kendon

et al. [85]:

$$\partial_t(\rho u_\alpha) + \partial_\beta(\rho u_\alpha u_\beta) = -\partial_\beta P_{\alpha\beta}^{th} + \partial_\beta\left[\rho\nu\left(\partial_\alpha u_\beta + \partial_\beta u_\alpha - \frac{2}{3}\partial_\gamma u_\gamma \delta_{\alpha\beta}\right) + \rho\nu_B\partial_\gamma u_\gamma\delta_{\alpha\beta}\right]$$
$$- \frac{3\nu}{\rho}\partial_\beta(u_\alpha\partial_\gamma P_{\beta\gamma}^{chem} + u_\beta\partial_\gamma P_{\alpha\gamma}^{chem} + u_\gamma\partial_\gamma P_{\alpha\beta}^{chem})$$
$$- \frac{3\nu}{\rho}\partial_\beta\partial_\gamma(\rho u_\alpha u_\beta u_\gamma) \tag{A.28}$$

Here, $\nu_B$ is the bulk viscosity and assumed as $\nu_B = (2\nu/3)$ [85]. Also, the similar Navier-Stokes equations with additional terms were obtained during the derivation for the pure system by [51] as well.

The terms on the second and third lines of Eq. (A.28) are the additional terms in the original Navier-Stokes equation. The term on the third line of Eq. (A.28) is a non-Galilean-invariant term and is related to the fluid velocity. This term can be neglected because $u_\alpha \ll c_s$ is usually the case for the multiphase flows [51]. The term on the second line of eq. (A.28) is not Galilean-invariant but according to [85], this term can be decomposed into the Galilean-invariant and non-Galilean-invariant terms. The Galilean-invariant term is the product of gradients of the chemical pressure tensor and the velocity, these product terms are small compared to the linear product terms present in the first line of eq. (A.28). When these product terms become weak, both Galilean-invariant and non-Galilean-invariant terms can be neglected under the condition that all hydrodynamic fields vary smoothly on the lattice scale. Following these considerations, the Navier-stokes equations (2.1b) can be recovered.

# Appendix B: MRT matrices

The transformation matrix $\mathbf{M}$ derived following Ref. [94] reads:

$$
\begin{pmatrix}
1 & 1 & 1 & 1 & 1 & 1 & 1 & 1 & 1 & 1 & 1 & 1 & 1 & 1 & 1 & 1 & 1 & 1 & 1 \\
-30 & -11 & -11 & -11 & -11 & -11 & -11 & 8 & 8 & 8 & 8 & 8 & 8 & 8 & 8 & 8 & 8 & 8 & 8 \\
12 & -4 & -4 & -4 & -4 & -4 & -4 & 1 & 1 & 1 & 1 & 1 & 1 & 1 & 1 & 1 & 1 & 1 & 1 \\
0 & 1 & 0 & -1 & 0 & 0 & 0 & 1 & -1 & -1 & 1 & 1 & -1 & -1 & 1 & 0 & 0 & 0 & 0 \\
0 & -4 & 4 & 0 & 0 & 0 & 0 & 1 & -1 & 1 & -1 & 1 & -1 & 1 & -1 & 0 & 0 & 0 & 0 \\
0 & 0 & 1 & 0 & -1 & 0 & 0 & 1 & 1 & -1 & -1 & 0 & 0 & 0 & 0 & 1 & -1 & -1 & 1 \\
0 & 0 & 0 & -4 & 4 & 0 & 0 & 1 & 1 & -1 & -1 & 0 & 0 & 0 & 0 & 1 & -1 & 1 & -1 \\
0 & 0 & 0 & 0 & 0 & 1 & -1 & 0 & 0 & 0 & 0 & 1 & 1 & -1 & -1 & 1 & 1 & -1 & -1 \\
0 & 0 & 0 & 0 & 0 & -4 & 4 & 0 & 0 & 0 & 0 & 1 & 1 & -1 & -1 & 1 & 1 & -1 & -1 \\
0 & 2 & 2 & -1 & -1 & -1 & -1 & 1 & 1 & 1 & 1 & 1 & 1 & 1 & 1 & -2 & -2 & -2 & -2 \\
0 & -4 & 2 & -4 & 2 & 2 & 2 & 1 & 1 & 1 & 1 & 1 & 1 & 1 & 1 & -2 & -2 & -2 & -2 \\
0 & 0 & 0 & 1 & 1 & -1 & -1 & 1 & 1 & 1 & 1 & -1 & -1 & -1 & -1 & 0 & 0 & 0 & 0 \\
0 & 0 & 0 & -2 & -2 & 2 & 2 & 1 & 1 & 1 & 1 & -1 & -1 & -1 & -1 & 0 & 0 & 0 & 0 \\
0 & 0 & 0 & 0 & 0 & 0 & 0 & 1 & -1 & -1 & 1 & 0 & 0 & 0 & 0 & 0 & 0 & 0 & 0 \\
0 & 0 & 0 & 0 & 0 & 0 & 0 & 0 & 0 & 0 & 0 & 0 & 0 & 0 & 0 & 1 & -1 & -1 & 1 \\
0 & 0 & 0 & 0 & 0 & 0 & 0 & 0 & 0 & 0 & 0 & 1 & -1 & -1 & 1 & 0 & 0 & 0 & 0 \\
0 & 0 & 0 & 0 & 0 & 0 & 0 & 1 & -1 & 1 & -1 & -1 & 1 & -1 & 1 & 0 & 0 & 0 & 0 \\
0 & 0 & 0 & 0 & 0 & 0 & 0 & -1 & -1 & 1 & 1 & 0 & 0 & 0 & 0 & 1 & 1 & -1 & 1 \\
0 & 0 & 0 & 0 & 0 & 0 & 0 & 0 & 0 & 0 & 0 & 1 & 1 & -1 & -1 & -1 & -1 & 1 & 1
\end{pmatrix}
$$

The relaxation matrix $\mathbf{S}$ is diagonal in the moment space

$$
S = \mathrm{diag}(0, s_e, s_\varepsilon, 0, s_q, 0, s_q, s_\nu, s_\pi, s_\nu, s_\pi, s_\nu, s_\nu, s_\nu, s_m, s_m, s_m) \tag{B.1}
$$

where the relaxation rates other than $s_\nu$ are chosen as follows: $s_e = 1.19$, $s_\varepsilon = s_\pi = 1.4$, $s_q = 1.2$ and $s_m = 1.98$. These values were obtained by Lallemand and Luo [102] using linear analysis to achieve optimized stability of the model.

The kinematic viscosity $\nu$ of the system which is calculated using Eq. (2.72) defines the relaxation rate $s_v$ as follows:

$$
\nu = \frac{1}{3}\left(\frac{1}{s_v} - \frac{1}{2}\right) \tag{B.2}
$$